

FINAL REPORT

BRAYTON CYCLE RADIANT GAS HEATING SYSTEM

by

L. G. Desmon

Solar Division of International Harvester Company

2200 Pacific Highway

San Diego, California 92112

prepared for

NATIONAL AERONAUTICS AND SPACE ADMINISTRATION

April 1969

CONTRACT NAS 3-10945

Technical Management
NASA Lewis Research Center

Cleveland, Ohio

Space Power Systems Division

William T. Wintucky

CASSELL
COPY

NOTICE

This report was prepared as an account of Government-sponsored work. Neither the United States, nor the National Aeronautics and Space Administration (NASA), nor any person acting on behalf of NASA:

- A.) Makes any warranty or representation, expressed or implied, with respect to the accuracy, completeness, or usefulness of the information contained in this report, or that the use of any information, apparatus, method, or process disclosed in this report may not infringe privately-owned rights; or
- B.) Assumes any liabilities with respect to the use of, or for damages resulting from the use of, any information, apparatus, method or process disclosed in this report.

As used above, "person acting on behalf of NASA" includes any employee or contractor of NASA, or employee of such contractor, to the extent that such employee or contractor of NASA or employee of such contractor prepares, disseminates, or provides access to any information pursuant to his employment or contract with NASA, or his employment with such contractor.

Requests for copies of this report should be referred to:

National Aeronautics and Space Administration
Scientific and Technical Information Facility
P. O. Box 33
College Park, Md. 20740

CONTENTS

<u>Section</u>		<u>Page</u>
	ABSTRACT	xiii
	SUMMARY	xv
1	INTRODUCTION	1
	1.1 Description of Hardware	1
	1.2 Publications	2
2	HEAT TRANSFER ANALYSIS	5
	2.1 Task Description	5
	2.2 Evaluation of Gas Thermal and Transport Properties	5
	2.2.1 Core Energy Balance	8
	2.2.2 Fluid Flow	10
	2.2.3 Forced Convection Heat Transfer	13
	2.2.4 Combined Heat Transfer-Pressure Loss Solution	19
	2.2.5 Radiation Heat Transfer	19
	2.2.6 Heater Module Distribution	22
	2.2.7 Circumferential Temperature Distribution Analysis	28
	2.3 Arrangement of Lamp Modules Used	31
	2.4 Conclusions	36
3	STRESS ANALYSES AND MATERIAL SELECTION	37
	3.1 Design Criteria	37
	3.2 Material Properties	37
	3.3 Materials Selected	38
	3.4 Operating Stresses	38

<u>Section</u>		<u>Page</u>
4	FABRICATION	41
	4.1 Fabrication of Heat Exchanger	42
	4.2 Fabrication of Enclosure	44
	4.3 Fabrication of Assembly	44
	4.4 Fabrication of the Duct System	44
	4.4.1 Duct Assembly, Inlet	46
	4.4.2 Duct Assembly, Inlet Center	46
	4.4.3 Duct Assembly, Inlet	46
	4.4.4 Duct Assembly, Outlet	46
	4.4.5 Gimbal	48
	4.4.6 Snip-Open Joint	48
	4.5 Installation	50
5	CONTROL SYSTEM AND INSTRUMENTATION	53
	5.1 Control System	53
	5.1.1 Description	53
	5.1.2 Drawings	53
	5.1.3 Control System Analysis	54
	5.2 Instrumentation	54
	5.2.1 Description	54
	5.2.2 Thermocouple Readout	60
6	QUARTZ TUBE LAMP HEATER	63
	6.1 Heater Requirements	63
	6.2 Assumed Solution	63
	6.3 Development Program	64
	6.4 Final Configuration Lamp	69
	6.5 Lamp Module Description	75
	6.6 Description of the Iodine Cycle	77
	6.7 Operating Conditions	77
7	SURFACE COATING	79
	7.1 Coating Selection	79
	7.2 Coating Description	79
	7.3 Coating Tests	80
	7.4 Coating Performance During Heater Module Tests	81
	7.5 Effect on Performance of Deleting the Coating	81

CONTENTS (Cont)

<u>Section</u>		<u>Page</u>
	REFERENCES	83
Appendices		
A	NASA REVIEW OF SYSTEM THERMAL DESIGN	
B	EFFECTS OF TUBE SURFACE ABSORPTIVITY	
C	HEATER MODULE LIFE TESTS-PROGRESS REPORTS	
D	SINGLE-LAMP, LIFE-TEST - SUMMARY REPORT	

ILLUSTRATIONS

<u>Figure</u>		<u>Page</u>
1	Solar Brayton Cycle Gas Radiant Heating System; Outlet End	3
2	Solar Brayton Cycle Gas Radiant Heating System; Inlet end	4
3	Thermal and Transport Properties of Helium-Xenon Gas Mixture	6
4	Thermal and Transport Properties of Krypton	7
5	Theoretical Gas-Wall Temperature Distribution	9
6	Parametric Study of Pressure Loss	14
7	Parametric Study of Pressure Loss; Specification Values Incorporated	15
8	Comparison of Forced Convection Correlations	16
9	Parametric Study of Heat Transfer Coefficient	18
10	Parametric Study of Heat Transfer Area	18
11	Combined Heat Transfer-Pressure Loss Solution	19
12	Results of the Radiant Flux Distribution Survey	23
13	Conversion of Location on Module Plant to Location Along Tube Flow Length	26
14	Circumferential Temperature Distribution	30
15	Gas and Wall Temperature Distribution as a Function of Flow Length	31
16	Strip Heater Arrangement, Inlet Plane	32
17	Strip Heater Arrangement, Outlet Plane	32
18	Solution to Strip Heater Flux Related to Case II	33
19	Case I - Krypton Flux Values	33

ILLUSTRATIONS (Cont)

<u>Figure</u>		<u>Page</u>
20	Case III - Mixture Flux Values	34
21	Case I - Krypton Longitudinal Temperature Profile	34
22	Case II - Mixture Longitudinal Temperature Profile	35
23	Case III - Mixture Longitudinal Temperature Profile	35
24	Section Through Tube to Header Joint	42
25	Mass Spectrometer Leak Testing	43
26	Header Support Assemblies	43
27	Complete Assembly	45
28	Inlet Side of Assembly	45
29	Inlet Center Duct Assembly	47
30	Inlet Duct Assembly	47
31	Outlet Duct Assembly	48
32	Schematic Diagram of a Typical Gimbal	49
33	Components of a Typical Gimbal	49
34	Schematic Diagram of a Snip-Open Joint	50
35	Brayton Cycle Heater Installation	51
36	Schematic Wiring Diagram of the Control Assembly	55
37	Hot Spot Thermocouples Welded to the U-Tubes	60
38	Thermocouple Jack Box	61
39	Candidate 16-Lamp Heater Module	64
40	Development Test Apparatus and Instrumentation, Second Cast Module	65
41	Two-Lamp Module Fabricated at Solar	66
42	Five-Lamp Module Fabricated at Solar	67
43	Typical Lamp Modifications Tested	68
44	Five-Lamp Module After Test	69

ILLUSTRATIONS (Cont)

<u>Figure</u>		<u>Page</u>
45	Comparison of the Final 750-Watt T5 Lamp and a Special Design 300-Watt T4 Lamp	72
46	Typical Voids in Base Seal Potting	72
47	Sylvania Lamps After 1032-Hour Vacuum Test	73
48	Sylvania Lamps After 1007-Hour Atmosphere Test	73
49	Final Configuration Lamp	74
50	Lamp Module	76
51	Cross Section of Lamp Module	76
52	Amperes, Watts, and Average Filament Temperature Versus Operating Voltage	78
<u>Appendix B</u>		
1	Case II - He-Xe	B-4
2	Case II - He-Xe	B-6
3	Case II - He-Xe	B-7
<u>Appendix C</u>		
1	Test System Schematic	C-3
2	Thermocouple Locations	C-4
3A	Power Source Schematic	C-5
<u>Appendix D</u>		
1	Lamp Life Test Apparatus	D-2
2	Depotted Quartz Lamp; As-Received	D-3
3	Aerometrics-Potted Quartz Lamp After 51.5 Hours Operation at Low Pressure	D-4
4	Power Requirement to Maintain 1700° F Target Temperature Versus Time	D-5
5	Thermocouple Calibration, Low Pressure Test	D-6
6	Target Temperature Versus Hours, Air Operation	D-7
7	Solar-Potted Quartz Lamp After 1994 Hours Operation in Air and Vacuum	D-8

TABLES

<u>Table</u>		<u>Page</u>
I	Thermal Design Requirements	8
II	Nomenclature	11
III	Final Assembly Drawings	41
IV	List of R. I. Drawings	54
V	Summary of the Five-Lamp Module Tests in Vacuum Environment	70
VI	Summary of the Five-Lamp Module Tests in Air Environment	71
VII	List of Aerometrics Drawings	75

ABSTRACT

A radiant gas heating system for use in ground testing a Brayton Cycle Space Power System has been designed and fabricated. It is believed that this is one of the few, if not the only quartz tube lamp heater - heat exchanger system built to operate in vacuum at 1×10^{-8} Torr, in air at one atmosphere, and at any pressure in between.

Heat transfer and stress analyses are presented in brief, as are the activities in the fields of controls system design, quartz tube lamp development, and surface coating tests.

SUMMARY

This final report describes the work conducted by Solar Division of International Harvester Company under NASA Contract NAS 3-10945. The purpose and scope of the contract was to design and fabricate a radiant gas heating system for use in ground testing a Brayton Cycle Space Power System. The heart of the system delivered is a U-tube heat exchanger, radiantly heated by tungsten filament quartz tube lamps in water cooled modules. It is designed to operate at input power levels to 120-KW, in vacuum at 1×10^{-8} Torr, in air at one atmosphere, and at any pressure in between. Design problems, life tests, and the final configuration of the lamps are reviewed as are the activities in the fields of heat transfer analysis, absorptivity coating, and fabrication.

1

INTRODUCTION

This report describes the activities and results of the program conducted by Solar Division of International Harvester Company under NASA Contract NAS 3-10945. The scope of the program included the design, fabrication, and assembly of a radiant gas heating system for use in ground testing a Brayton Cycle Space Power System. This system provides a heat source that is easily controlled, infinitely adjustable, well understood, and similar in effect to its more complex and as yet unavailable counterpart, the flight heat source(s). Among the specification requirements was that the heater-exchanger assembly operate satisfactorily in air at one atmosphere, in vacuum at 1×10^{-8} Torr, and at pressures in between. For this and other reasons, including a design goal of 10,000 hours of operation, no assembly was available to serve as an example.

Work on this program began on 19 February 1968 and hardware was shipped on 16 January 1969. This report was generated to satisfy the final contractual requirement.

1.1 DESCRIPTION OF HARDWARE

The Solar Brayton Cycle Gas Radiant Heating System provides a radiant heat source for use in ground testing various components of a 10 kw NASA Brayton Cycle Power System. The basic components (shown in Figures 1 and 2) are a heat exchanger, heater, and ducting, along with a power control and distribution systems, and instrumentation.

Gas enters the system through the 51439⁽¹⁾ Duct Assembly and flows into the 51491 Duct Assembly. The gas proceeds on through the 51433 Duct Assembly and into the 51432 Heat Exchanger. Gas inlet and outlet temperature probes are located immediately upstream and downstream of the core, outside of the heater enclosure. From the inlet header of the heat exchanger, the gas passes through the U-tube bank, into the exit header, and out of the system through the 51434 Duct Assembly. While flowing through the tube bank, the gas is heated by the radiant energy from the quartz tube lamps in the lamp modules, bolted in panels on both sides which are hinged to the 51486 Enclosure.

1. Solar drawing number.

The electric power and control system has the capability of regulating the voltage to the lamps either manually or automatically.

1.2 PUBLICATIONS

Throughout the progress of this program, many formal reports were generated and transmitted to NASA. Most of these publications are referenced in this report; those not referenced but considered significant include:

- Solar ES 2058 - Installation, Operation and Maintenance Manual;
(24 January 1969)
- Brayton Cycle Radiant Gas Heating System - Monthly Technical Progress Narratives 1 through 9 (April through December 1968)

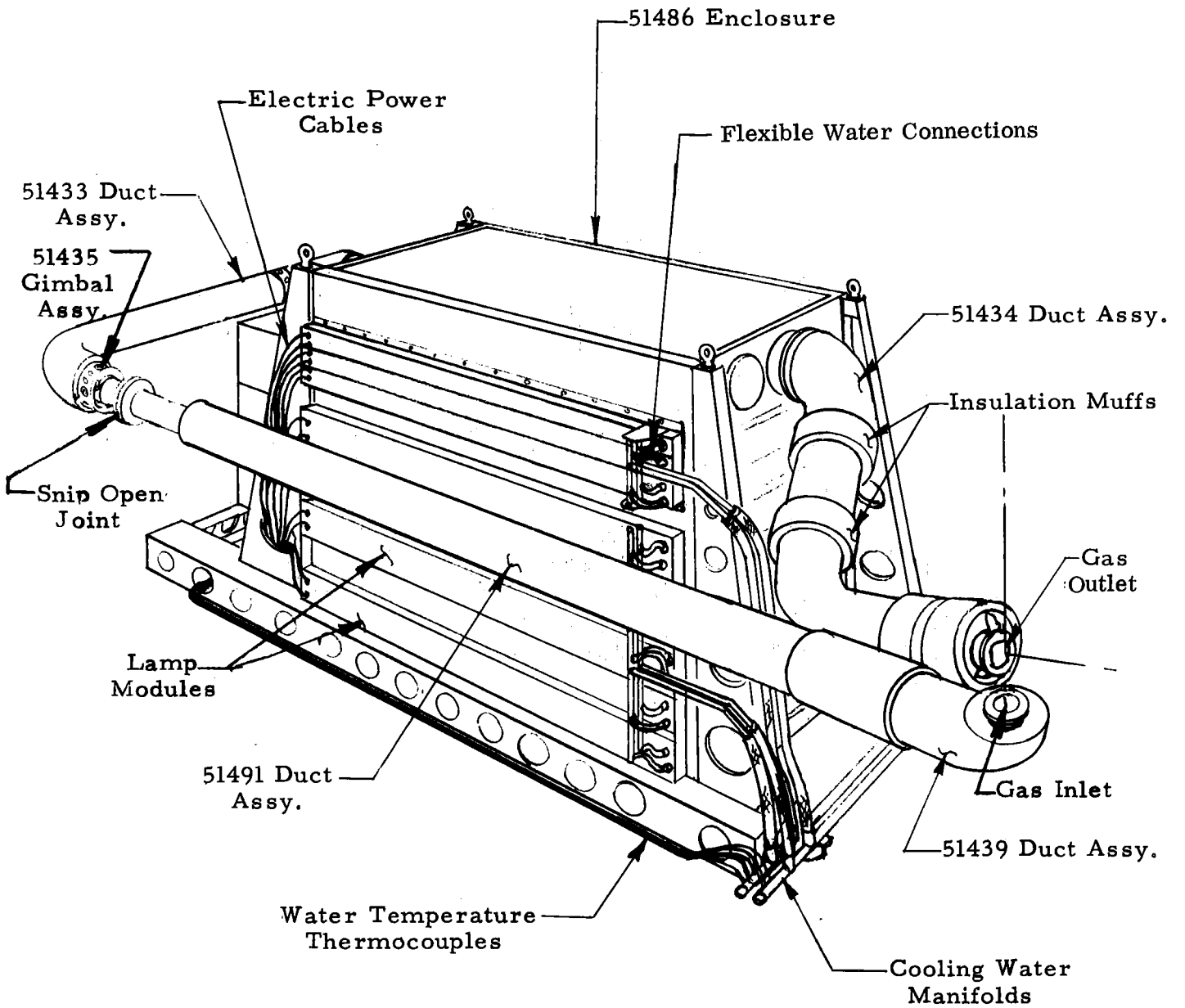


FIGURE 1. SOLAR BRAYTON CYCLE GAS RADIANT HEATING SYSTEM; Outlet End

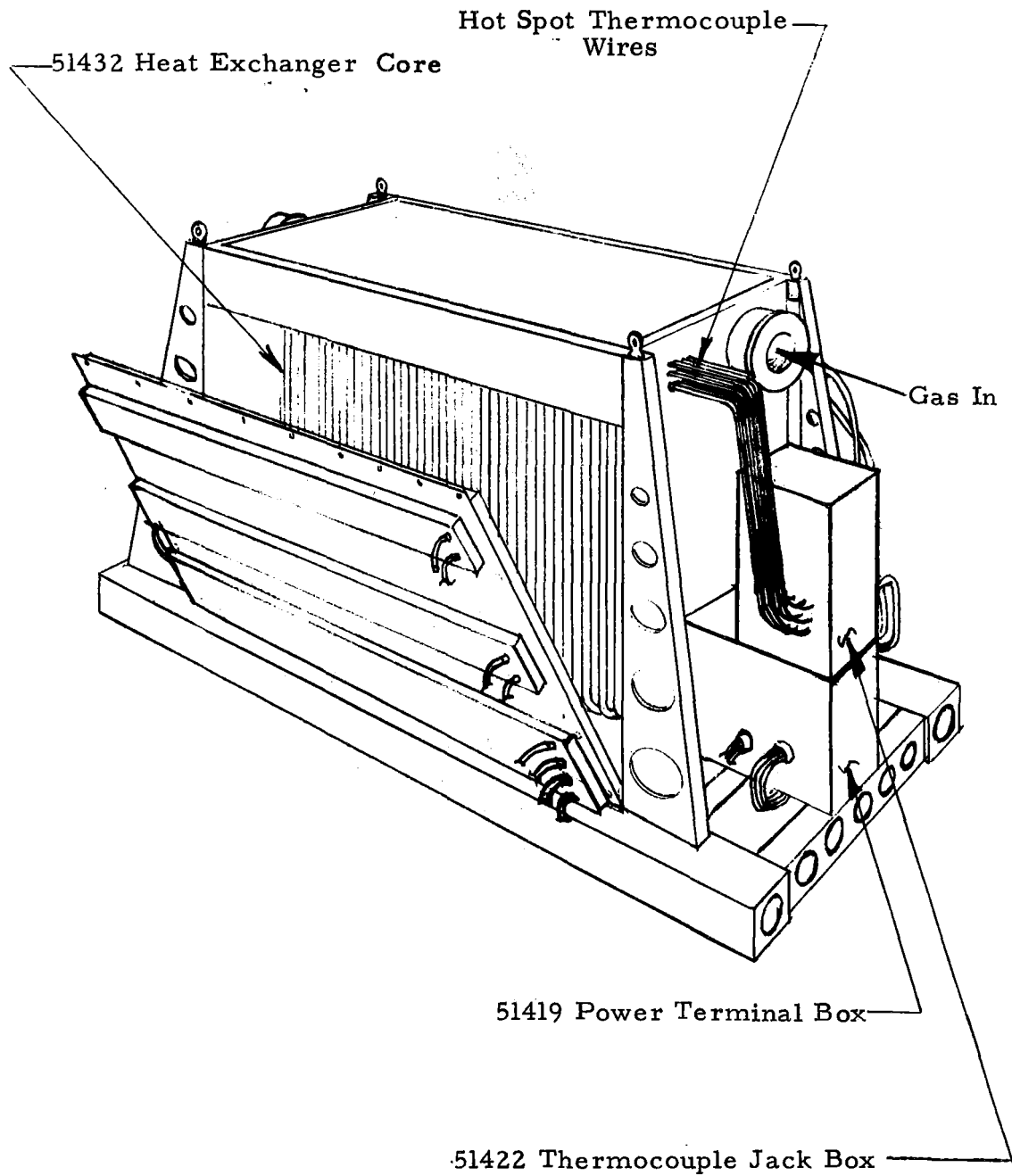


FIGURE 2. SOLAR BRAYTON CYCLE GAS RADIANT HEATING SYSTEM; Inlet End

2

HEAT TRANSFER ANALYSIS

2.1 TASK DESCRIPTION

In addition to establishing the quantity, diameter, length, and arrangement of the heat exchanger tubes, the task included sizing the ducting, designing the insulation system, and selecting the quantity and location of radiant heater modules. Two of the problem areas relating to this task included:

- The Prandtl number for the helium-xenon gas mixture is about 0.3 and no convection correlation could be found in the literature for a Prandtl number in the range of 0.1 and 0.5.
- The analytical technique required to determine the radiant flux distribution which may be obtained from a specified number and geometric distribution of heater modules did not appear in the literature. Dr. Paul F. Pucci, Professor of Mechanical Engineering at the Naval Postgraduate School, Monterey, California acted as consultant on thermal design and established the technique used.

2.2 EVALUATION OF GAS THERMAL AND TRANSPORT PROPERTIES

An IBM program was prepared to calculate the thermal and transport properties of low pressure gas mixtures as a function of temperature. The output of the program, which includes viscosity, thermal conductivity, specific heat, and Prandtl number, is shown in Figures 3 and 4.

SPECIFIC HEAT = 0.05927 Btu/Lb-°F
 MOLECULAR WEIGHT 83.8 Lb/Mol
 GAS PROPERTIES FROM NASA, TN D-2677

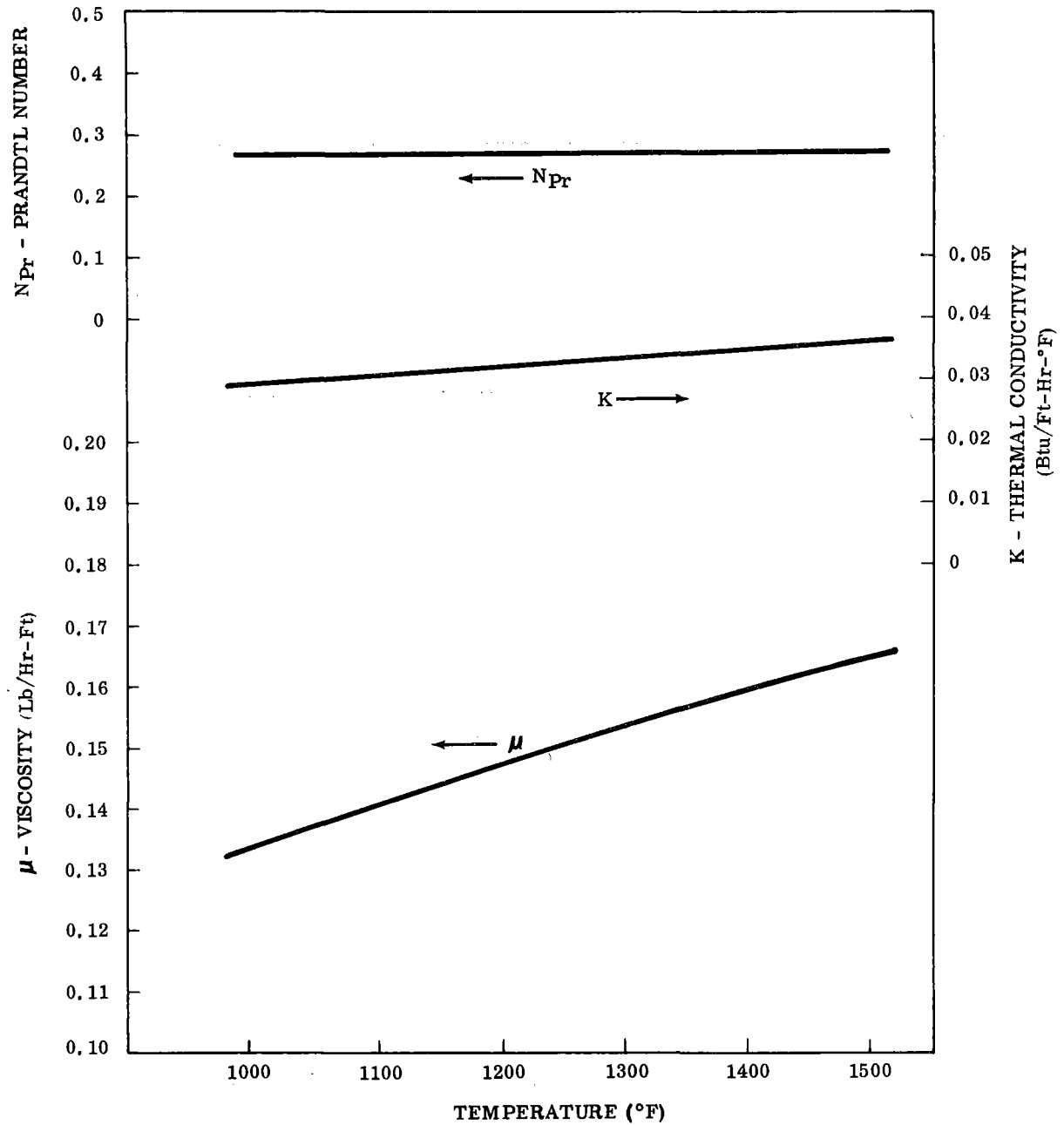


FIGURE 3. THERMAL AND TRANSPORT PROPERTIES OF HELIUM-XENON GAS MIXTURE

SPECIFIC HEAT = 0.05927 Btu/Lb-°F
 MOLECULAR WEIGHT = 83.8 Lb/Mol
 KRYPTON PROPERTIES FROM NASA, TR R132

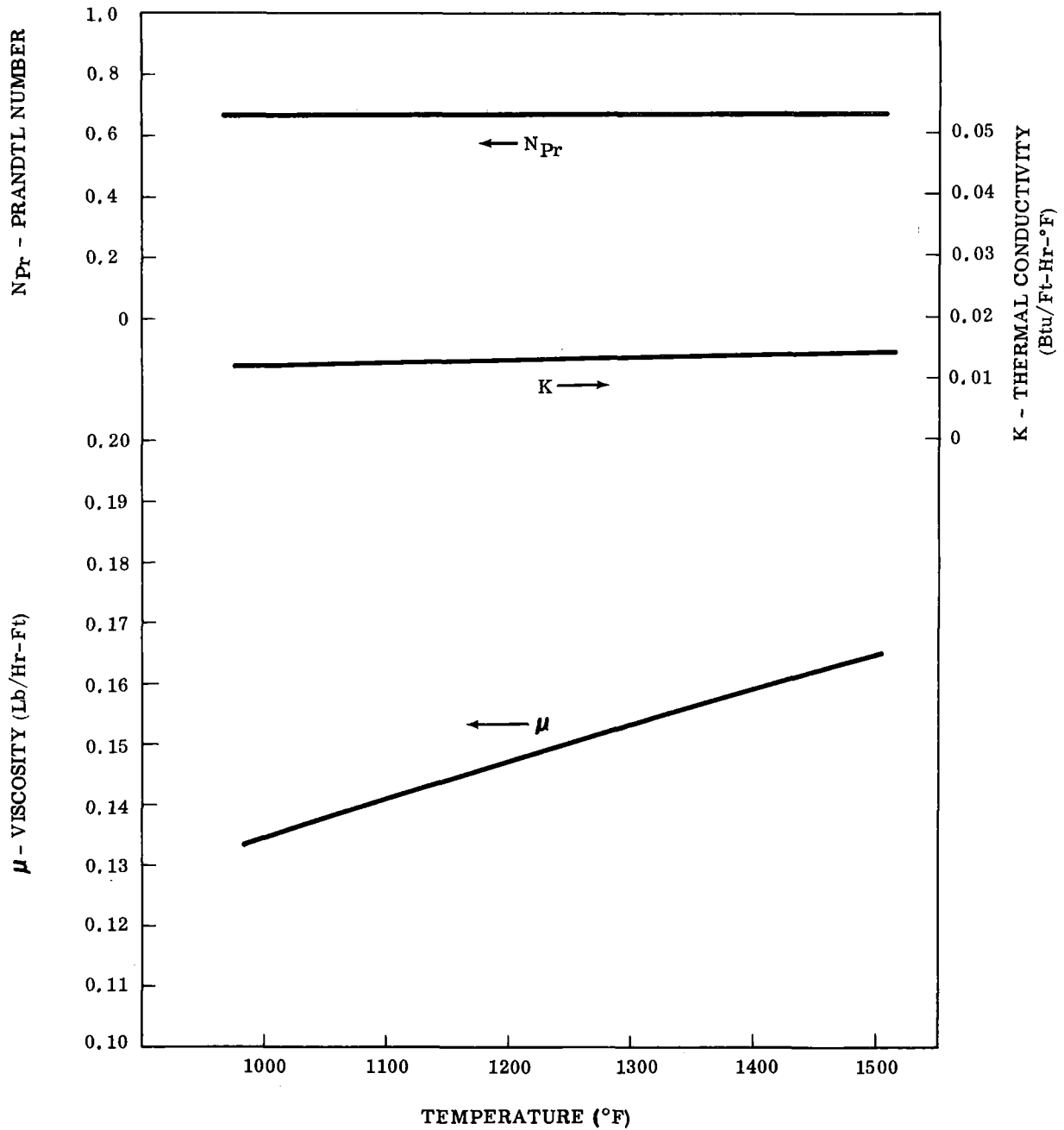


FIGURE 4. THERMAL AND TRANSPORT PROPERTIES OF KRYPTON

2. 2. 1 Core Energy Balance

The design gas temperatures specified in Table I do not include duct losses at entrance to and exit from the heat exchanger. These ducts are insulated with 2 inches of Johns-Manville Microquartz of 6.0 lb/ft³ density. The insulation is covered with a corrugated stainless steel foil outer wrap for protection.

TABLE I
THERMAL DESIGN REQUIREMENTS

	Case Number		
	I	II	III
Gas flow rate (lb/sec)	1.63	1.30	0.81
Temperature in (°R)	1560	1650	1660
Temperature out (°R)	1960	2060	2060
Pressure in (psia)	55.8	43.8	27.7
Pressure out (psia)	54.3	42.6	26.6

Another computer program (Insulation Design - High Temperature Ducting) was utilized to obtain the reduction in gas temperature in the inlet and outlet ducts due to the heat lost to ambient. The program computes radiation and natural convection losses to ambient considering a horizontal circular cylindrical configuration. The results are presented in the following tabulation:

Case	I	II	III
Temperature to inlet duct (°F)	1100	1190	1200
Temperature loss, inlet duct (°F)	9.88	14.34	23.4
Temperature to H/X (°F)	1090	1176	1177
Temperature to outlet duct (°F)	1500	1600	1600
Temperature loss, outlet duct (°F)	13.45	19.0	30.6
Temperature discharge from outlet duct (°F)	1513	1619	1631

As indicated from the preceding tabulation the 2-inch insulation thickness satisfied all flow conditions.

Core overall duty, including the duct losses, is shown in the following tabulation:

Case	Δt_g -F	w- lb /sec	Q- Btu /hr	η -KW
I	423	1.63	147,115	43.10
II	443	1.30	122,879	36.00
III	454	0.81	78,460	22.99

Theoretical Gas-Wall Temperature Distribution

Theoretical gas-wall temperature distribution, as a function of dimensionless flow length, is shown in Figure 5; the associated gas temperature differences and the theoretical log mean temperature differences are also included. These diagrams are consistent with a fixed wall temperature of 1700°F together with terminal gas temperatures which reflect ducting temperature drops.

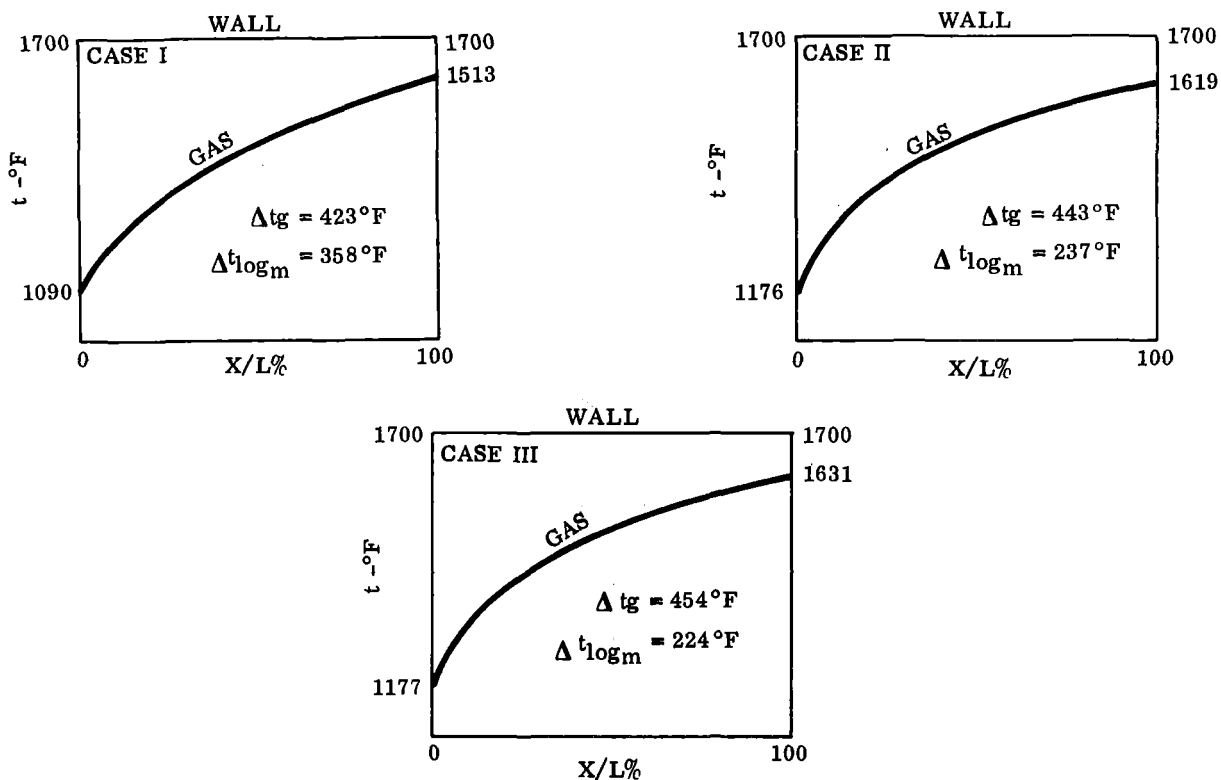


FIGURE 5. THEORETICAL GAS-WALL TEMPERATURE DISTRIBUTION

2.2.2 Fluid Flow

The next requirement was to determine which case produced the most critical flow-pressure loss condition. Assuming fully developed turbulent flow in circular smooth bore tubes, then:

$$f = \frac{\text{Const}}{(N_{\text{Re}})^{0.2}} \quad (1)$$

Assume that the kinetic theory of gas applies, then gas viscosity is proportional to the square root of the absolute temperature:

$$\mu \sim T^{1/2} \quad (2)$$

Then for a given gas and fixed surface geometry:

$$\frac{\Delta P}{P_1} \sim \frac{w^{1.8} (T_m)^{1.1}}{(P_1)^2} \quad (3)$$

Hence the most critical flow-pressure loss case occurs when:

$$\frac{w^{1.8} (T_m)^{1.1}}{(P_1)^2} \left/ \left(\frac{\Delta P}{P_1} \right) \right. = \text{Max} = \Omega \quad (4)$$

The results of these analyses are shown in the following tabulation. Nomenclature used in the preceding calculations are included in Table II.

Case	I	II	III
Ω	107.0	120.0	88.9

TABLE II
NOMENCLATURE

Symbols

A	Area
C_p	Specific heat, constant pressure
c	Bend loss correction factor
D	Diameter
F	Radiation view factor
f	Fanning friction factor
g_c	Constant; Newton's second law
h	Coefficient of heat transfer
K	Thermal conductivity
K_t	Pressure loss coefficient
L	Length
N_{Nu}	Nusselt number
N_{Pr}	Prandtl number
N_{Re}	Reynolds number
n	Number of tubes
P	Pressure; area per unit length; pitch distance
Φ	Electrical power
Q	Heat flow rate
q	Dynamic head; heat flux, area basis
q(x)	Heat flux, length basis
R	Thermal resistance
r	Bend radius

TABLE II (Cont)

NOMENCLATURE

Symbols

T	Temperature - °R
t	Temperature - °F
v	Specific volume
W	Mass flow rate - lb/hr
w	Mass flow rate - lb/sec
X	Distance from entrance
X/L	Dimensionless flow length
α	Absorptivity
β	Defined by equation 10
ϵ	Emissivity
θ	Temperature difference; circumferential length
λ	Wave length
μ	Dynamic viscosity
Ω	Defined by equation 4

Subscripts

CD	Conduction
CV	Convection
D	Elemental area
g	Gas
i	Inner
m	Mean
o	Outer; entrance
P	Plane
S	Static
T	Tube

TABLE II (Cont)
NOMENCLATURE

Subscripts

W	Wall
x	Flow length 'x'
Δ	Difference
λ	Wave length
Σ	Sum
ϕ	Function of
1	Inlet; source; element No.
2	Outlet
90	90 degree bend
II	Case II
∞	Infinity

Evaluation Temperature

Fluid property evaluation temperature for this particular configuration was selected as the wall temperature minus the log mean temperature difference.

Parametric Study

A detailed study of component pressure losses was made over the range of duct and U-tube diameters and lengths (Fig. 6). Specification values of flow rate, pressure, and temperature as well as allowable pressure drop were then incorporated into Figure 7.

2.2.3 Forced Convection Heat Transfer

Flux Distribution

A steady-state temperature limitation at 2160°R was imposed (in the contract) on the heat exchanger wall which was not much higher than the desired gas temperature. To maximize the heat transfer and minimize the size of the heat exchanger within this limitation, an exponential axial heat flux distribution was used for the tubes. A constant heat flux to the heat exchanger wall would have resulted in a unit nearly three times greater in size.

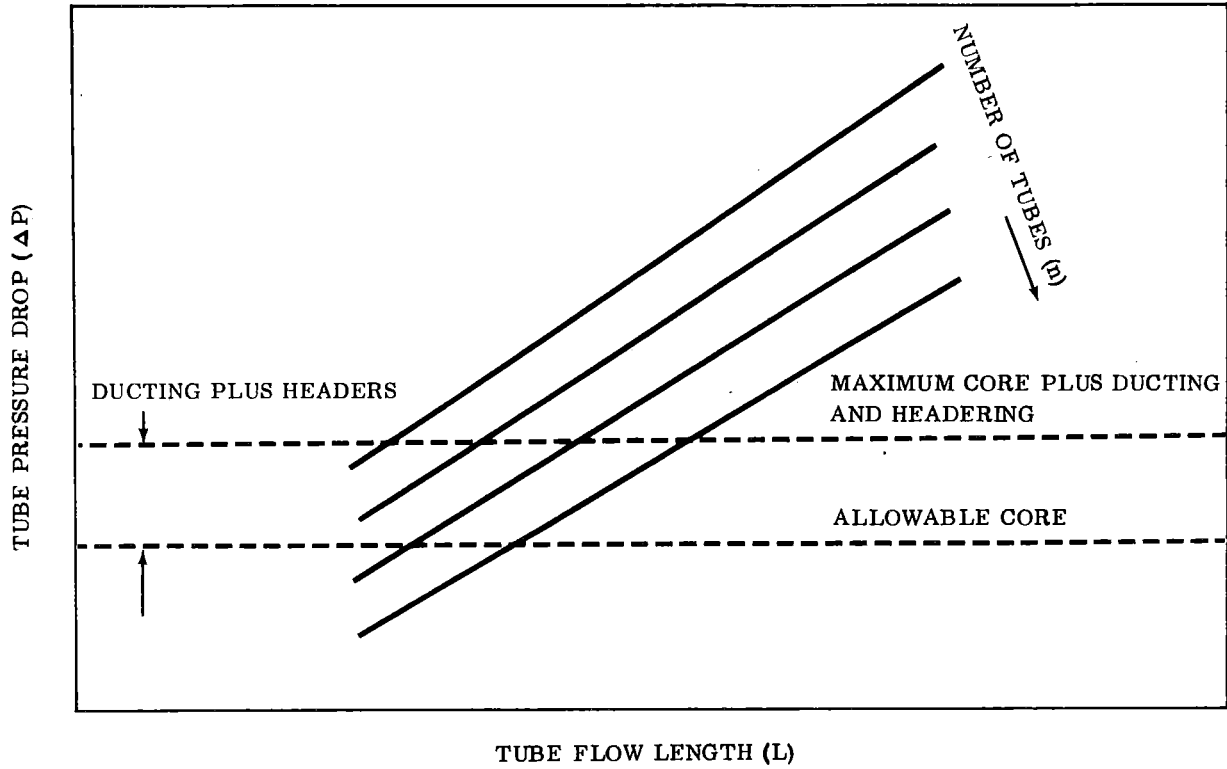


FIGURE 6. PARAMETRIC STUDY OF PRESSURE LOSS

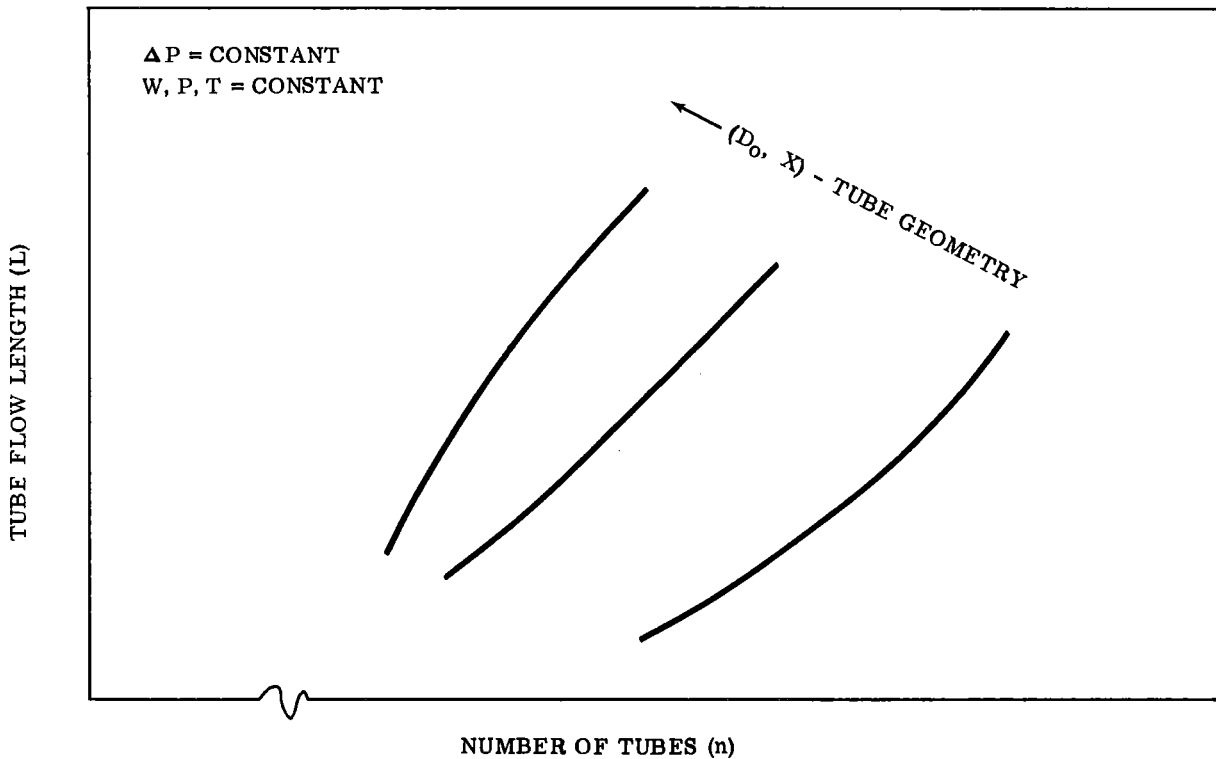


FIGURE 7. PARAMETRIC STUDY OF PRESSURE LOSS; Specification Values Incorporated

Correlation

A review of the literature showed no recommended correlating equation for internal forced convection for the mixture Prandtl number of interest (0.27 , Fig. 3). This Prandtl number is substantially less than that for normal gas range ($0.7 \leq N_{Pr} \leq 1$) and is substantially greater than for a low Prandtl number fluid ($N_{Pr} \leq 0.1$). Therefore, the bounding correlations were extrapolated into the Prandtl number range of interest and the most conservative selected.

The recommended (Ref. 1) bounding correlations for a fully developed turbulent flow in circular tubes for the constant wall temperature case are:

for $N_{Pr} < 0.1$

$$N_{Nu} = 4.8 + 0.003 (N_{Re} \cdot N_{Pr}) \quad (5)$$

and for $0.5 < N_{Pr} < 1.0$

$$N_{Nu} = 0.021 N_{Re}^{0.8} N_{Pr}^{0.6} \quad (6)$$

Equation 6 raises another point in that the 0.6 power exponent on Prandtl number is somewhat higher than normally given in the traditional gas range correlations, viz:

$$N_{Nu} = 0.023 N_{Re}^{0.8} N_{Pr}^{1/3} \quad (7)$$

Equation 7 is quoted as being valid for $0.5 \leq N_{Pr} \leq 100$, when suitably modified for temperature variation in the radial direction (Ref. 2).

The three correlating equations are plotted as a function of N_{Pr} in Figure 8 for two levels of Reynolds number, 10^4 and 10^5 . (Reynolds number for the final design geometry varies from about 1.0 to 2.2×10^4 for all flow conditions and fluids.) Examination of Figure 8 reveals that the Kays correlation clearly matches the "low N_{Pr} " correlation better than does the "traditional" correlation, everywhere in the range $0.1 \leq N_{Pr} \leq 0.5$. On this basis the Kays correlation was chosen.

NOTE: FULLY DEVELOPED TURBULENT
FLOW IN CIRCULAR TUBE

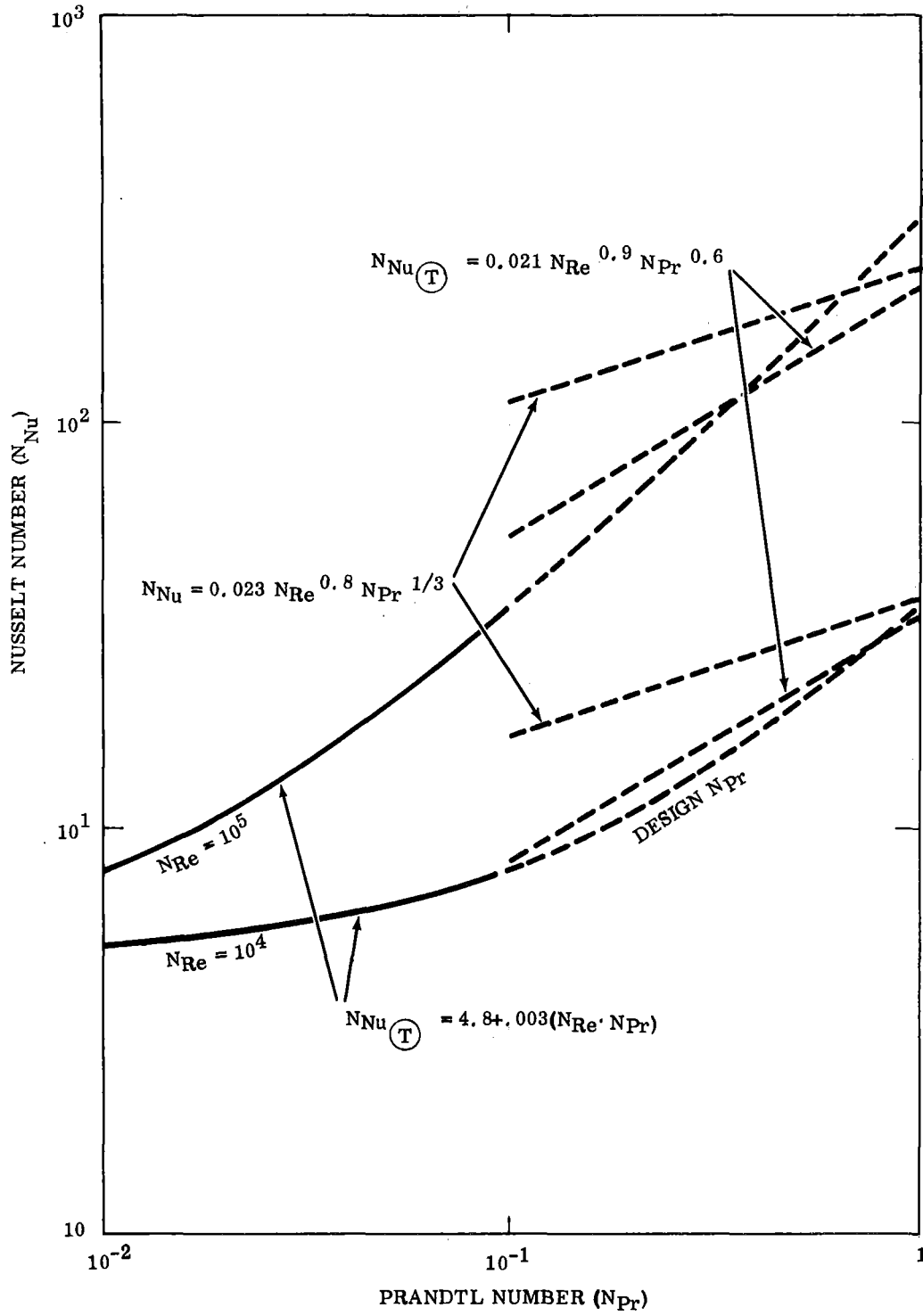


FIGURE 8. COMPARISON OF FORCED CONVECTION CORRELATIONS

In addition to the major considerations discussed, the effects of entry conditions, tube bends and roughness, and the influence of radial temperature distribution on thermal properties were examined. The internal forced convection heat transfer correlation equation used in this analysis was:

$$N_{Nu} = \left[0.021 N_{Re}^{0.8} N_{Pr}^{0.6} \right] \left[1 + \frac{1.4}{L/D} \right] \left[\frac{T_m}{T_w} \right]^{0.5} \quad (8)$$

Most Critical Case

The most critical case from the viewpoint of heat transfer was defined as that particular combination of flow conditions and demand (duty) which dictates the largest heat exchanger. In addition to these variables, it was necessary to consider the effect of changing from the gas mixture to krypton for Case I. Establishment of a figure of merit for this particular set of conditions was accomplished by writing the basic energy balance and solving for the relative surface area requirements which is tabulated below:

Case	w - lb/sec	$\Delta t_g - ^\circ F$	$\Delta t_{\log_m} - ^\circ F$	h/h_{II}	A/A_{II}
I Kr	1.63	423	358	0.825	0.959
I Mix	1.63	423	358	1.175	0.673
II	1.30	443	237	1.000	1.000
III	0.81	454	224	0.685	0.975

As indicated, Case II is the most critical for design purposes.

Parametric Study

As with the pressure drop analysis, a detailed parametric heat transfer study was made; Figure 9 typifies the trend of heat transfer coefficient versus number of tubes. From Figure 9, the required and available surface area versus length of tube flow was plotted for a finite number of tubes (Fig. 10); the combined heat transfer - pressure loss plot is shown in Figure 11.

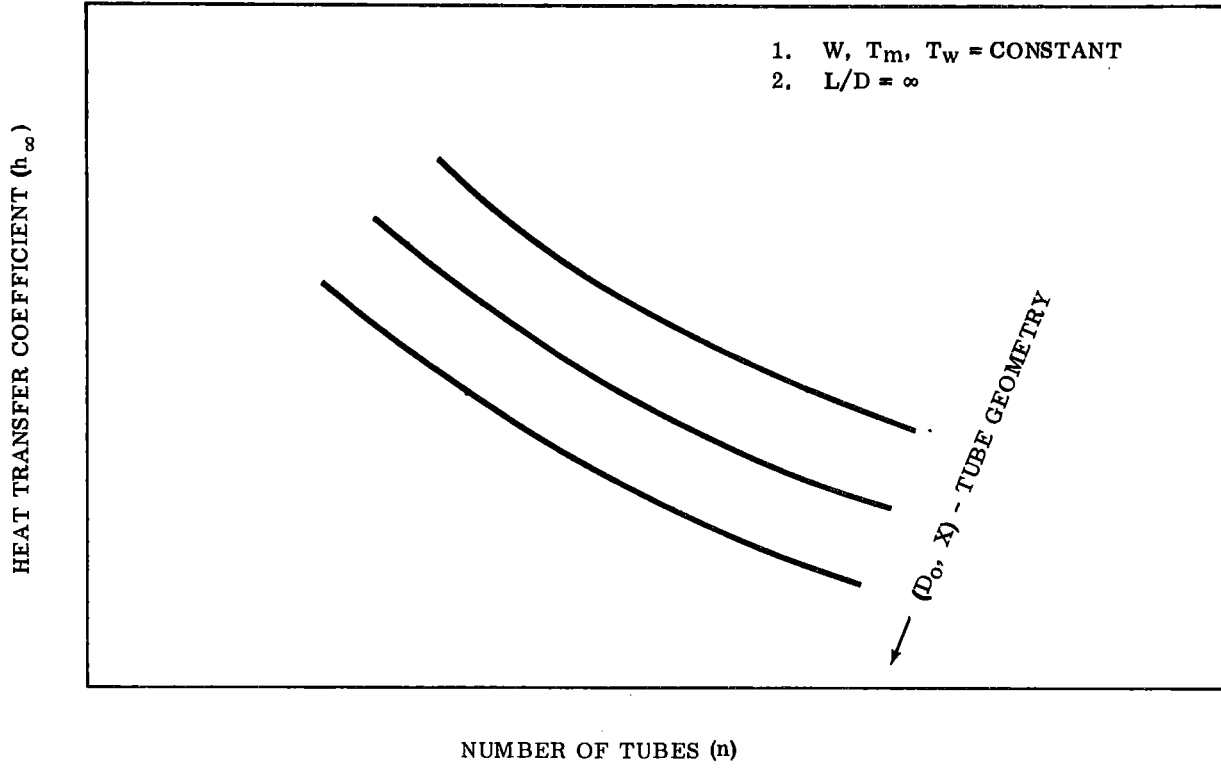


FIGURE 9. PARAMETRIC STUDY OF HEAT TRANSFER COEFFICIENT

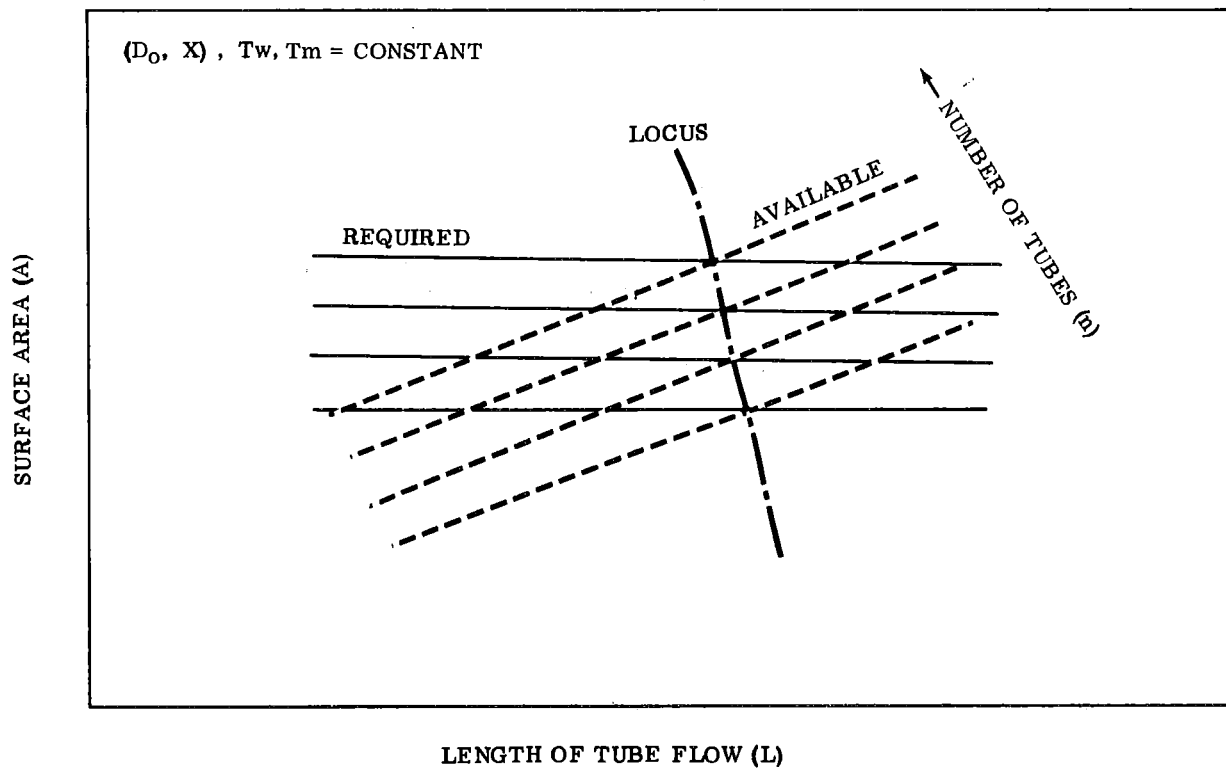


FIGURE 10. PARAMETRIC STUDY OF HEAT TRANSFER AREA

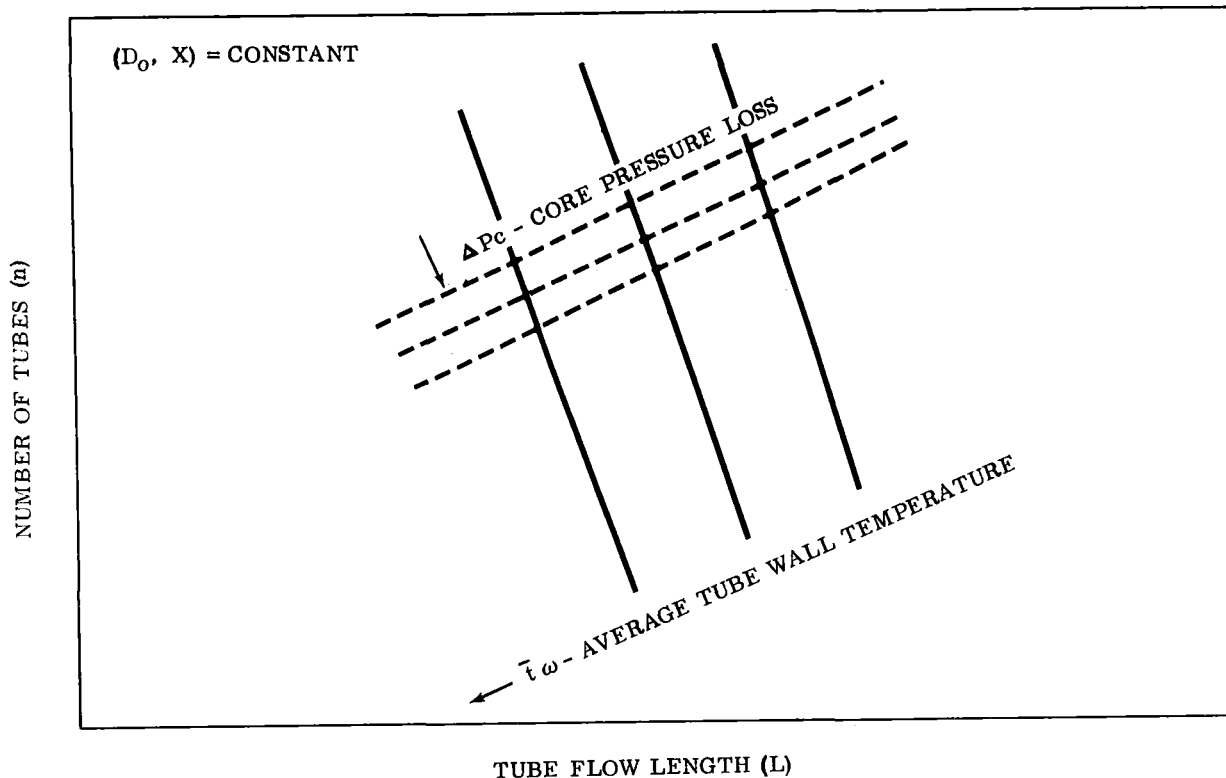


FIGURE 11. COMBINED HEAT TRANSFER-PRESSURE LOSS SOLUTION

2.2.4 Core Geometry

The heat exchanger was optimized for Case II for the number and length of tubes and the flux distribution selected. However, when the requirements of the other cases were imposed on the Case II heat exchanger with its flux distribution, it was found that this configuration was not adequate due to the different heat demand rates. Therefore, a composite curve was made that took into account the different demand rates. After a configuration was obtained, the tube area was increased by 10 percent to compensate for the tube circumferential temperature gradient. This gradient was due to the fact that only one side of the tube would be seeing direct radiation from the lamps. The final core geometry consists of 40 U-tubes, 3/4 OD by 0.042 inch wall, and a flow length of 8.5 feet. The calculated pressure drop for Case II is 0.075 psi less than the 1.200 psi contractual allowance, or a margin of 6 percent.

2.2.5 Radiation Heat Transfer

The heater configuration and a number of simplifying assumptions directly affected the radiation heat transfer analysis. Those of major significance are discussed in the subsequent paragraphs.

Refractory Wall

The heat exchanger is radiantly heated from two sides. Since the tubes are "U" shaped, they are directly heated on one side. Also, the relative heat flux on the inlet side of the U-tube bundle is greater than on the outlet side to attain the exponential flux distribution along the tube axis. In order not to overheat the outlet side from inlet side radiation and to minimize flux maldistribution around the tube circumference, the two sides were separated by a sheet of material in the plane of symmetry of the U-tube bank. From a radiation viewpoint, this reduced the system to two tube banks with a common wall. For simplification of analysis it was assumed that this common wall was a "refractory wall". This then allowed use of the radiation design method and data developed for use in the design of tube banks in fired furnaces for each side separately. (A discussion of the wall as an adiabatic shield is included in Appendices A and B).

Tube Coating

A detailed discussion of the coating is included in Section 7. Initially it was assumed that the heat exchanger tubes would be coated for consistent high absorptivity in air and vacuum, and the analysis was performed with this assumption. Subsequent long term testing in vacuum revealed an adherence problem on Inconel 600. In addition, during the course of the lamp tests, significant contamination of the lamp's cooled reflector surfaces occurred which was attributed to the coated Inconel 600 targets. With these two problems, the coating was deleted from the tubes. An analysis of the effect of tube surface absorptivity was conducted by NASA and the results are included as Appendix B.

Heater Modules

A series of lamp modules are located in planes on either side of the U-tube heat exchanger and only directly radiant-heat one side of the tube. An initial module considered, which was commercially available, consisted of 16 lamps in two rows of eight each. The lamps were a quartz tube with a tungsten filament of 750-watt rated capacity. The lamps were located on 1.5-inch centers. Testing in vacuum showed that this particular lamp and reflector resulted in very early failure due to overheating. The reflector was redesigned and in conjunction with an improved life lamp a redesigned module resulted. This new module contained a single row of 24 lamps on 2.5-inch centers which run the entire width of the bank of U-tubes. Early thermal analysis used the 16-lamp module as its basis; however, the analysis procedure is independent of module configuration.

Enclosure

In all areas of the enclosure not covered by heater modules, 2 inches of Johns-Manville Microquartz insulation with a density of 6 lb/ft³ was used. The insulation was clad with 0.010 inch Inconel 600 foil internally and type 321 stainless steel externally.

Source Radiation Flux Distribution

The problem was one of arranging a relatively small number of heater modules in an orientation that would produce an acceptably close approximation to an axial exponential flux distribution and a relatively uniform longitudinal distribution.

First an equivalent gray plane was substituted for the combined tube bank and backing refractory wall. The gray plane was located in the plane of the tube row. Second, it was assumed that the heater modules behaved as strip (finite rectangular plane) sources rather than as individual arrays of point sources. The relatively close spacing of the lamps and the composition and wide angle construction of the reflectors made this assumption reasonable.

Radiation view factors were computed as a function of source geometry. A computer program (RAFLX) was prepared to perform these calculations. Input to the RAFLX consisted of the number of heater modules and their size and location in the source plane together with sink plane size and its distance from source plane. Output consisted of a matrix of elemental area to plane source area view factors, as shown in the gray plane. In addition, a contour map is obtained which illustrates the relative flux distribution from the gray plane. Flux intercepted by a particular point on the sink plane was now computed.

RAFLX does not consider the effects of the enclosure or of tube surface absorptivity.

- The commonly used factor F for a black enclosure accounts for all energy arriving at a sink surface, including that which has traveled via "no flux" surfaces due to reradiation or reflections. This factor always exceeds in value the view factor which considers only the direct energy transfer rate from source to sink surfaces. Thus, the direct view factors generated by the subject program result in calculated energy transfer rates in the enclosure, which are lower than those which will actually be encountered.
- When the absorptivity is high, energy absorption rates can be reasonably predicted by multiplying the impinging flux rate by an appropriate absorptivity. In the case of a tube bank, the term absorptivity should be replaced by the "equivalent gray plane emissivity".

Module Flux Distribution Test

To check the ability of the RAFLX program to predict heater module flux distribution, the relative flux distribution of a 16-lamp heater module was measured using a light meter. The test objective was to measure the relative flux level at various locations before the module, thus the units of measurement were of no particular concern.

Four relative flux level measurement surveys were taken, with three located in a plane 18 inches in front and parallel to the module face. The details of geometric location of test measurements, in addition to a tabulation of test data are shown in Figure 12. The survey was redefined as the relative flux distribution impinging upon a quarter section of 70 x 70-inch plane centered at 18-inch distance and parallel to a 3 x 12-inch heater module. The test values and the analytical predictions of flux distribution given by the RAFLX program were normalized by expressing the relative flux in terms of a fraction of peak flux.

2.2.6 Heater Module Distribution

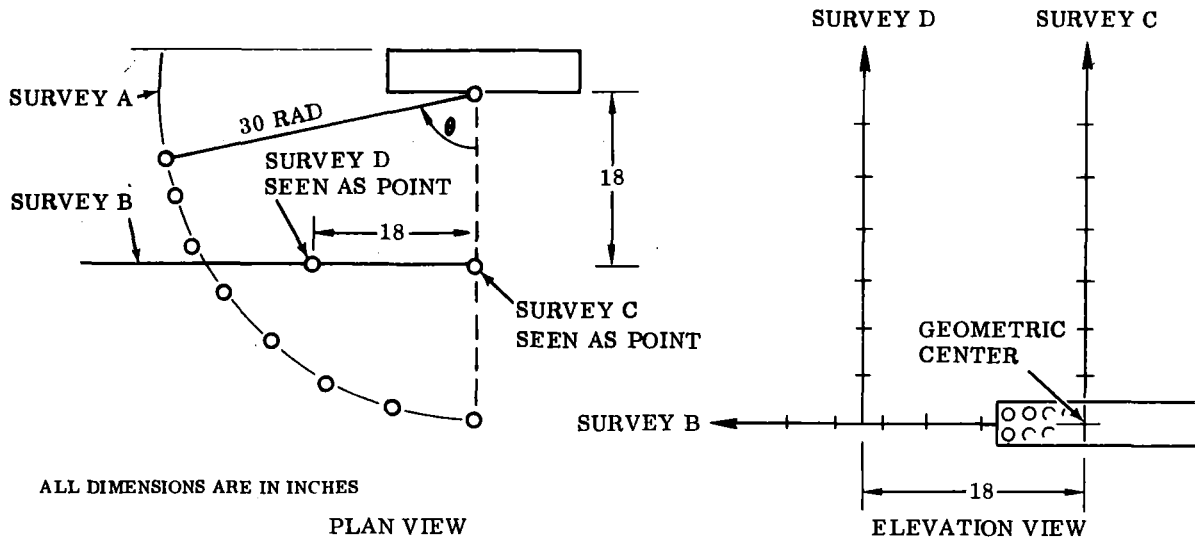
The external (radiation) axial flux distribution expression had been previously developed:

$$q(X) = \frac{Q}{A_1} F_{D1} \frac{A_D}{\Delta X} \epsilon_p \frac{-\text{Btu}}{\text{hr-ft}} \quad (9)$$

where:

$$\begin{aligned} \frac{Q}{A_1} &= \text{total emitted heat flux of modules divided by the total area of modules} \\ F_{D1} &= \text{point to plane strip source view factor} \\ A_D/\Delta X &= \text{elemental area per unit length in tube direction} \\ \epsilon_p &= \text{effective gray plane emissivity} \end{aligned}$$

Utilizing this external flux distribution expression, it was possible to predict the axial flux distribution as absorbed by the tube bank for any given arrangement of heater modules. If the results are plotted as a function of flow length, integration under the resulting curve yields the total heat energy flow rate, which must be equal



Notes

1. Single-phase power supply from SCR
2. LH of module 73 volts; RH 78 volts
3. Current: RH and LH 35 amps

TEST DATA							
A		B		C		D	
θ Degrees	Illumination	Distance From Datum (in.)	Illumination	Distance From Datum (in.)	Illumination	Distance From Datum (in.)	Illumination
0	100	0	250	0	260	0	56
10	100	5	200	5	180	5	50
20	64	10	100	10	92	10	46
30	48	15	62	15	64	15	32
40	40	20	44	20	44	20	24
50	34	25	30	25	28	25	16
60	27	30	20	30	16	30	12
70	16	35	12				

FIGURE 12. RESULTS OF THE RADIANT FLUX DISTRIBUTION SURVEY

to or exceed the required duty for any given case. Further, by superimposing this external flux distribution curve upon the internal flux distribution curve:

$$\frac{q(x)}{q(o)} = e^{-\beta X} = \frac{\theta(x)}{\theta(o)} \quad (10)$$

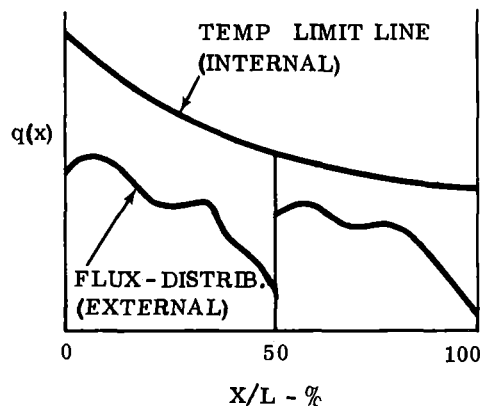
An effective surface temperature limit line is generated.

For this procedure to produce a valid 1700°F temperature limit line, accurately account for the excess surface area, and ensure an outlet gas temperature not in excess of the design value, a fictitious value of β was used. If the correct value of β were used, together with an initial temperature difference consistent with 1700°F wall temperature, the outlet fluid temperature would be in excess of design value due to excess surface area.

The fictitious β was computed by first establishing the heat flow rate which would be achieved by utilizing the actual surface area uniformly with design gas boundary temperatures and the developed mean film coefficient. The related unit flux at entrance was then computed; finally β was obtained from equation 11. Substitution of this value of β and the related $q(o)$ to equation 10 provides a flux distribution which implicitly represents a 1700°F temperature limit line.

$$Q_{o \rightarrow x} = \int_0^x q(X) dx = \frac{q(o)}{\beta} \left[1 - e^{-\beta X} \right] - \text{BTU/HR} \quad (11)$$

Due to the fact that the integrated area under the temperature limit line will yield an energy flow rate greatly in excess of the required duty, it is not essential that the external axial flux distribution be uniform nor need it "fill in" more than a fraction of the area under the internal flux distribution (temperature limit line). A typical curve illustrating the flux distribution and the temperature limit line is shown in the following sketch:



These curves now produce the means of establishing a suitable heater module distribution which satisfies the prime design requirements of achieving or exceeding the duty, while ensuring that the surface does not exceed 1700°F at any point. The design procedure is as follows:

- Establish the locations of a selected number of heater modules in the source wall (inlet and outlet sides); specify source wall-sink plane distance; compute the flux distribution impinging upon the sink planes by the RAFLX program.
- Compute the absorbed axial flux distribution resulting from this particular heater module arrangement and plot as a function of flow length.
- Over-plot the temperature limit line (external flux distribution).
- If the flux distribution exceeds the flux value of the temperature limit line at any point, it indicates that the surface temperature was close to 1700°F at that point and a new module arrangement is calculated.
- If the flux distribution does not exceed the temperature limit line, a graphical integration under the external flux distribution curve is performed to determine if the duty has been achieved.
- Repeat until both requirements have been satisfied for all flow conditions.

After considering many arrangements of modules on the inlet and outlet source planes, a final solution with 12 modules was obtained. The geometric arrangement of modules for this distribution is discussed in Section 2.3. Conversion of source plane location to the tube flow length location is shown in Figure 13 for final core geometry.

A summary of all pertinent final design geometry and predicted performance values includes:

GEOMETRY

<p>Tubes, type 3/4-0.042 inch⁽¹⁾ flow length 8.5 feet quantity 40</p> <p>Header, inlet OD 5.0 inches⁽¹⁾, 0.250 inch wall length 64 inches</p> <p>Header, outlet OD 5.0 inches⁽¹⁾, 0.250 inch wall length 63 inches</p> <p>Duct, inlet OD 5.0 inches⁽¹⁾, 0.187 inch wall length 61.5 inches 3 90° elbows and 1 transition</p>	<p>Duct, inlet 4.5 inches⁽²⁾, 0.083 inch wall length 126 inches 3 90° elbows and 1 transition</p> <p>Duct, outlet OD 5.0 inches⁽¹⁾, 0.187 inch wall length 82.0 inches 2 elbows (75° and 90°) and 1 transition</p> <p>Distance of lamp modular plane to tube plane: inlet 9.6 inches outlet 14.0 inches</p> <p>Number of lamp modules: inlet 8 outlet 4</p>
<p>1. Material: Inco 600 2. Material: Type 316</p>	

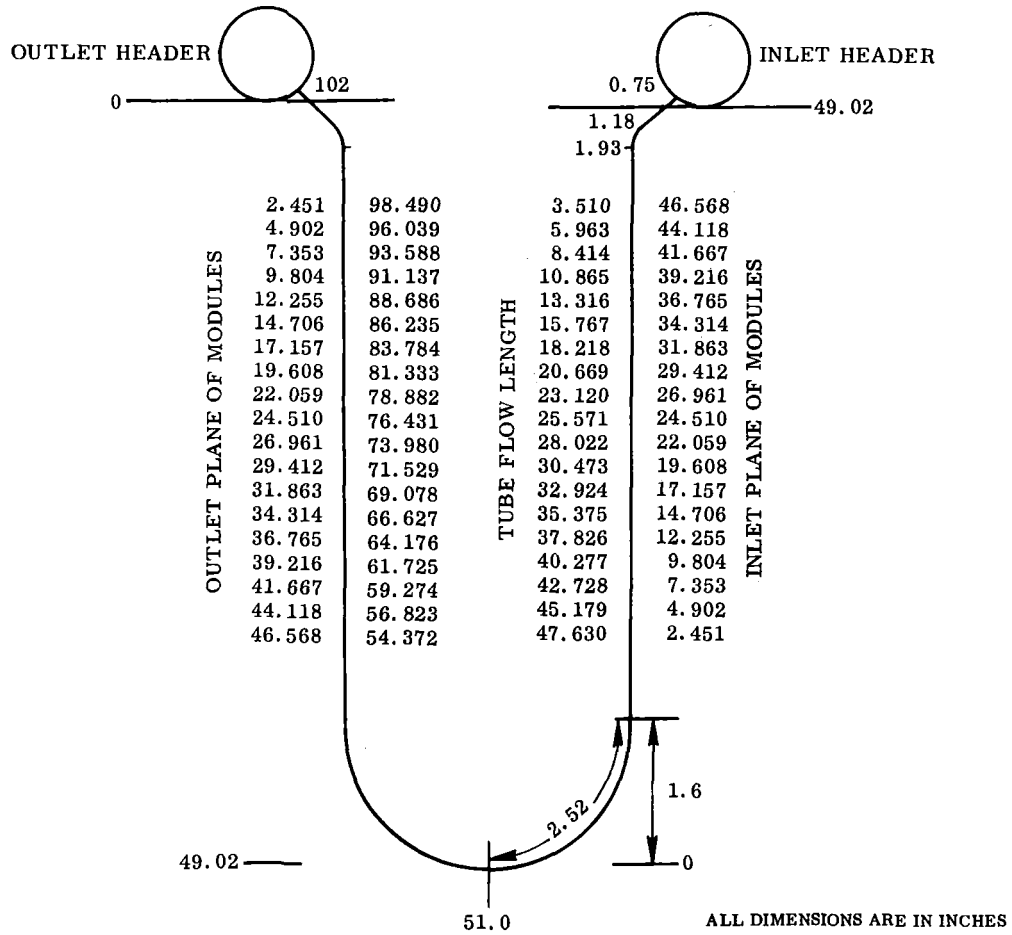


FIGURE 13. CONVERSION OF LOCATION ON MODULE PLANE TO LOCATION ALONG TUBE FLOW LENGTH

PRESSURE LOSS

Case	I	II	III
Core Entrance	0.110	0.094	0.057
Inlet expansion	0.013	0.011	0.007
Inlet bend	0.009	0.009	0.009
Friction	0.681	0.621	0.421
U-bend	0.024	0.028	0.027
Outlet bend	0.013	0.014	0.014
Outlet expansion	0.017	0.015	0.009
Exit	0.143	0.122	0.076
$\Sigma\Delta P$ Core	1.010	0.914	0.620
Duct in	0.083	0.080	0.063
Duct out	0.089	0.086	0.070
Header in	0.024	0.021	0.014
Header out	0.028	0.024	0.017
$\Sigma\Delta P$ Ducts and headers	0.224	0.211	0.164
$\Sigma\Delta P$ Heat exchanger	1.234	1.125	0.784
Allowable ΔP	1.50	1.20	1.10

HEAT TRANSFER COEFFICIENTS (Btu/hr-ft²-° F)

Case	Krypton		Mixture		
	I	II	I	II	III
h_m	11.40	9.49	16.21	13.80	9.45

HEAT BALANCE

Case	Krypton	Mixture			
	I	I	II ⁽¹⁾	III	
Output	Btu/hr	147,115	147,115	122,879	78,460
	KW	43.1	43.1	36.0	23.0
Losses, radiation to modules ⁽²⁾	Btu/hr	38,600	38,600	38,600	38,600
	Conduction through walls				
	Btu/hr	53,200	53,200	53,200	53,200
Input	Btu/hr	238,915	238,915	214,679	170,260
	KW	70.0	70.0	62.9	50.0

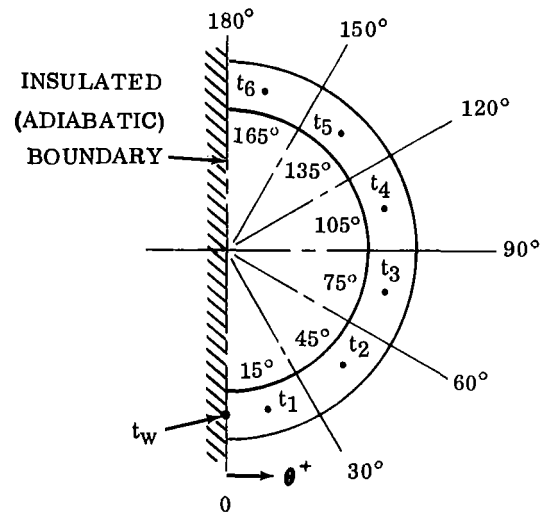
1. It is estimated that Case II operating on krypton will produce a gas outlet temperature of 1511°F, consistent with a heat flow rate to the gas of 93,000 Btu/hr.

2. Radiation losses to modules calculated on the basis of tube wall and module face temperatures of 1700 and 288°F respectively.

2.2.7 Circumferential Temperature Distribution Analysis

The flux distribution around the tube circumference is not uniform; therefore, a temperature gradient will be induced. The peak temperature may be expected to occur at the tube leading edge, adjacent to the heat sources. Results of the tube wall axial temperature distributions implicitly assume these temperatures to be integrated mean values around the circumference. It was, therefore, essential to determine the relative significance of the tube circumferential temperature distribution.

This analytical model evaluated the circumferential temperature gradient, utilizing a finite element, steady-state energy balance approach:



Assumptions upon which the analysis was based were:

- Heat flow in the axial (flow) direction is negligible compared to the circumferential direction.
- Radial temperature difference across the tube wall is negligible.
- The solution is symmetrical about the 0 to 180-degree axis.
- Internally, the local value of mean heat transfer coefficient applies and is uniform about the circumference.

The analysis was arbitrarily confined to include one tube diameter in the flow direction for any particular axial flow length station selected for analysis.

A steady-state energy balance was written for each element in the model at a selected flow length; e. g. , element t_1 :

$$\frac{(t_w - t_1)}{R_{CD_{o-1}}} + Q_1 = \frac{(t_1 - t_{gx})}{R_{CV_{1-gx}}} + \frac{(t_1 - t_2)}{R_{CD_{1-2}}}$$

- where:
- R_{CD} = circumferential conduction resistance
 - = $\frac{\theta}{KA}$
 - θ = circumferential distance between temperature modes
 - K = tube material thermal conductivity
 - A = tube wall cross-sectional area along circumference, one diameter in flow length
 - Q_1 = heat input to element 1 due to radiation
 - R_{CV} = convection resistance
 - = $\frac{1}{hA}$
 - h = local mean heat transfer coefficient
 - A = tube internal surface area swept by gas for a 30-degree circumferential segment

The results of the circumferential temperature distribution as a function of angular location and the parameter "dimensionless flow length", are shown in Figure 14. Apart from the entrance region (X/L to 30 percent or less), the maximum differential along the circumference is not significant due to substantial convective resistance increase in the flow direction. In the entrance region, the maximum circumferential differential has been greatly attenuated due to relatively low average tube wall temperature. For the resulting distribution, the leading edge (maximum wall) temperature was over-plotted on Figure 15. As indicated in Figure 15, the circumferential temperature distribution problem is not significant in the final 50 percent of flow length where concern is the greatest. Based on the analytically demonstrated behavior of the system for Case II flow conditions, analysis of other flow conditions did not appear necessary.

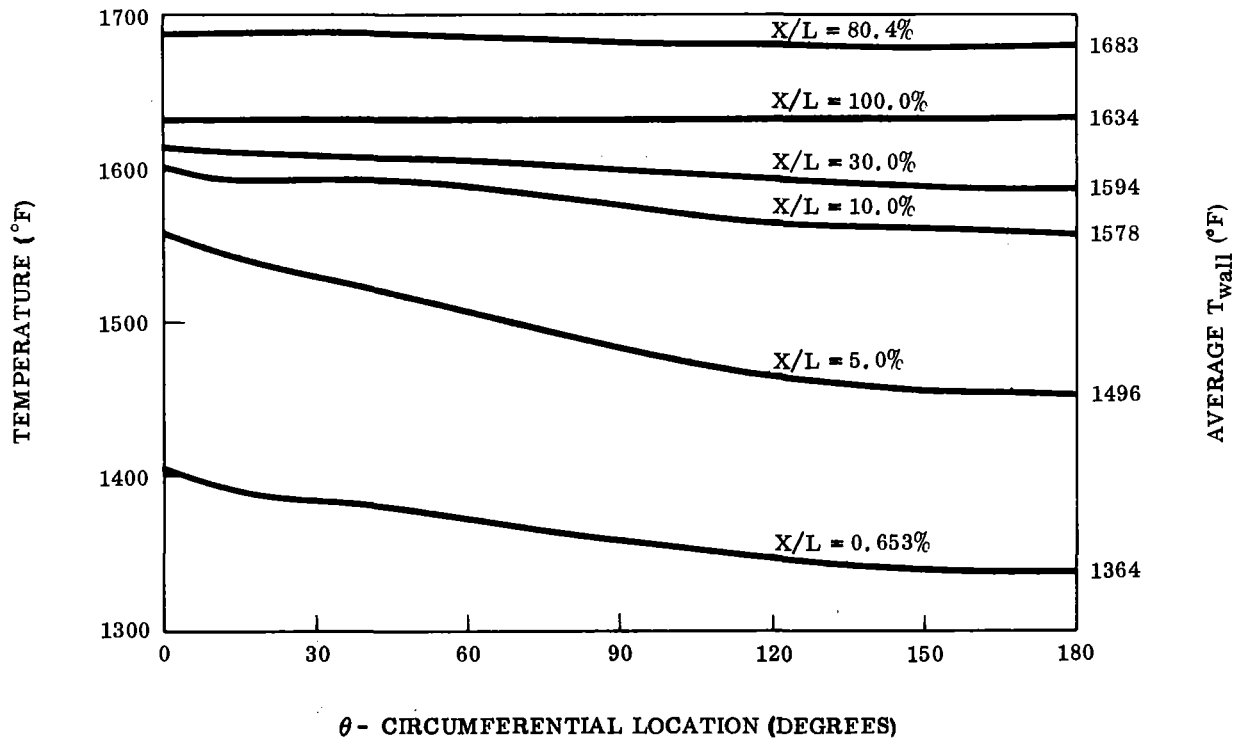


FIGURE 14. CIRCUMFERENTIAL TEMPERATURE DISTRIBUTION

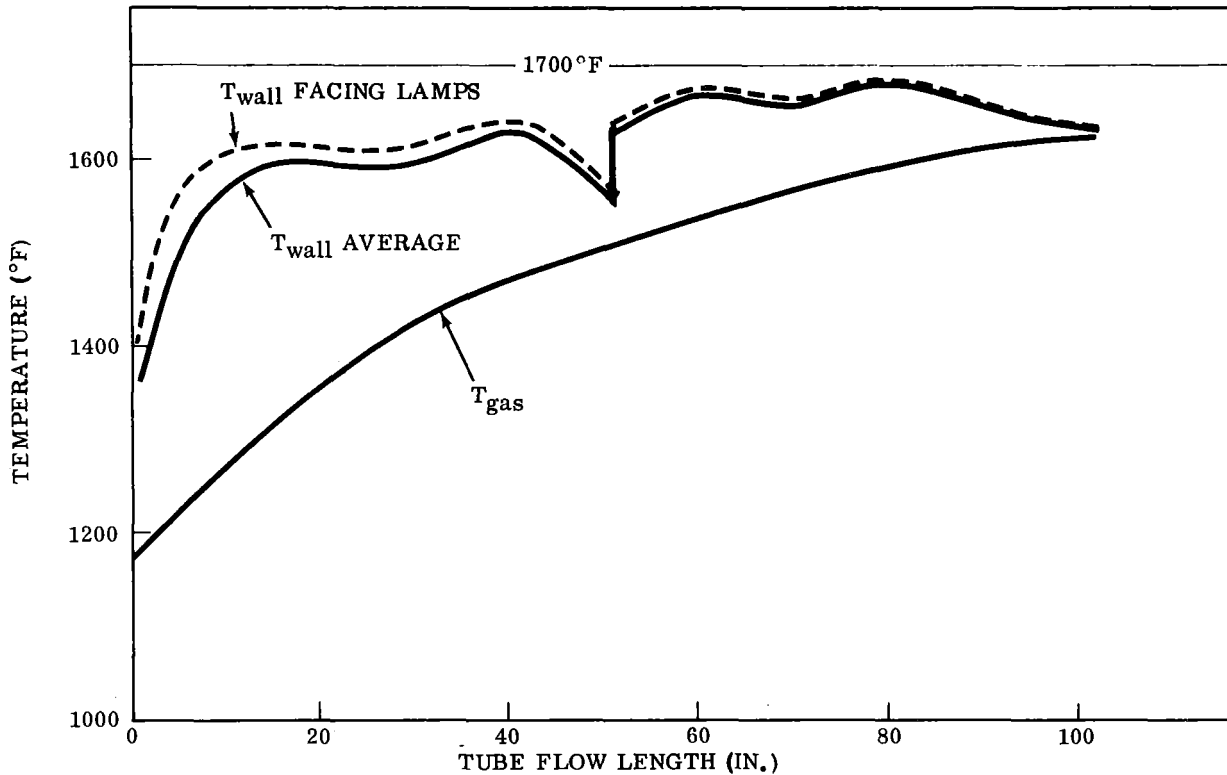


FIGURE 15. GAS AND WALL TEMPERATURE DISTRIBUTION AS A FUNCTION OF FLOW LENGTH

2.3 ARRANGEMENT OF LAMP MODULES USED

After testing several geometries, the final module arrangements arrived at are shown in Figures 16 and 17. The module-to-heat exchanger tube face distances are 9.6 and 14.0 inches for the inlet and outlet sides of the enclosure.

Plots of flux per tube versus tube length for Case II, Case I - Krypton, and Case III Mixture are shown in Figures 18, 19, and 20. Figure 18 also shows a value of Q total (external flux) of 132,000 Btu/hr compared to the required value of 122,879 Btu/hr.

Average wall and gas temperatures versus flow length are shown in Figures 21, 22, and 23. Figure 21 shows the plot for Case I - Krypton (which presents a more critical wall temperature problem than Case I - Mixture). Figures 22 and 23 show the results for Case II - Mixture and Case III - Mixture. Figure 22 is directly comparable with Figure 15 (for the 16-lamp module). In both cases, the average wall temperature reaches a value about 12°F below the design maximum of 1700°F . As indicated, the 24-lamp module provides 1.08 times as much external flux as is required.

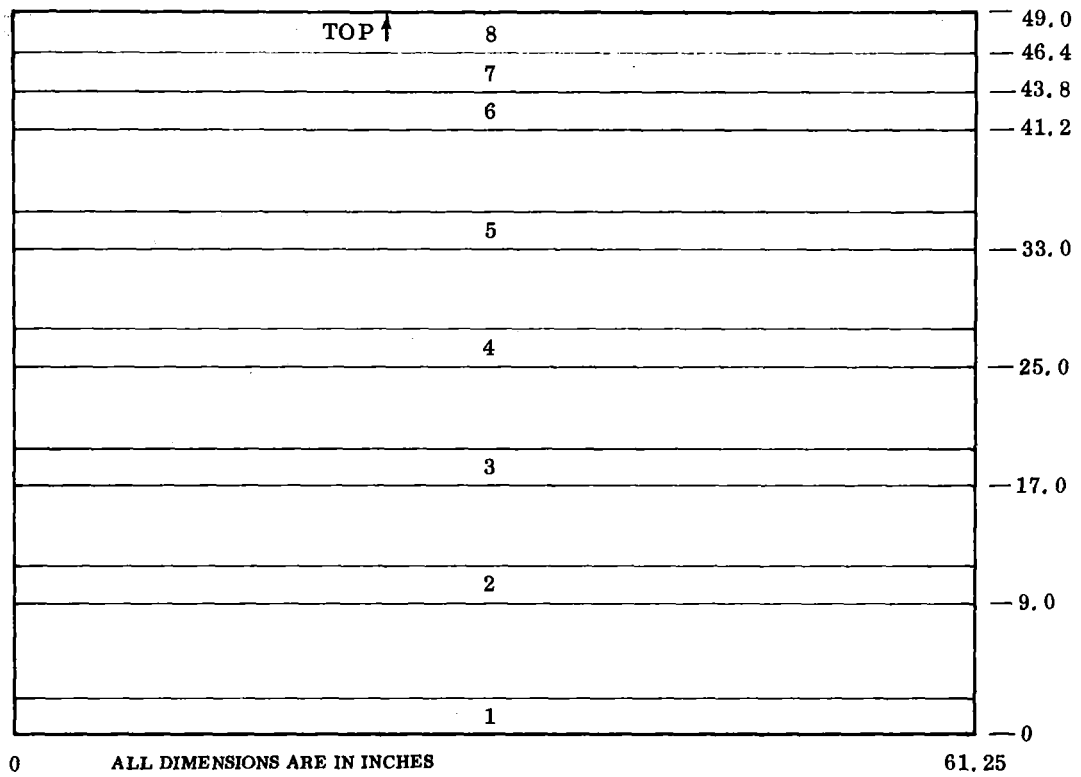


FIGURE 16. STRIP HEATER ARRANGEMENT, INLET PLANE

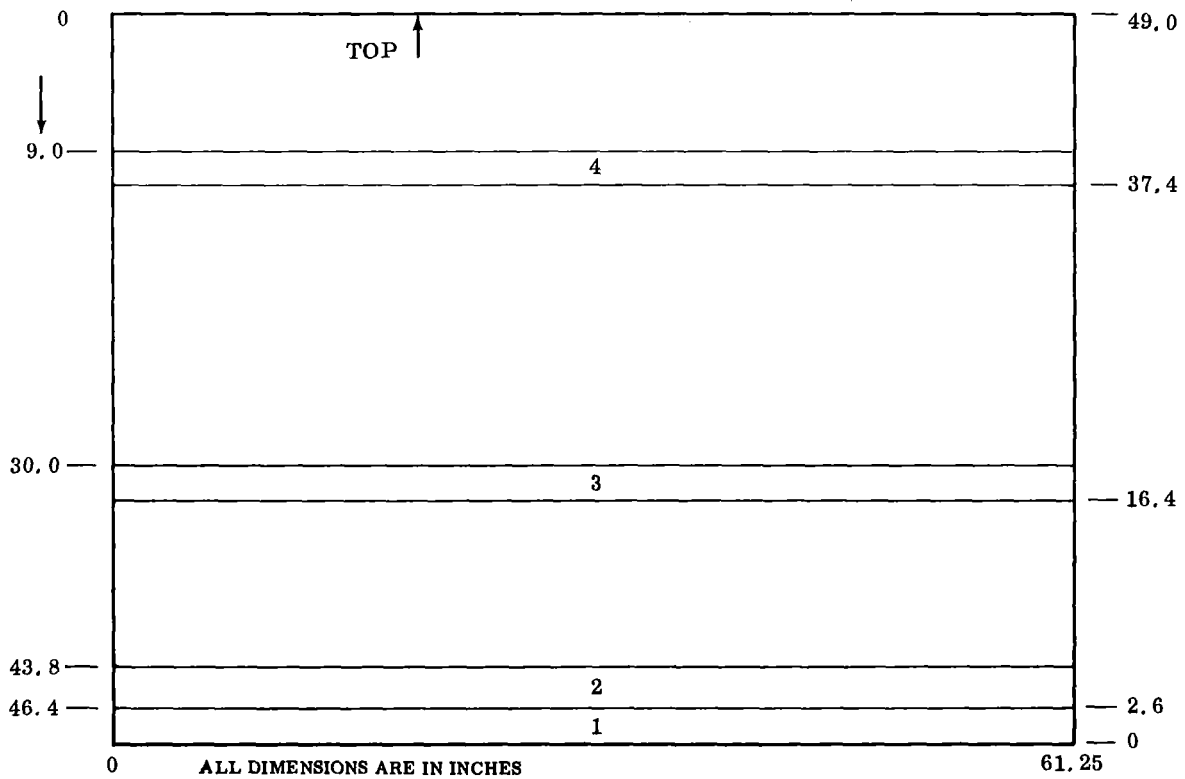


FIGURE 17. STRIP HEATER ARRANGEMENT, OUTLET PLANE

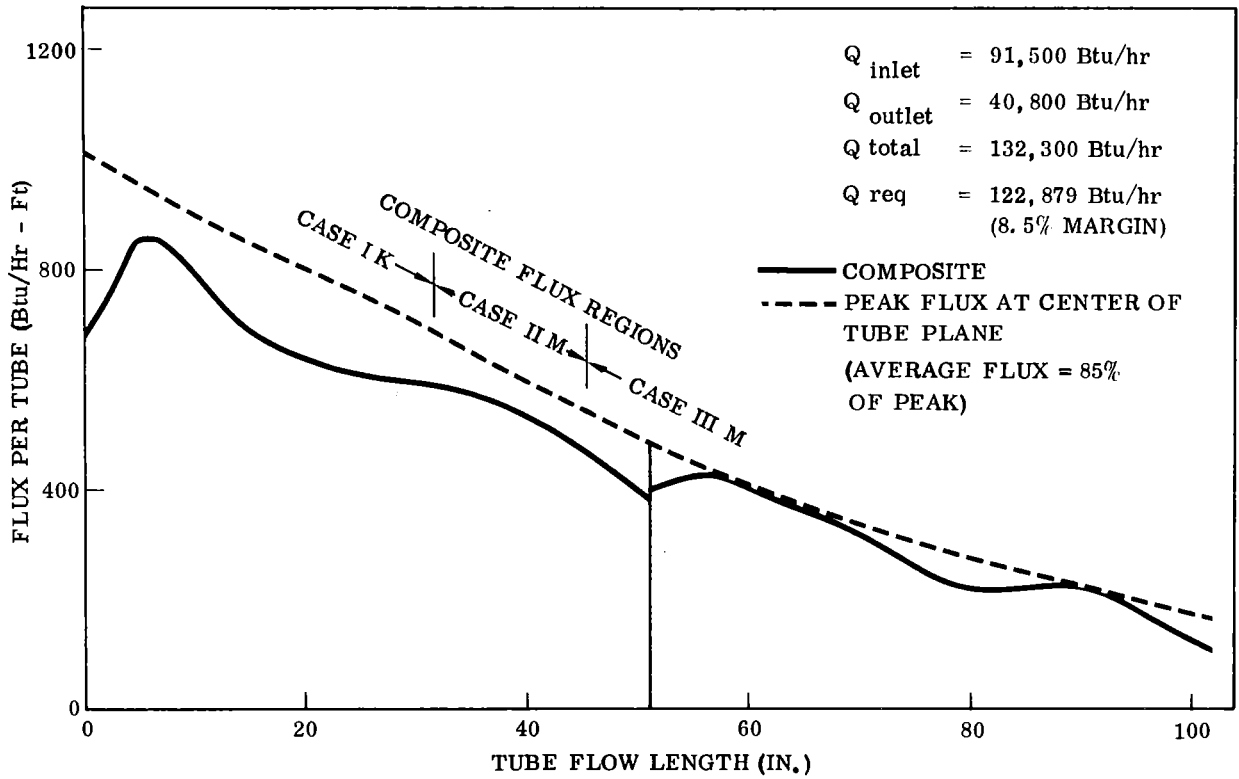


FIGURE 18. SOLUTION TO STRIP HEATER FLUX RELATED TO CASE II

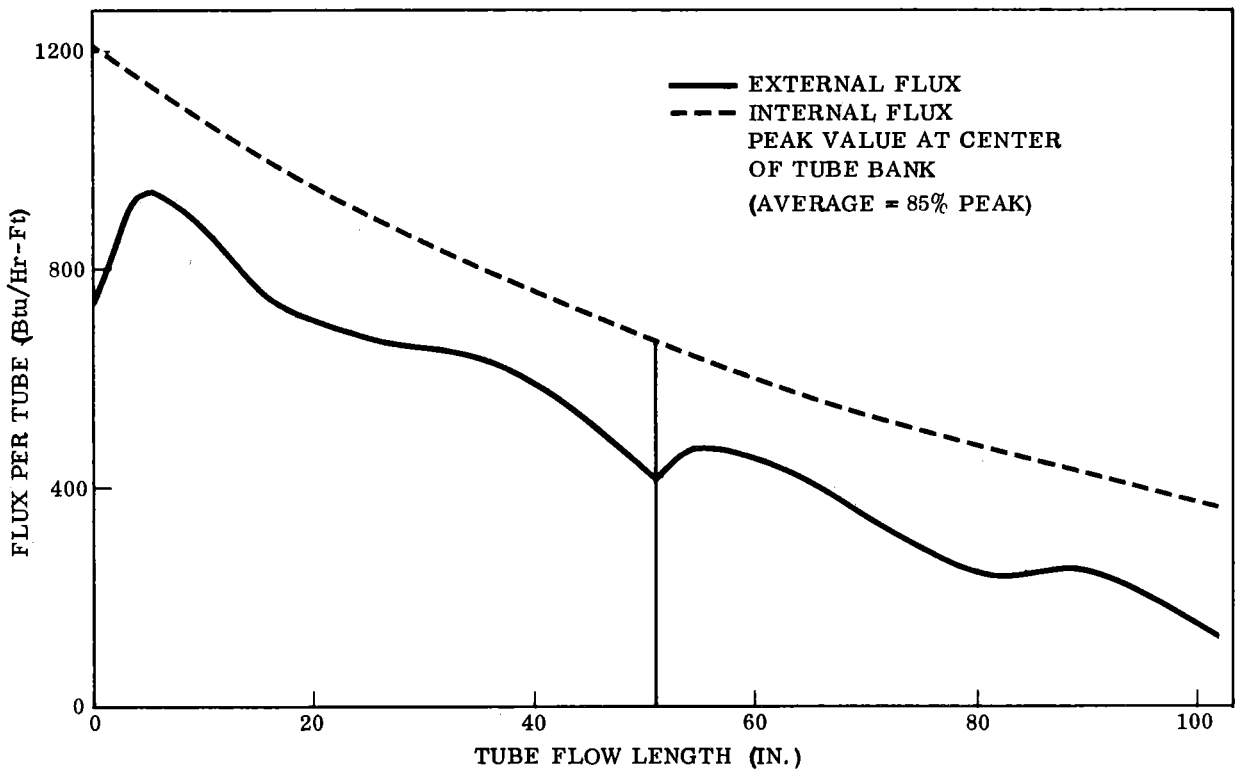


FIGURE 19. CASE I - KRYPTON FLUX VALUES

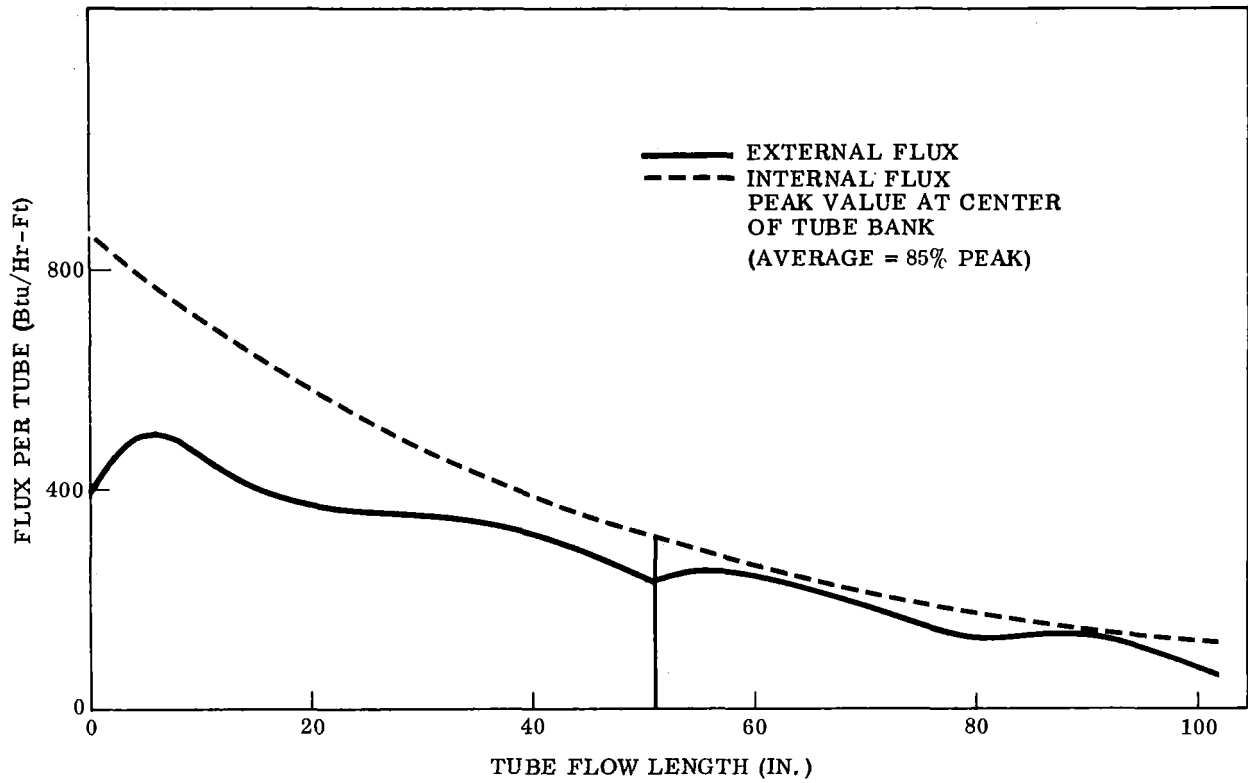


FIGURE 20. CASE III - MIXTURE FLUX VALUES

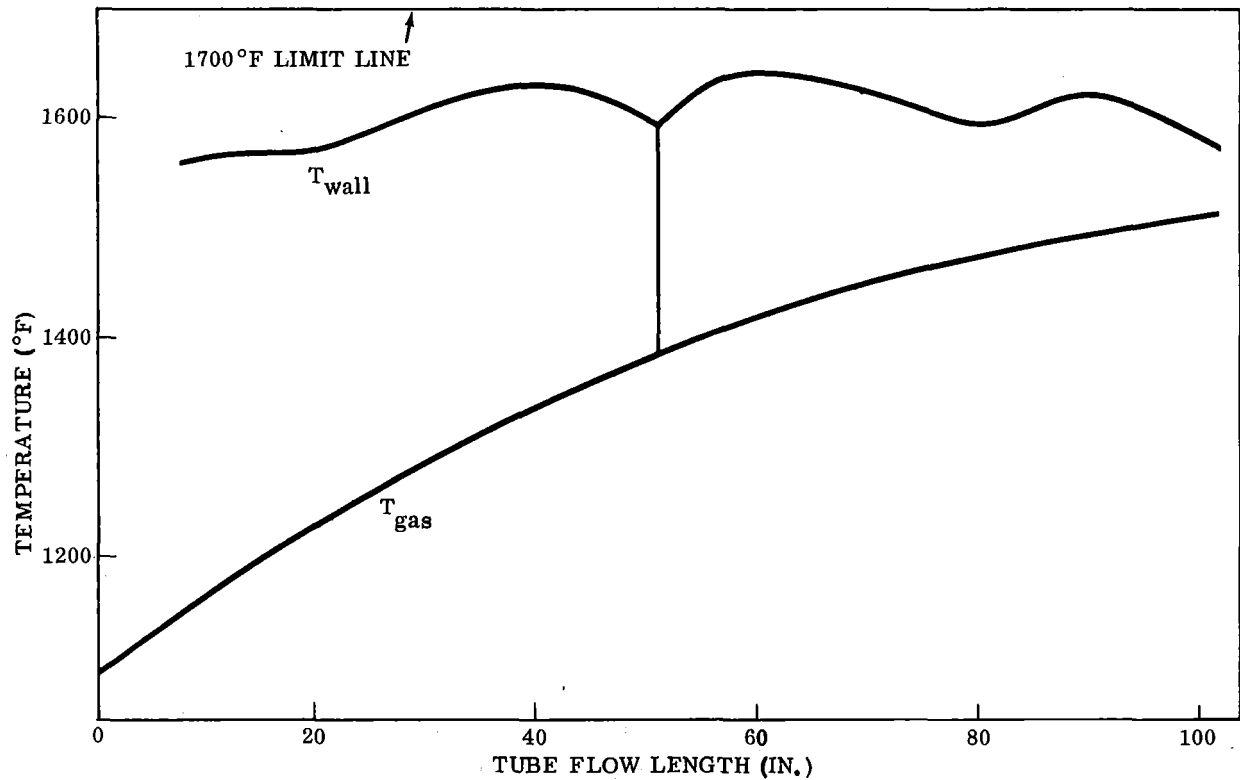


FIGURE 21. CASE I - KRYPTON LONGITUDINAL TEMPERATURE PROFILE

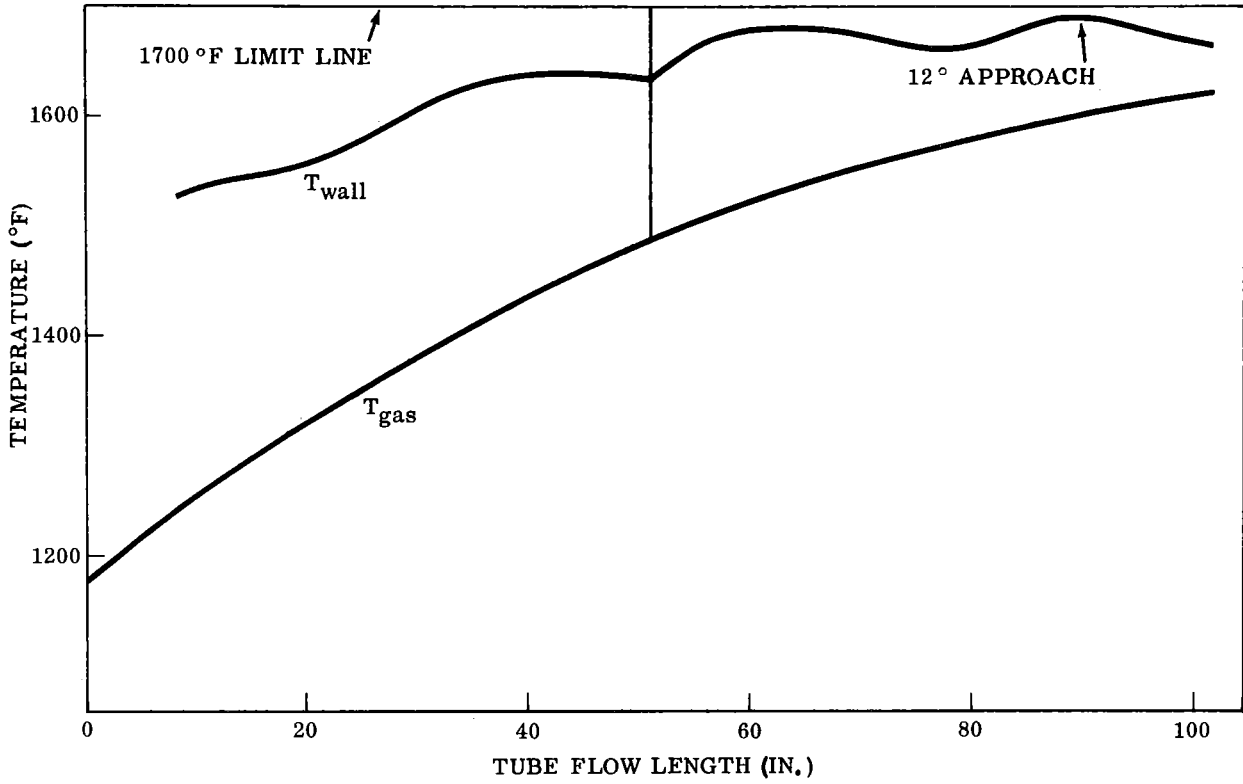


FIGURE 22. CASE II - MIXTURE LONGITUDINAL TEMPERATURE PROFILE

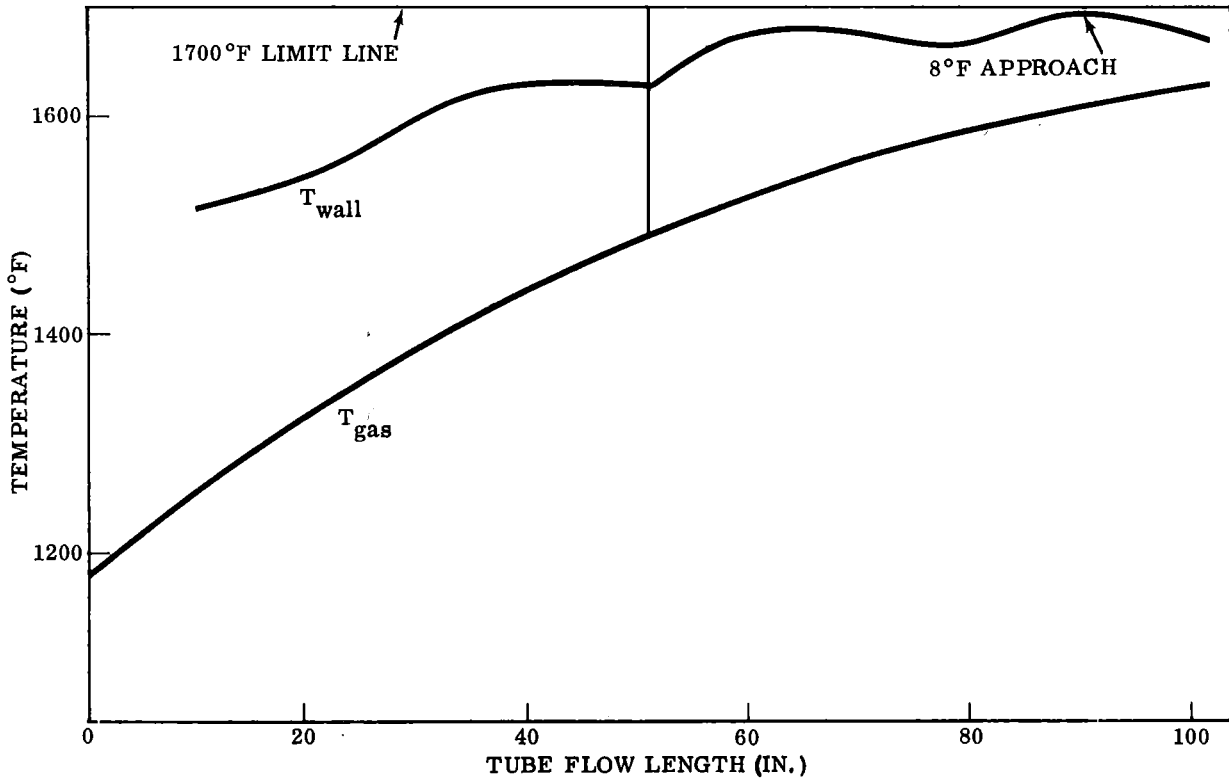


FIGURE 23. CASE III - MIXTURE LONGITUDINAL TEMPERATURE PROFILE

2.4 CONCLUSIONS

As a result of the heat transfer analyses, the following conclusions are made:

- The heat transfer design is conservative, therefore the heat exchanger surface area is greater than required.
- The temperature increases indicated on the outlet side of the heat exchanger are small, and in the actual operation should be lower due to the heat transfer across the dividing plane, an effect which was not considered in this analysis.

The calculated stresses were:

Inlet and Outlet Tube

$$\sigma_H = \frac{4.627 \times 55.8}{0.374} = 690 \text{ psi}$$

U-Tube

$$\sigma_H = \frac{0.666 \times 55.8}{0.084} = 443 \text{ psi}$$

Gimbal Joint - Bellows Hoop Stress

$$\sigma = \frac{PR_m W}{A}$$

where:

P = internal pressure

W = bellows pitch

R_m = mean radius

A = area of section in one pitch

σ = average hoop stress

$$\sigma = \frac{55.8 \times 2.674 \times 0.50}{0.081}$$

$$\sigma = 920 \text{ psi}$$

Gimbal Joint - Bellows Bulging Stress

Considered as membrane stress in the omega skin:

$$\sigma = \frac{Pr}{t} = \frac{55.8 \times 0.21}{0.020} = 585 \text{ psi}$$

Gimbal Joint - Bellows Angulation Stress

Considered as a low cycle fatigue condition. From Solar computer program No. 224 for 5 degrees total angulation and Reference 4:

$$\sigma = 68,000 \text{ psi (hot)}$$

$$\sigma = 88,000 \text{ psi (cold)}$$

Using the method of Halford and Manson, a minimum life of 1000 cycles with total angulation is indicated, which is considerably more than the 200 start/stop cycle requirement. The maximum total angulation expected is 4.5 degrees.

Gimbal Ring

The results of the gimbal ring calculations are:

$$\tau_S = 575 \text{ psi (max. shear)}$$

$$\sigma_B = 2260 \text{ psi (max. bending)}$$

$$\tau_T = 2310 \text{ psi (max. torsion)}$$

Gimbal Clevis

Shear at pin hole:

$$\tau = 1500 \text{ psi (max.)}$$

4

FABRICATION

A complete list of all Solar-released drawings is presented in Table III.

TABLE III
FINAL ASSEMBLY DRAWINGS

Drawing Number	Description	Revision
51418	Probe Assy - Gas Temperature	B
51419	Box Assy - Power Terminal	E
51420	Master Wiring Diagram	B
51422	Box Assy - Thermocouple Jack	B
51431	Heat Exchanger Installation	C
51432	Core Assy - Heat Exchanger	B
51433	Duct Assy - Inlet	B
51434	Duct Assy - Outlet	B
51435	Gimbal Assy - Duct	B
51436	Flange Assy - Duct	A
51437	Flange - Duct	A
51439	Duct Assy	B
51440	Gimbal Insulation Assy - Removable	-
51465	Harness - Gas Temperature - Inlet & Outlet	-
51466	Harness - Water Temperature - Inlet & Outlet	-
51469	Harness - Hot-Spot Thermocouples	-
51482	Elbow Insulation Assy - Removable	-
51483	Boss Insulation Assy - Removable	-
51484	Flange Assy - Duct	A
51485	Flange - Duct	B
51486	Enclosure Assy - Heat Exchanger	B
51487	Panel Assy - Inlet Lower	C
51488	Panel Assy - Outlet	C
51489	Manifold Assy - Cooling	B
51491	Duct Assy - Center Inlet	B
51504	Probe Assy - Water Temperature	A
51505	Probe Assy - Duct Surface Temperature	A
51506	Probe Assy - Hot Spot Temperature	A
51508	Insulation - Removable	-
51510	Insulation - Elbow	-
51518	Panel Assy - Upper Inlet	-
51522	Heater Assy	-

4.1 FABRICATION OF HEAT EXCHANGER

Work was started on the core (tube bank) assembly 51432 by installing the 40 pre-bent (3/4-inch diameter by 0.042-inch wall) U-tubes in holes in the half headers (5-inch OD x 0.250-inch wall) then bulging the tubes as indicated in Figure 24. The purpose of the bulge was to lock the tubing in place mechanically; the sole function of the braze was to seal the joint. Both tubes and headers were solution annealed Inconel 600.

Solar NX-1 braze alloy was placed on the concave side of the headers and the assembly placed in the fixture for brazing. After brazing, the assembly was mass spectrometer leak tested (Fig. 25). Subsequent to brazing, the half-header section and the end caps required to seal the blind ends were heliarc welded in place. Additional leak, dye penetrant, and X-ray tests were performed after assembly.

The support assemblies placed on the ends of the headers are shown in Figure 26. Each support assembly consisted of a dish made from 0.125-inch type 321 stainless steel containing 2 inches of Microquartz. The inside surface of the assembly was faced with 0.010-inch Inconel 600. Nutplates welded to the inside surface of the "dish" permitted attachment of the core assembly to the structure. The headers at the inlet end of the core were inserted through the large openings in the assembly, supported by the arc-shaped titanium carbide bearings, and are free to grow with temperature. The collar provides an attachment ring for the duct insulation.

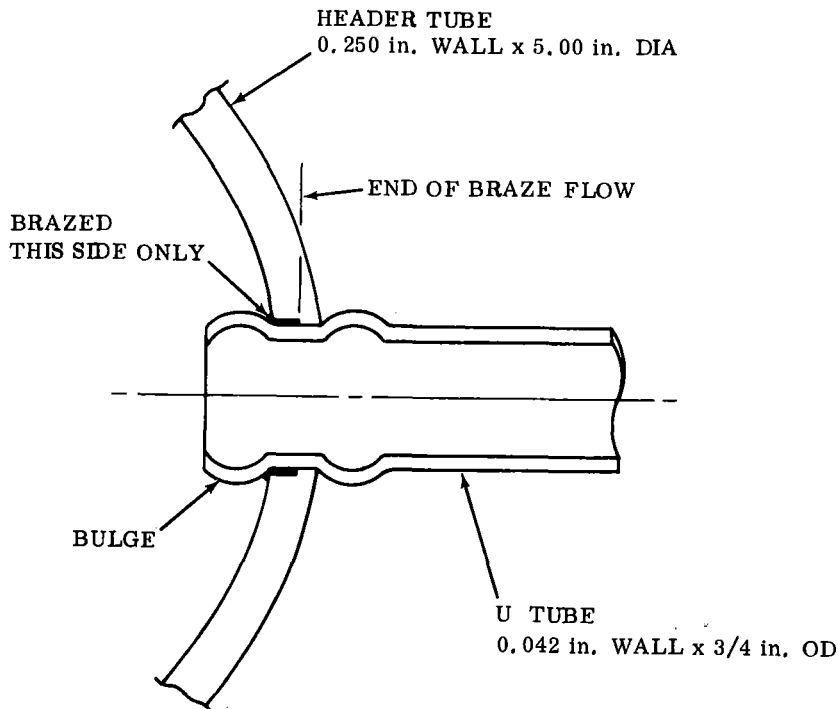


FIGURE 24. SECTION THROUGH TUBE TO HEADER JOINT

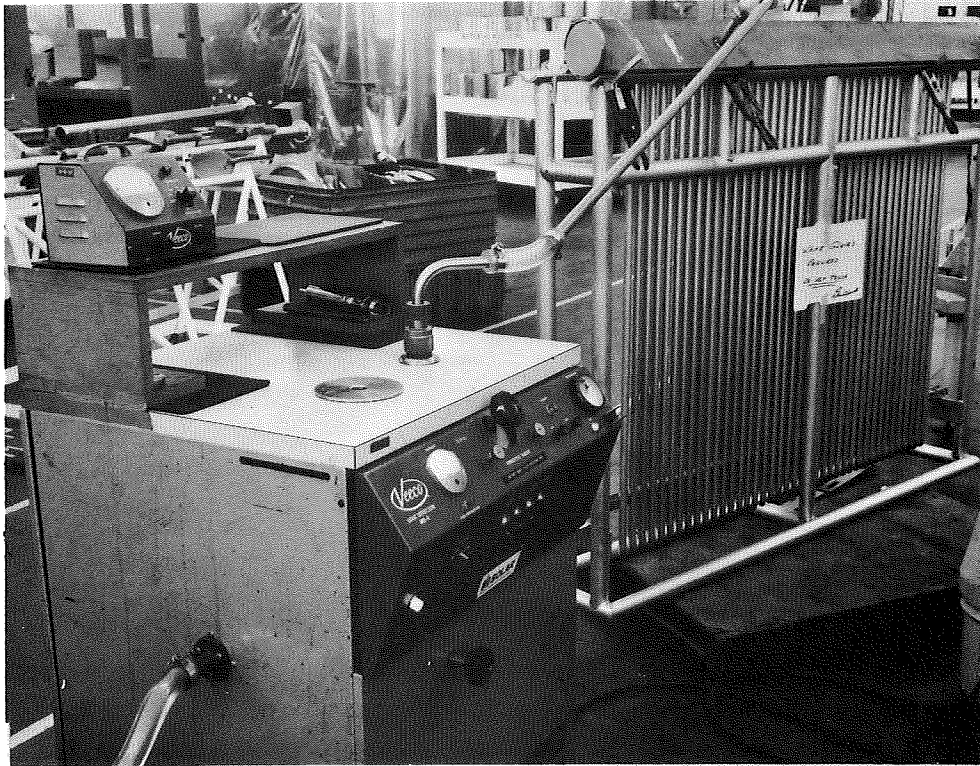


FIGURE 25. MASS SPECTROMETER LEAK TESTING

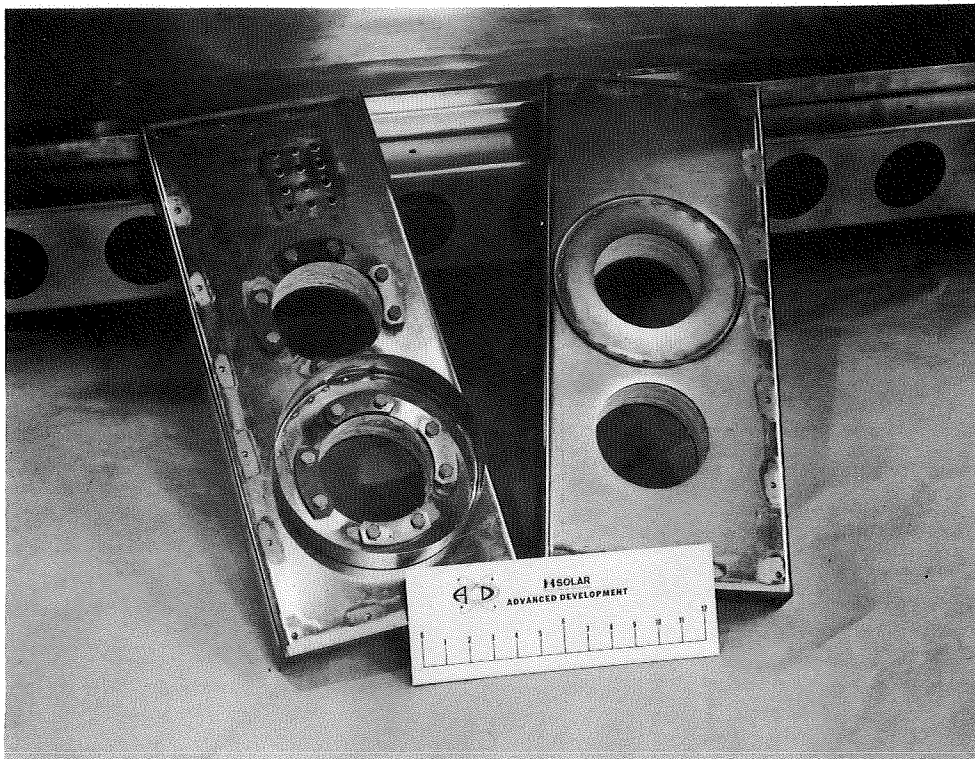


FIGURE 26. HEADER SUPPORT ASSEMBLIES

Hot spot thermocouple leads exited through the 12 small openings at the top of this assembly. The other support assembly (shown on the right in Figure 26) was welded to the outlet headers of the heat exchanger core during assembly.

4.2 FABRICATION OF ENCLOSURE

The structure consists of the 51486 enclosure and its three hinged panels. The enclosure is a parallelepiped setting on two longitudinal box beams. Its two ends and bottom are permanently fixed; the top is removable to allow insertion of the heat exchanger core. Channel frames in the side panels of the enclosure allow installation of the hinged panels.

The lower inlet side panel (51487) has openings for five lamp modules. The upper inlet side panel (51518) was similar except that it held three lamp modules immediately adjacent to each other. All interior surfaces were of 0.010-inch Inconel 600; exterior surfaces were made from Type 321 stainless steel sheets, with thickness ranging between 0.060 and 0.090 inch. Except where structural members of lamp modules intrude, the space between the surfaces was filled with 6 lb/ft³ density Microquartz. All interior surfaces of the enclosure were polished to improve reflectivity.

4.3 FABRICATION OF ASSEMBLY

The complete assembly with both inlet side panels open is shown in Figure 27. The core assembly was lowered into the enclosure and the support assemblies through which the 5-inch OD headers protrude were bolted to the structure. The reflector separating the two legs of the U-tubes and 5 of the 24-lamp modules is also shown in Figure 27, as is the 51422 thermocouple jack box (upper left) and the 51419 power terminal box. The white electric power cables connect the bussbars on the lamp modules to the power terminal box. Lamp modules fit snugly into the hinged panels. Figure 28 is the inlet side of the assembly with the panels closed. Cooling water manifolds are located at the right edge of the assembly and cooling water thermocouple leads are at the bottom. The inlet support assembly was bolted in place at the top of the structure; the hot spot thermocouple leads were not yet connected to the thermocouple jack box terminals.

4.4 FABRICATION OF THE DUCT SYSTEM

The duct system included the 51439/51491 inlet duct assemblies, the 51433 inlet duct assembly, and the 51434 outlet duct assembly.

Except where noted on the drawings, all ducts were insulated with 2 inches of 6 lb/ft³ density Microquartz retained by bellows made from corrugated Type 321 stainless steel foil 0.003 inch thick. The insulation was applied by:

- Wrapping Microquartz blanket onto the duct
- Bagging the insulation in vinyl

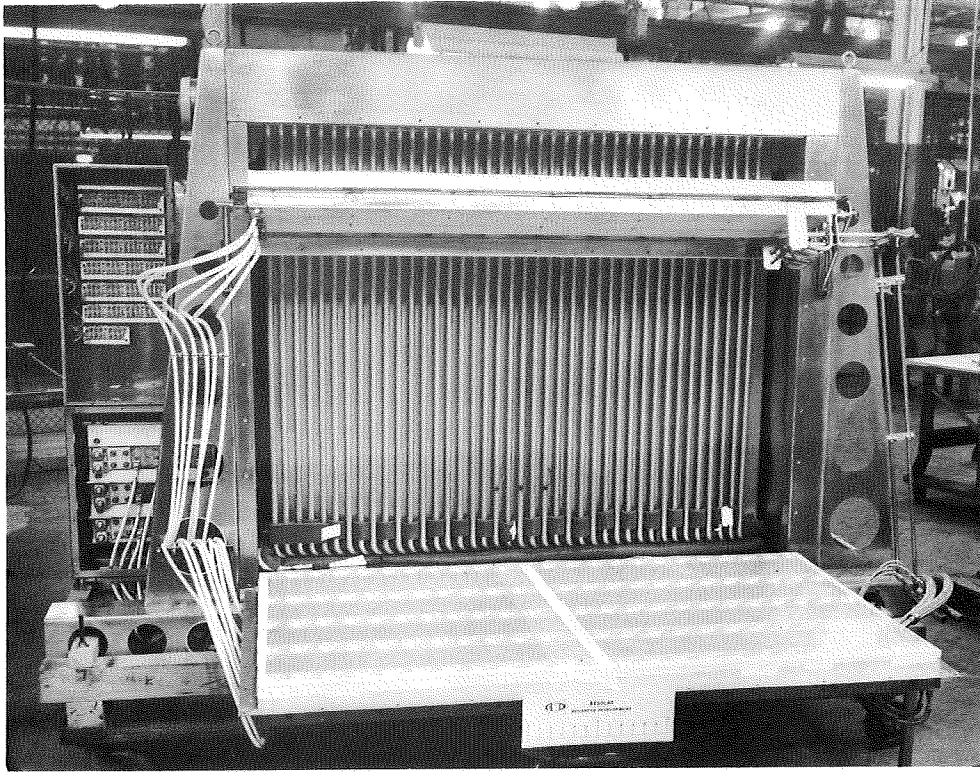


FIGURE 27. COMPLETE ASSEMBLY

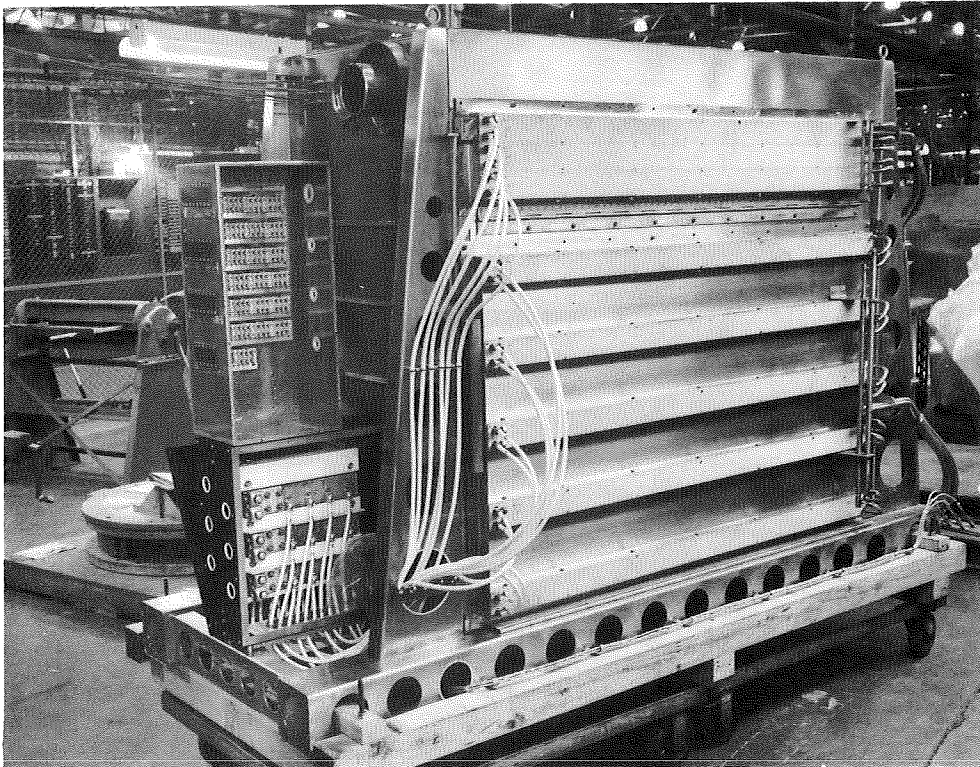


FIGURE 28. INLET SIDE OF ASSEMBLY

- Evacuating the bag to compress the blanket below the final OD
- Sliding the corrugated foil in position
- Removing the vinyl sheet before the insulation could expand

Removable muffs, fabricated from Microquartz blanket insulation covered with Type 321 stainless steel foil, were used to bridge the insulation gaps.

4.4.1 Duct Assembly, Inlet

The inlet duct assembly (51439) consisted of a 4.5-inch OD by 0.083-inch wall, Type 316 stainless steel elbow and tubes; a 51435 gimbal made entirely from Inconel 625; and half of a snip-open joint made from Type 316 stainless steel (Fig. 29). As shipped, the -5 stub duct was welded to the -2 elbow.

All gimbals are identical and have a 5-inch diameter; therefore, 4.5- to 5-inch diameter transition tubes were used to accommodate the difference.

4.4.2 Duct Assembly, Inlet Center

The inlet center duct assembly consisted of two snip-open joint sections connected by a length of 4.5-inch OD by 0.083-inch wall tube. All components were made from Type 316 stainless steel. The 51439 assembly is shown in Figure 29. Special bolts are used to secure these joints and will be discussed in a subsequent section along with the snip-open joints.

4.4.3 Duct Assembly, Inlet

The third inlet duct assembly (51433) began with half of a Type 316 stainless steel snip-open joint and consisted of (in order of flow direction) a 4.5-inch OD by 0.083-inch wall Type 316 stainless steel sleeve, a Type 316 stainless steel transition tube, a 51435 (Inconel 625) gimbal, a 5-inch OD by 0.187-inch wall Inconel 600 elbow, another gimbal, and a 5-inch OD by 0.187-inch wall Inconel 600 elbow having tubes of varying lengths for the inlet gas temperature thermocouples. The complete assembly is shown in Figure 30.

4.4.4 Duct Assembly, Outlet

The outlet duct assembly (51434) shown in Figure 31 consisted primarily of a three-gimbal system connected by 5-inch OD by 0.187-inch wall Inconel 600 tubes and elbows in addition to an Inconel 600 (and 625) snip-open joint. The upstream elbow has tubes for the outlet gas temperature thermocouples. Eight bosses for attachment of probes were welded in the duct between the final gimbal and the snip-open joint.

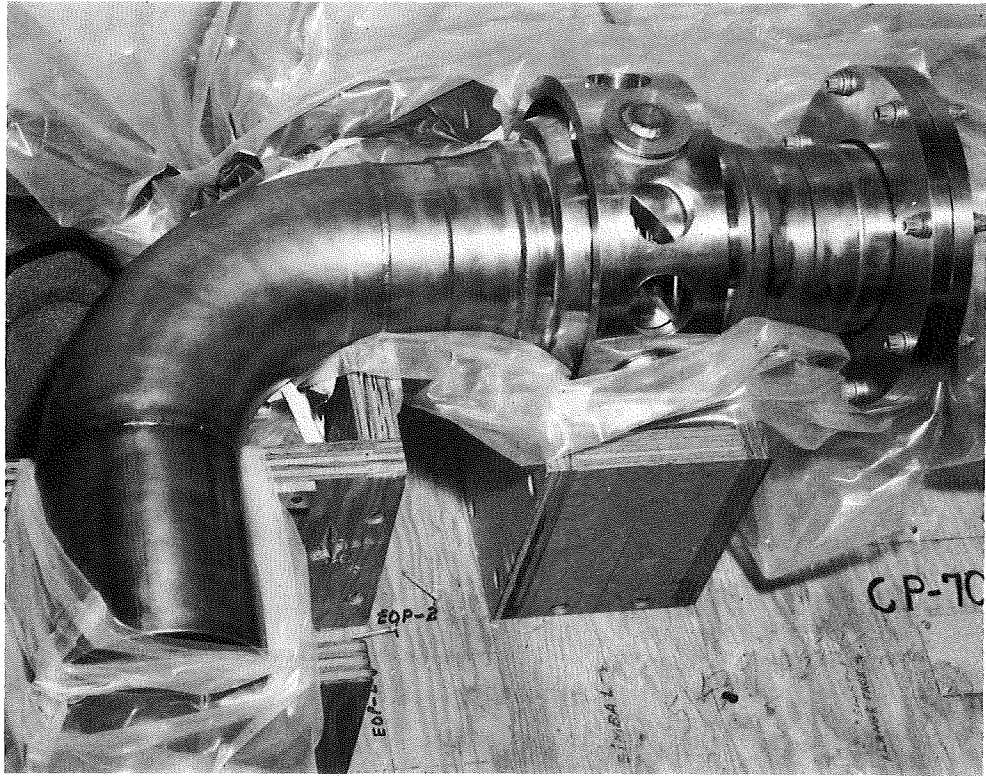


FIGURE 29. INLET CENTER DUCT ASSEMBLY

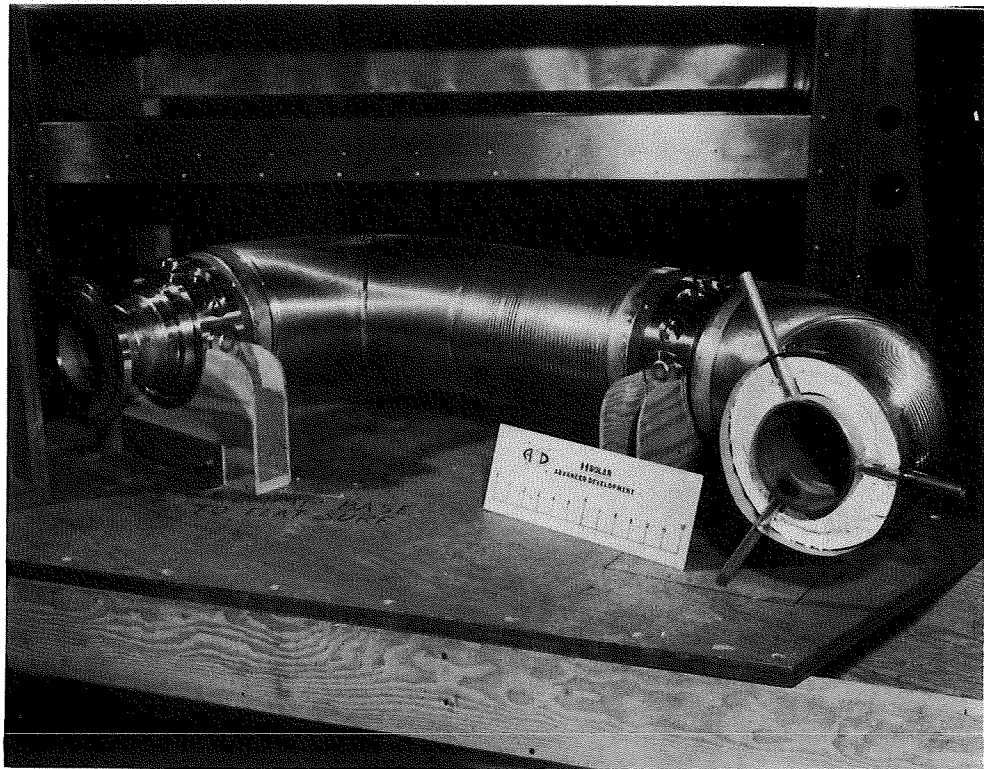


FIGURE 30. INLET DUCT ASSEMBLY

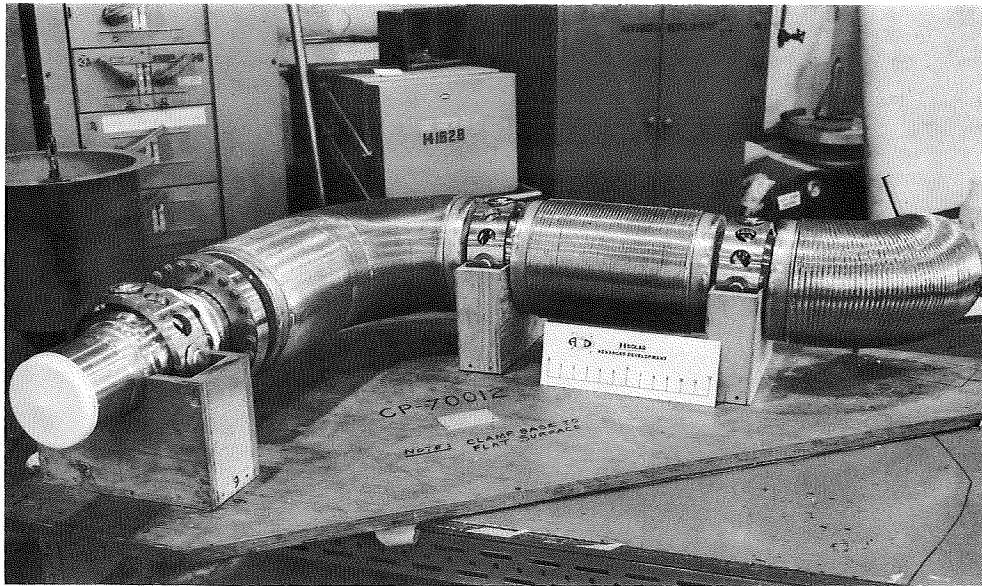


FIGURE 31. OUTLET DUCT ASSEMBLY

4.4.5 Gimbal

All gimbals (51435) built for this program were identical and matched a 5-inch duct. Where necessary, a transition sleeve was used to accommodate ducts having a different diameter. The schematic diagram shown in Figure 32 identifies all components and Figure 33 shows all hardware components for one gimbal.

The gimbal was made from Inconel 625 with the exception of the titanium carbide bearings. The bellows were made from two plies of 0.010-inch material; each convolution was formed around a root ring. A second operation (to form the omega shape) was performed to prevent the shape from changing during use. The function of the root rings was to provide additional resistance to hoop stress at high temperatures. Inner liners were incorporated to reduce system pressure drop.

4.4.6 Snip-Open Joint

The major components of the snip-open joint were foil-flange assemblies welded to adjacent tubes (Fig. 34). The outside diameters of the washer-shaped foils were then peanut welded together; the loose flanges were bolted to support the sides of the foils.

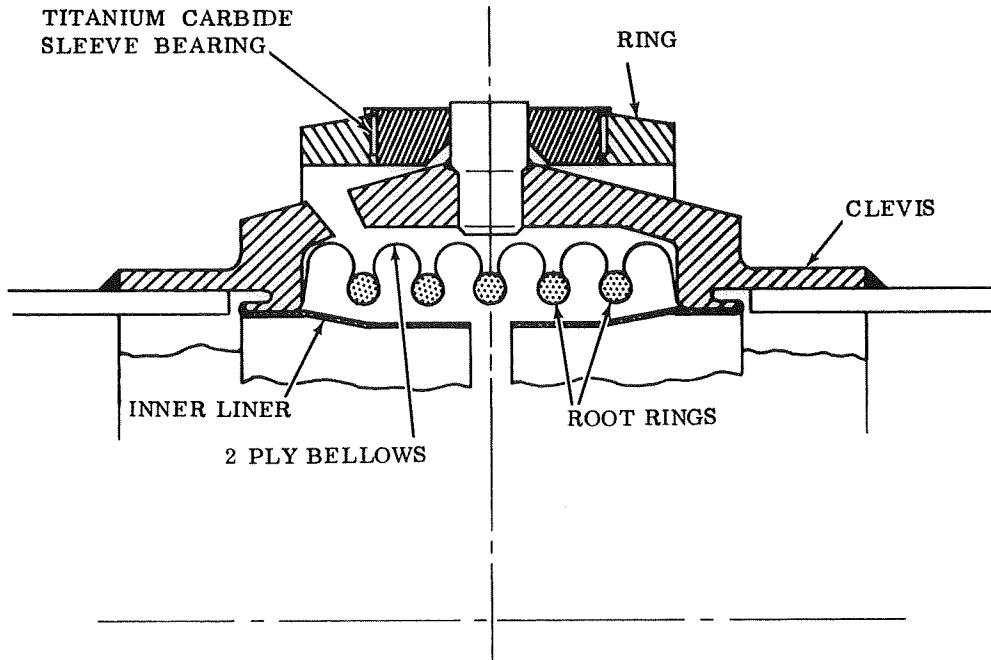


FIGURE 32. SCHEMATIC DIAGRAM OF A TYPICAL GIMBAL

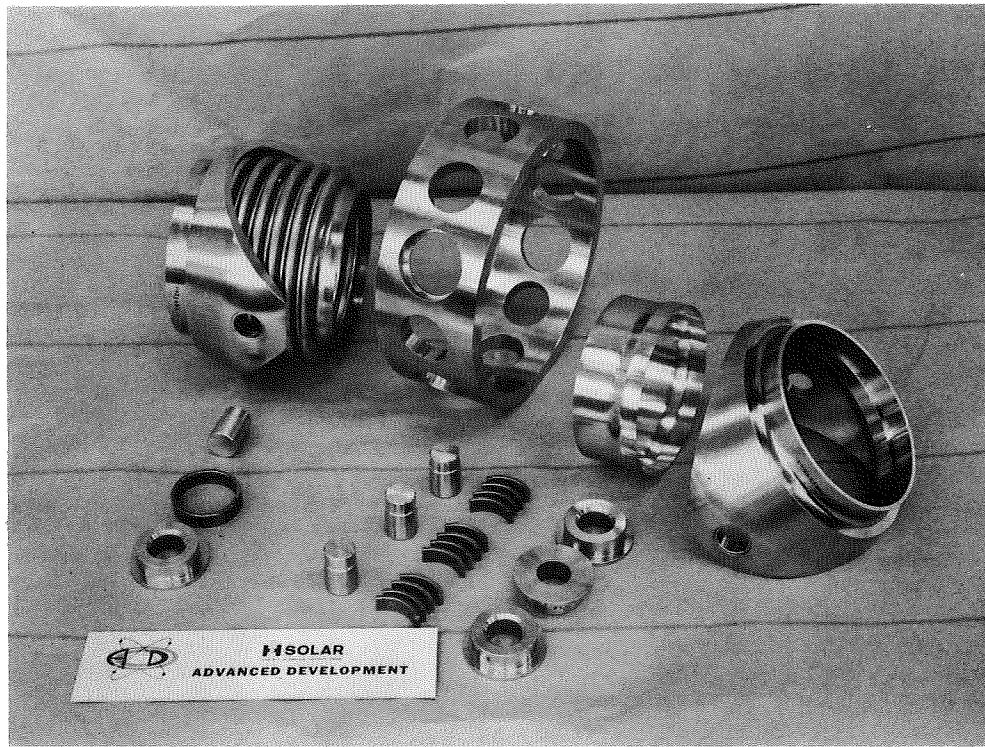


FIGURE 33. COMPONENTS OF A TYPICAL GIMBAL

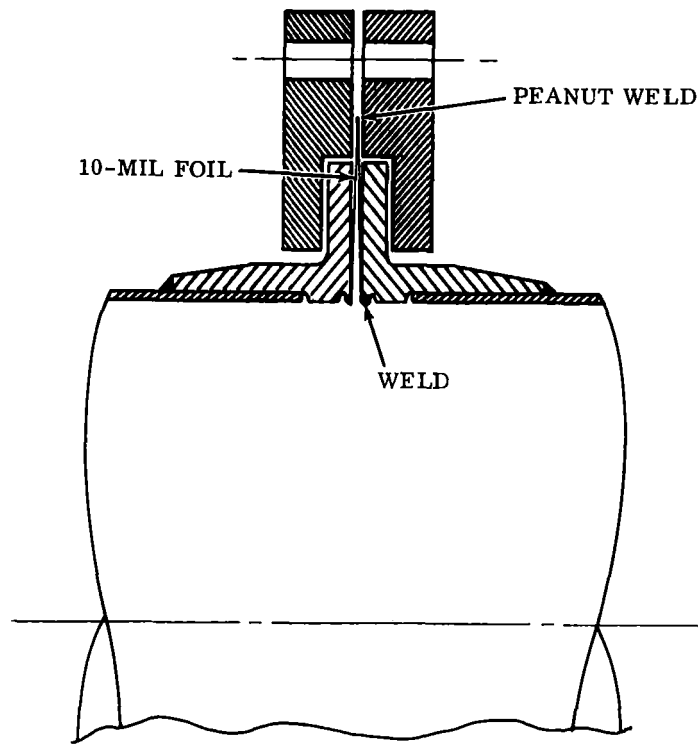


FIGURE 34. SCHEMATIC DIAGRAM OF A SNIP-OPEN JOINT

The advantages of incorporating snip-open joints in this assembly were:

- Provide leak-proof joints and allow the flow system to be disconnected without difficulty.
- Allow disconnection to be performed using a metal working snip which eliminates grinding, filing, or sawing residues from the inside of the duct.
- Capable of being rewelded numerous times before new foils are required; only the peanut weld is "snipped" off when opened.

This heater system used two models of the snip-open joint. The hot duct (51434) incorporated a joint made from Inconel 600 foil and weld flanges with Inconel 625 bolted support flanges. The "cold" 51439/51491 duct used two joints made entirely from Type 316 stainless steel.

All bolts and nuts (40 sets) used to clamp the support flanges were made from Rene' 41 with a lubricant "Silver Goop" applied to the bolt threads before the nut was run on. This was required both to prevent galling and to allow nut removal after the threads were heated.

4.5 INSTALLATION

The complete assembly appears on installation drawing 51431 (Fig. 35). The heat exchanger, structure, terminal boxes, ducts, and other assemblies are shown in proper orientation.

5

CONTROL SYSTEM AND INSTRUMENTATION

5.1 CONTROL SYSTEM

The prime function of the control system is to regulate the electrical power input to the quartz tube lamps.

5.1.1 Description

The major components of the control system include the remote power temperature control panel (controller) and the power control device. A schematic wiring diagram showing these components and the necessary interconnection is shown in Figure 36.

The system will accept 130-kw, 3-phase, 480 volts, and deliver up to 120-kw, 3-phase, 80 volts to the quartz tube lamps. In addition to manual operation, three control modes are available to the operator: Temperature, Power, and Automatic.

When the mode selector is in the Temperature position, the output from a gas outlet temperature thermocouple is fed back to a variable set point device which then controls the power supply. The Power position on the mode selector provides closed loop power control from a power input feed back. In Automatic position, power control is affected by nulling an input signal from a Dynamic Controller.

The control system was obtained from the R. I. Controls Division of Research Incorporated (Minneapolis, Minn.).

5.1.2 Drawings

A list of the drawings generated by R. I. Controls is shown in Table IV.

TABLE IV
LIST OF R. I. DRAWINGS

Drawing Number	Description
D35364	Schematic - Power Control Device
D35365	Schematic - Remote Control Panel
D35373	40 KVA Power Controller Model 6429
C35374	3 Rack Configuration of 40 KVA Power Controller
D35380	Power Temperature Control Panel Assy
A35331	Millivolt Range Card, 0-100 MV
A35382	Thermocouple Range Card
D35383	Schematic - TC5192 Temperature Controller
C35385	Interconnect Cable - Power Control Device Remote Control Panel

5. 1. 3 Control System Analysis

An analysis of the transient overshoot, stability, settling time, and steady-state error characteristics was performed and the results determined by computer solution to be within NASA specification requirements. The results of this analysis are presented in Solar Report M-1973 (Ref. 5). Both the heat exchanger and heater configuration have been revised since publication of this report; however, Solar has been informed that subsequent analyses performed by the NASA controls group are in substantial agreement with the results of M-1973.

5. 2 INSTRUMENTATION

The instrumentation (thermocouples only) provides input to the control system or raw data for computation.

5. 2. 1 Description

Instrumentation is defined here as those sensing devices and accessories built or procured directly by Solar for use with the Brayton Cycle Gas Radiant Heater.

By this definition, instrumentation consists of the following items, all of which were fabricated by Thermowells Incorporated:

<u>Quantity</u>	<u>Solar Drawing No.</u>	<u>Description</u>
6	51418	Gas Temperature Thermocouples
4	51504	Water Temperature Thermocouples
12	51506	Hot Spot Temperature Thermocouples
2	51515	Duct Surface Temperature Thermocouples
1	51422	Thermocouple Jack Panel Box

All thermocouples were made from Inconel 600 sheathed, magnesium oxide insulated, chromel-alumel stock. In addition, all thermocouple sheaths are isolated from ground potential except at the hot junction and terminal connection ends. Features considered important and/or unique to certain items of instrumentation are described in the subsequent paragraphs.

Gas Temperature Thermocouples

Three of the gas temperature thermocouples are immersion type units located in the inlet and outlet ducts. The depth of immersion varies so that a temperature traverse can be obtained.

Hot Spot Thermocouples

Hot spot thermocouples have plug welded tips and are welded to the U-tubes at selected locations. Three of the twelve hot spot thermocouples welded to the heat exchanger are shown in Figure 37.

Duct Surface Temperature Thermocouples

One of these thermocouples is welded to the surface of the duct at each of the gas temperature thermocouple stations to permit computation of piping heat losses.

Thermocouple Jack Panel Box

The thermocouple jack box is shown in Figure 38. The 6 three-pin (the third line is a ground wire) receptacles in the bottom strip and the first six positions (from the left) on the strip above receive signals from hot-spot thermocouples. Any four of these twelve positions may be selected as inputs to the control system by installing a jumper between it and one of the four middle positions on the top row. Twenty-two jumpers have been provided.

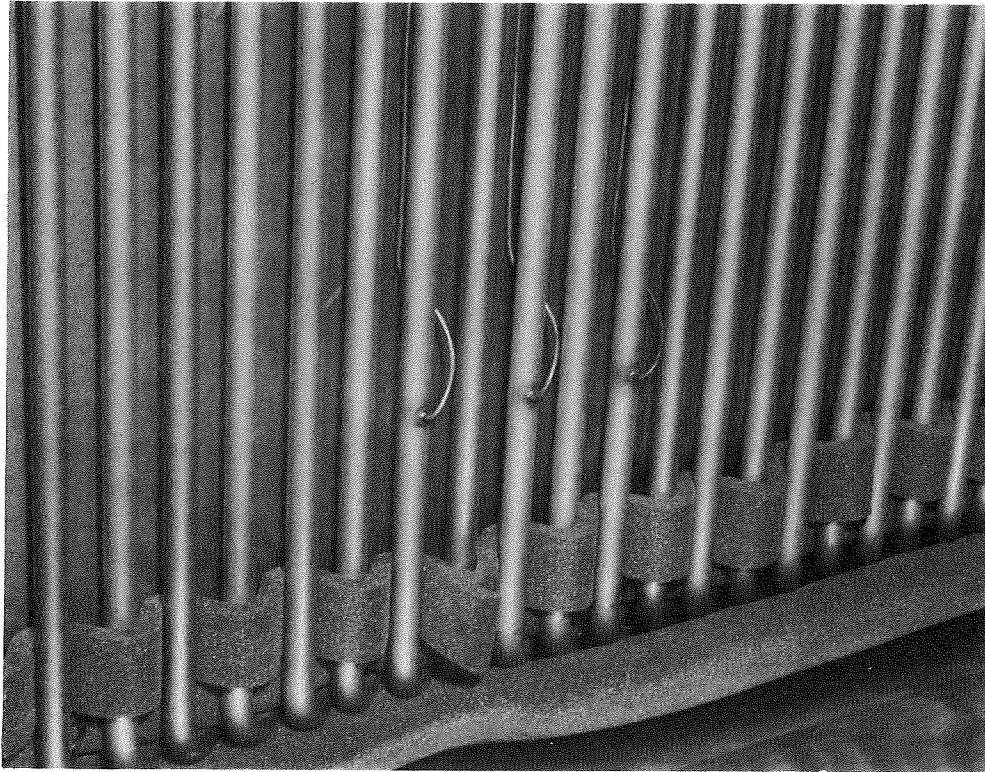


FIGURE 37. HOT SPOT THERMOCOUPLES WELDED TO THE U-TUBES

Similarly, one of the three gas inlets, one of the three gas outlets, one of the two water inlets, and one of the two water outlets, may be jumpered to provide input to the control system. No provision has been made in this panel box to accommodate the duct surface temperature thermocouples.

5. 2. 2 Thermocouple Readout

Of the eight thermocouple signals fed to the output terminal strip, all but the gas inlet temperature continue through to the Remote Control Panel.

The outlet gas temperature signal is read on a relay type display meter and also supplies temperature feedback for power control through a manually adjustable setpoint.

Cooling water temperature (switch selectable between inlet and outlet) is fed to a relay type display meter.

The four hot-spot temperatures are connected to a selector switch from which a single signal is fed to a relay type display meter which will open the main circuit breaker in the event of an overtemperature indication.

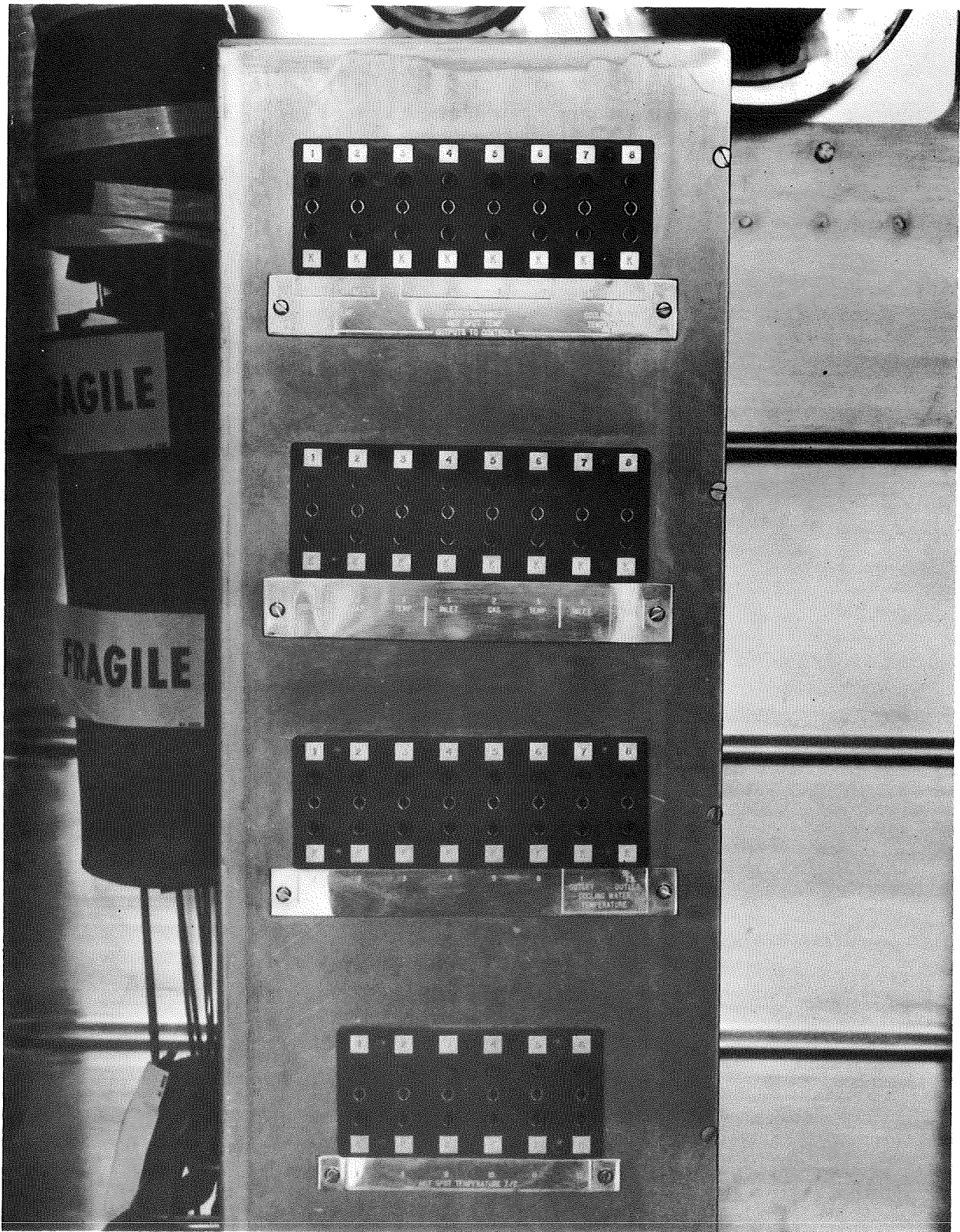


FIGURE 38. THERMOCOUPLE JACK BOX

6

QUARTZ TUBE LAMP HEATER

6.1 HEATER REQUIREMENTS

The heater specification requirements of the contract are summarized as:

- An array of quartz lamps with tungsten filaments.
- Capable of operating at a pressure of one atmosphere in air, at a vacuum level of 1×10^{-8} Torr, and at all conditions in between.
- Provide sufficient power into the heat exchanger to get 40 kw out of the heat exchanger for 10,000 hours and 80 kw out for 100 hours with a maximum of 200 start-stops.

6.2 ASSUMED SOLUTION

A survey of commercial quartz lamps indicated that the prime candidate was available as the essentially "off-the-shelf" item shown in Figure 39. This 16-lamp module was offered by Solar's subcontractor, the Aerometric Division of Aerojet General. Predesign calculations indicated that 18 of these 120 volt modules operating at a maximum of 80 volts would supply the necessary energy. Further, information provided to Aerometrics by Sylvania (the lamp manufacturer) predicted an associated tube life in air of 50,000 hours at the maximum anticipated voltage. The only unknown was lamp operation in a vacuum. There was only a few hours actual experience and no life test data for vacuum.

In retrospect, the establishment of a quartz tube lamp radiant heat source was the result of an arduous development program which could not have succeeded without the extensive testing by Solar and the complete cooperation of Aerometrics, Sylvania, and the NASA Program Manager.

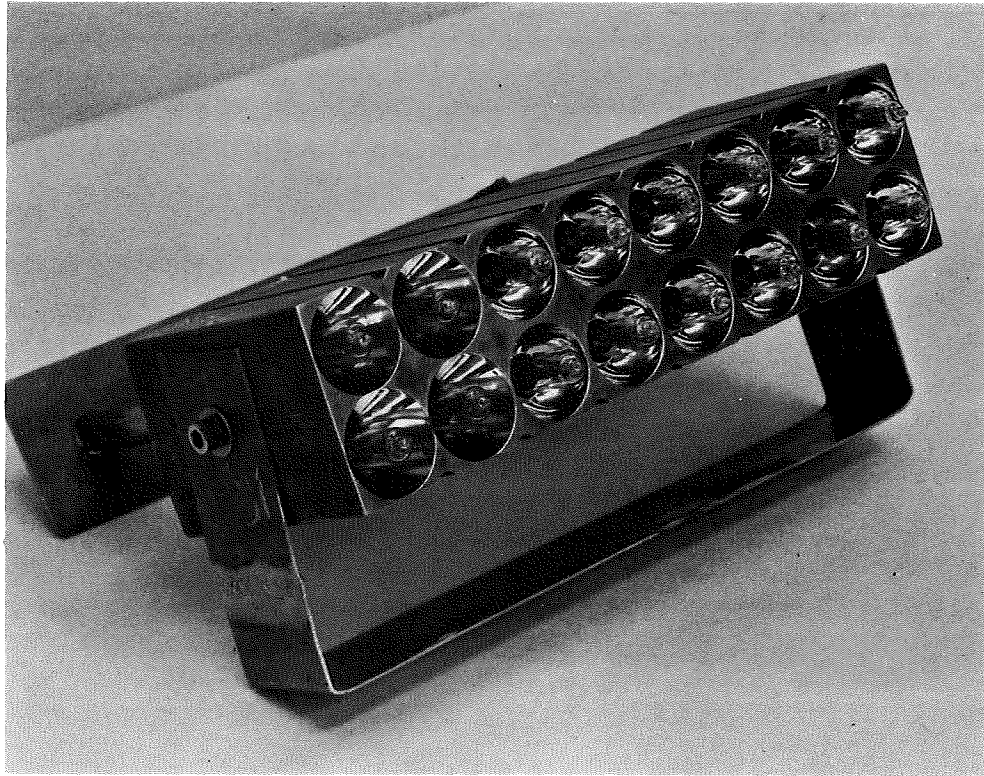


FIGURE 39. CANDIDATE 16-LAMP HEATER MODULE

6.3 DEVELOPMENT PROGRAM

A review of the test results is presented in this section. Progress reports with the data sheets prepared during the course of the development program are included as Appendix C. The information contained in reports No. 4 through 7 is repeated in report No. 8; therefore they are omitted from the Appendix.

The first 16-lamp module obtained was made from an aluminum casting with porosity which allowed helium to leak from the cooling water passage. This module was replaced with one in which the aluminum was cast around a stainless steel water passage.

The second cast module was set into a sheet metal target with thermocouples attached (Fig. 40). The apparatus with ancillaries was installed in a vacuum chamber and connected to power measuring and control devices and a temperature recorder. This second cast module was tested in vacuum using four sets of 750-watt, T-4 lamps operating at 80 volts and a target temperature of 1700° F. (These lamps were the

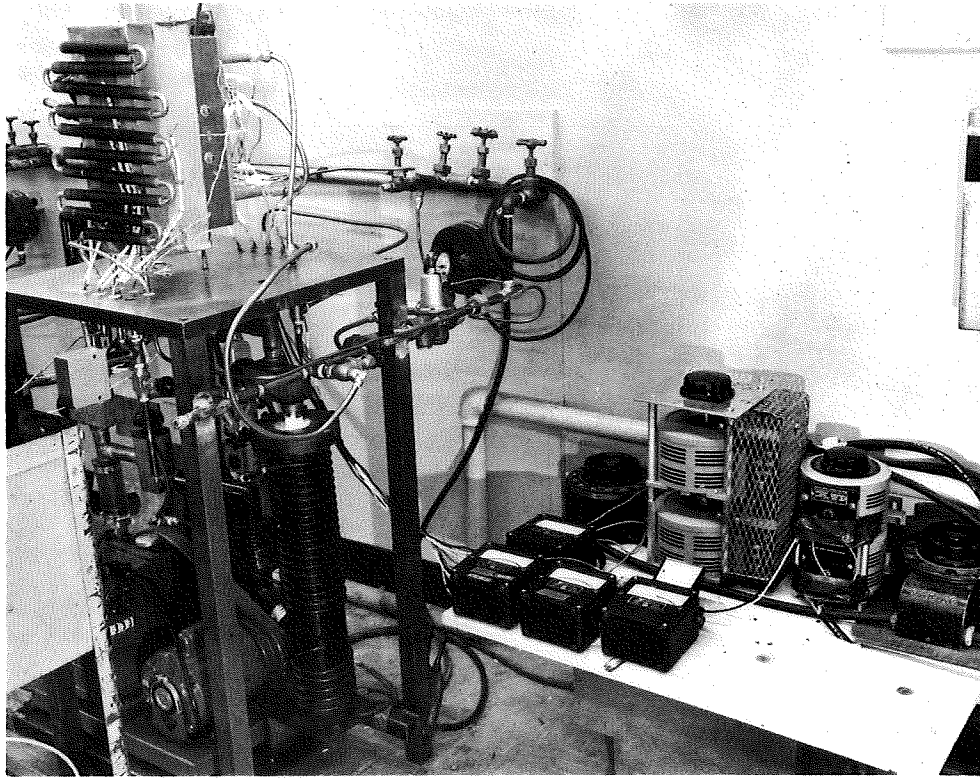


FIGURE 40. DEVELOPMENT TEST APPARATUS AND INSTRUMENTATION, SECOND CAST MODULE

standard configuration, having a 750-watt rating at 120 volts and a T4 (1/2-inch OD) quartz envelope,) The following problem areas were revealed:

- The lamp pin-to-lead wire joint overheated and frequently burned
- The lead wire insulation decomposed
- The pores of the cast module retained contaminants from machining or cleaning

To eliminate the contamination retention problem a third module, machined from wrought 6061 aluminum alloy, was obtained and used in testing. With this machined module, lengthy lamp-time at test-temperature (1700°F target) was obtainable and a quartz devitrification problem became apparent. Devitrification is the process whereby the oxygen separates from the silicon dioxide (quartz) leaving a porous silicon matrix. This porosity allowed air to get into the quartz envelope and cause burnout of the tungsten filament. Also, the inert gas leaks out and causes the tungsten-iodide cycle to fail resulting in tungsten deposition on and eventual melting of the quartz.

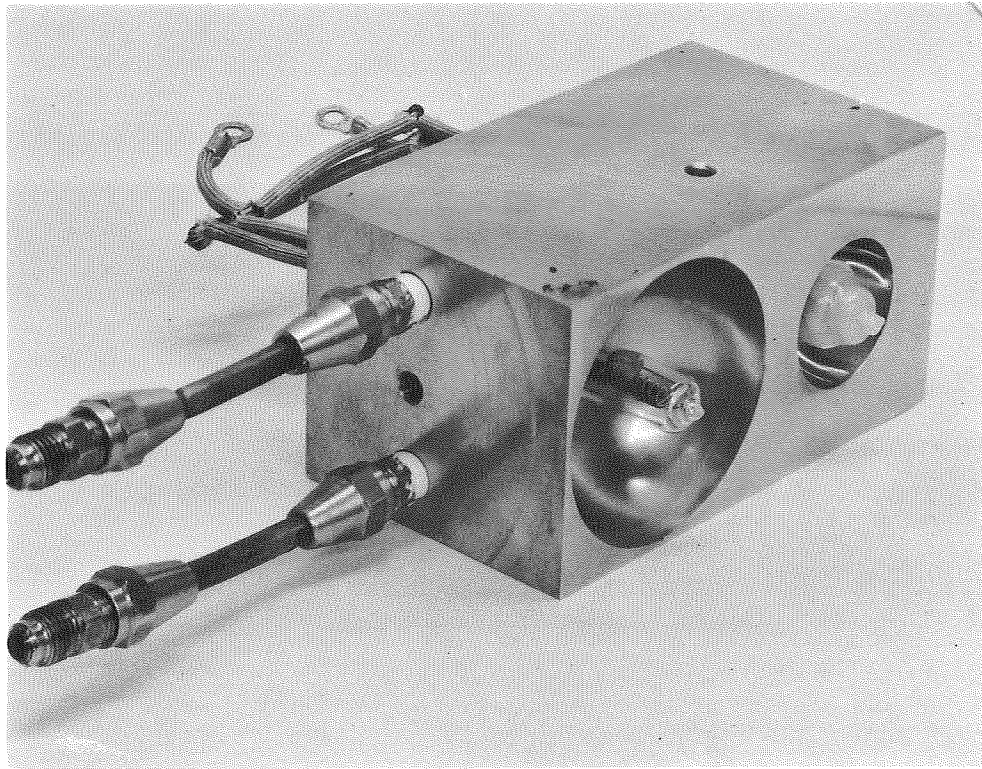


FIGURE 41. TWO-LAMP MODULE FABRICATED AT SOLAR

A 2-lamp module was fabricated at Solar in which one lamp reflector duplicated the 1-1/2 inch diameter configuration of the commercial module; the second reflector had an outside diameter of 2-1/2 inches and was designed both to minimize the reflection of rays from the filament through the quartz envelope and to submerge the filament completely within the module body. This module, after 40 hours of test at 100 volts and a target temperature of 1700°F, is shown in Figure 41. The lamp envelope in the 1-1/2 inch reflector is almost completely devitrified, whereas the other lamp showed no evidence of any change.

A single-lamp module having a 2-1/2 inch reflector was fabricated at Solar and testing was started using an as-furnished lamp. The lead wires burned off at the base seal in 52 hours and the lamp fell into the target while the filament was still hot. The next test used a T4 quartz tube lamp modified at Solar by brazing solid nickel leads to the pins at the lamp base seal. This lamp endured 600 hours at temperature in vacuum and additional testing in air for a total of 1994 hours. (The single-lamp life test report is included as Appendix D.) The test was terminated when a low-resistance bridge of tungsten crystals was formed due to mass transfer resulting from cycle failure. The envelope in the immediate area of the hot spot softened and bulged. This lamp had a design rated life of 500 hours at 120 volts in air ambient conditions.

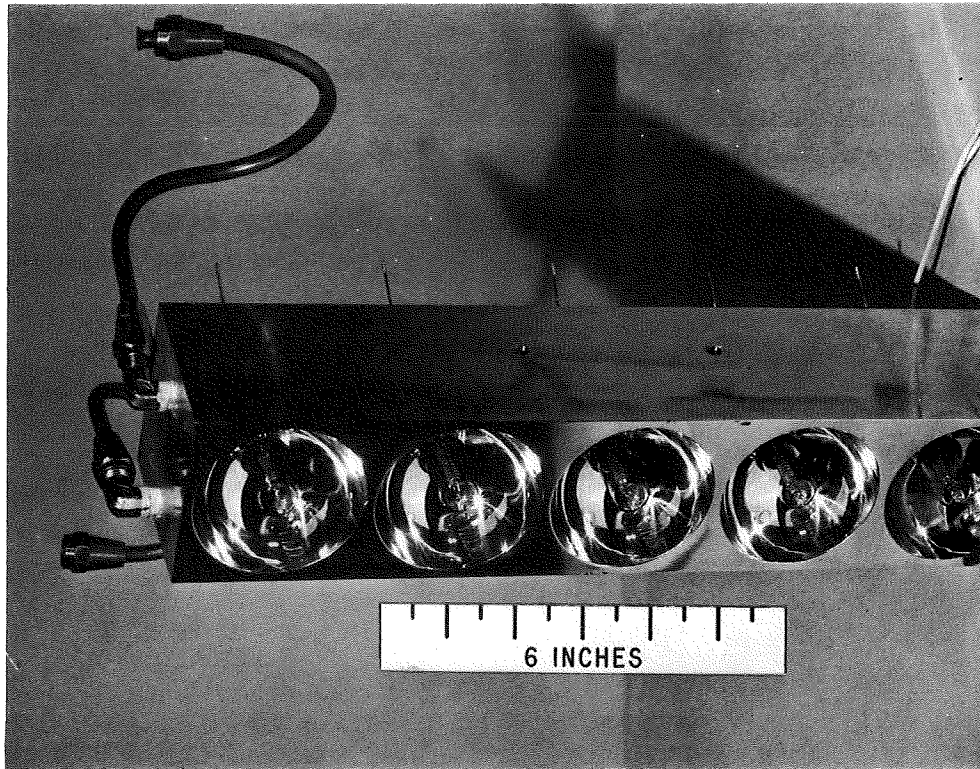


FIGURE 42. FIVE-LAMP MODULE FABRICATED AT SOLAR

Two 5-lamp modules (Fig. 42) were fabricated at Solar; one was set-up in a vacuum chamber, and the second similarly set up for operation in air. The Inconel 600 targets were coated with SE-8A to simulate the heat exchanger design. Some of the many lamp modifications tested are shown in Figure 43.

The first 5-lamp module after 45 hours in the vacuum chamber using as-received T4 lamps is shown in Figure 44. The lamps were potted in a ceramic base and fitted with Teflon-insulated, stranded-nickel leads spot welded to the lamp pins. One lamp failed when the lead-wire to lamp-pin joint burned. Lamp pins were platinum-clad molybdenum which had a tendency to oxidize during spot welding thereby causing a high resistance joint. A dull appearance of the reflector surfaces was caused by contaminants generated by decomposing lead wire insulation as well as products leaving the surface of the SE-8A coating on the target. (The SE-8A coating contamination of the lamp reflector resulted in no coating being used with the heater.) Unfortunately, additional tests were required before all sources of contaminants were identified. Note also in Figure 44 that lamp-reflector concentricity was a problem.

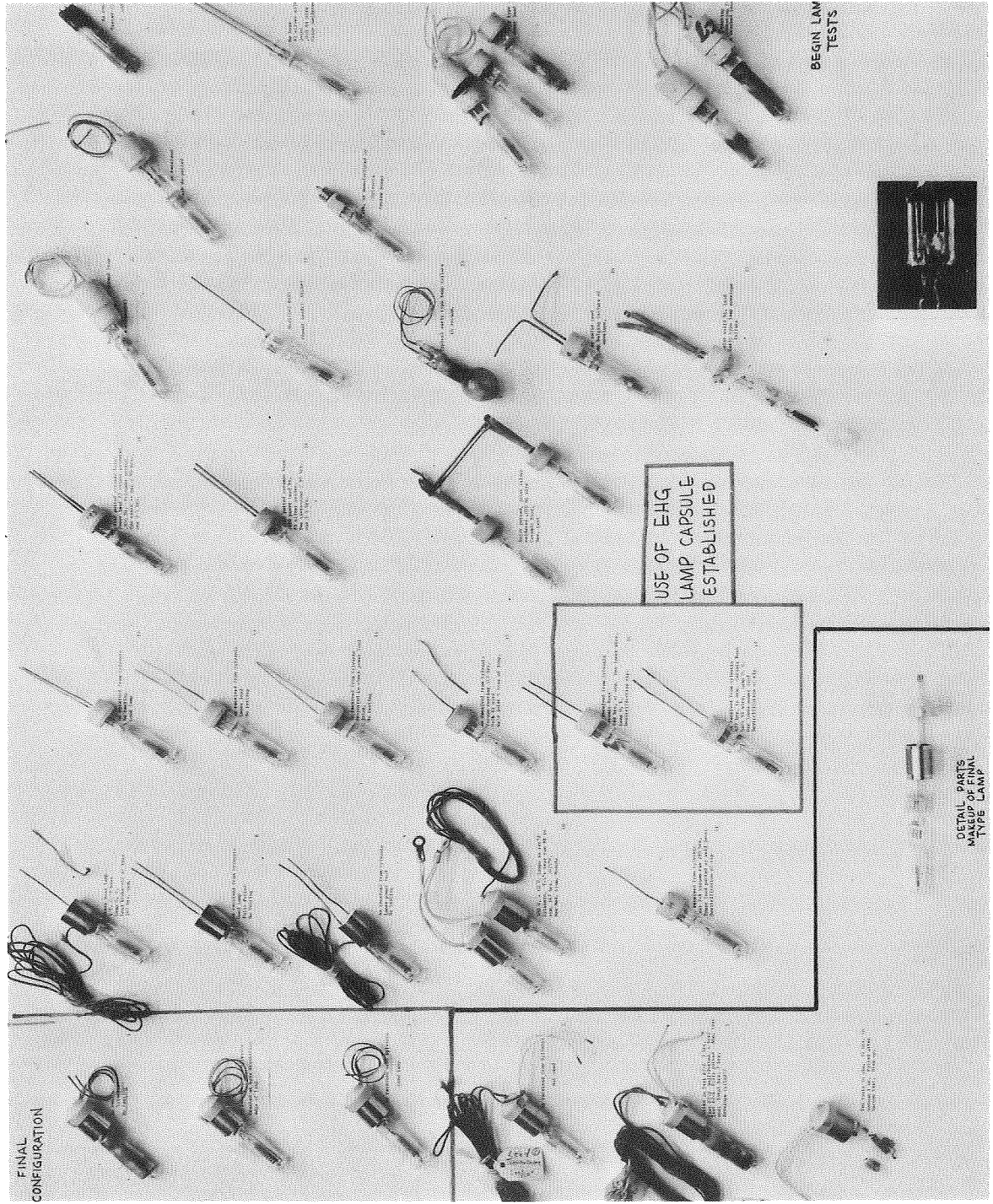


FIGURE 43. TYPICAL LAMP MODIFICATIONS TESTED

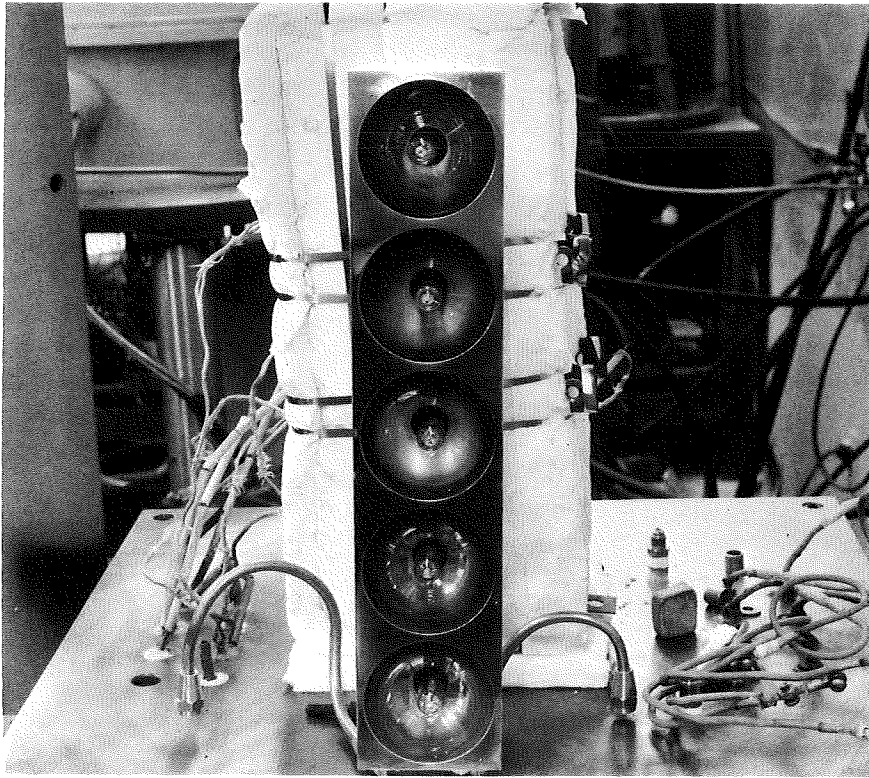


FIGURE 44. FIVE-LAMP MODULE AFTER TEST

Subsequent tests performed on a 5-lamp module in the vacuum chamber are summarized in Table V; Table VI is a summary of the tests conducted in an air environment. Figures 45 through 48 are typical of the lamps used in these module tests and include both the T5 and T4 capsules. The particles in the T4 quartz envelope (Fig. 45) are iodine crystals. Voids in the base seal potting were a problem throughout the program and a typical void is shown in Figure 46. However, two ceramic base T5 lamps ran 1060 hours in vacuum and helped establish confidence in the final lamp configuration. Five final configuration lamps (Fig. 48) ran more than 1000 hours in air. Both the vacuum and air tests were terminated due to near end of the contract.

6.4 FINAL CONFIGURATION LAMP

The final configuration lamp fabricated by Sylvania is shown in Figure 49. The lamp is based on Sylvania's iodine cycle EHG capsule which is a 750-watt, 120-volt lamp in a T5 (5/8-inch dia) quartz envelope. At rated voltage this lamp has a color temperature of 3000°K and an average rated life of 2000 hours at 120 volts at normal room temperature.

TABLE V

SUMMARY OF THE FIVE-LAMP MODULE TESTS IN VACUUM ENVIRONMENT

Date	Hours	Target T (°F)	Volts	Remarks
Sept 4, 1968	55			Target was coated - shutdown to install new lamps and clean reflectors.
9,	--	1700	58	Started test of new T5 ⁽¹⁾ lamps in ceramic base.
11,	40.5	1590	82	Reflectors contaminated-cleaned reflectors and removed coating from target.
17,	25	1638	85	Lost 1 lamp at 3 hours; base at 1590°F.
30,	265	1560	83	4 lamps have 44 additional hours - cleaned.
Oct 21,	590	1690	60	Removed module from bell-jar - Installed air module.
24,	25	1695	68	1 FC ⁽²⁾ leads burned at 79 hours in air plus 25 hours in vacuum - excess potting - seal at 1150°F.
Nov 6,	306	1660	71.5	In vacuum on FC lamp plus 79 in air = 385 hours. Add 754 hours in air for ceramic base lamps = 1060 hours.
12,	92.5	1660	71.5	3 new FC lamps and 2 new ceramic base lamps.
Dec 11,	696	1687		On 2 FC lamps.
	80			On 1 FC (repeated at 616 hours).
	85			On 2 ceramic base lamps (replaced at 616 hours).
30,	1032	1710	78	On 2 FC lamps.
	416			On 1 FC lamp.
	421			On 2 ceramic base lamps.
Stopped Test				
1. 750-watt T5 in ceramic base; nickel wire spot welded to molybdenum pins and then potted.				
2. Final configuration lamps.				

TABLE VI

SUMMARY OF THE FIVE-LAMP MODULE TESTS IN AIR ENVIRONMENT

Date	Hours	Target T (°F)	Volts	Remarks
Sept 13, 1968	45	1700	82	New T5 ⁽¹⁾ in ceramic base - 870°F seal temperature - coated target.
17	147	1665	84	895°F seal temperature - clean reflectors
30	450	1638	85	Reflectors contaminated - tips divitrified - target coating removed.
Oct 3	575	1660	82	Ceramic base seal 700°F - brass base seal 275°F ⁽²⁾ .
15	673	1660	85	Brass base lamp removed - installed 3 new FC ⁽³⁾ lamps.
21	752	1695	80	2 ceramic base lamp - 685°F base seal temperature - moved air module to vacuum bell-jar.
	79			3 FC lamps - 450°F base seal temperature - moved air module to vacuum bell-jar.
29	18.5	1620	59	5 T4 FC base type lamps - top base seal temperature 932°F - bottom 830°F - lead 320°F (base test)
Nov 4	160	1630	63	5 new lamps - complete final configuration
12	152	1660	76	5 new FC lamps.
Dec 20	1007	1705	78	Stopped test.

1. 750-watt T5 in ceramic base; nickel wire spot welded to molybdenum pins and then potted.
2. Similar to final configuration lamp except has brass sleeve.
3. Final configuration lamps.

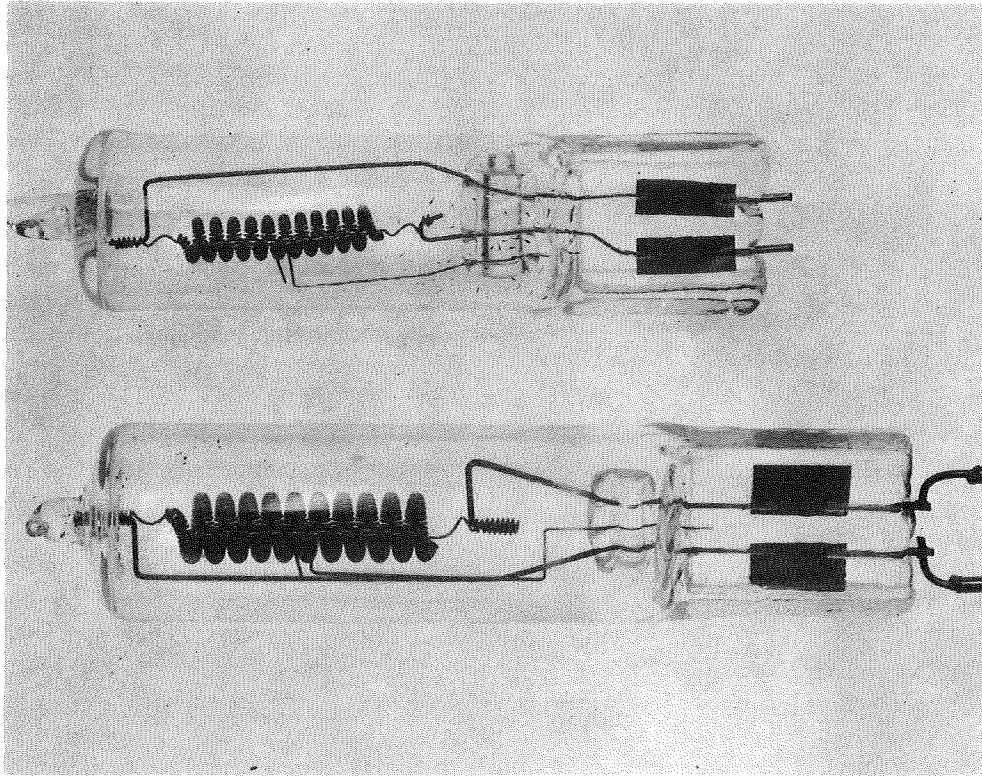


FIGURE 45. COMPARISON OF THE FINAL 750-WATT T5 LAMP AND A SPECIAL DESIGN 300-WATT T4 LAMP

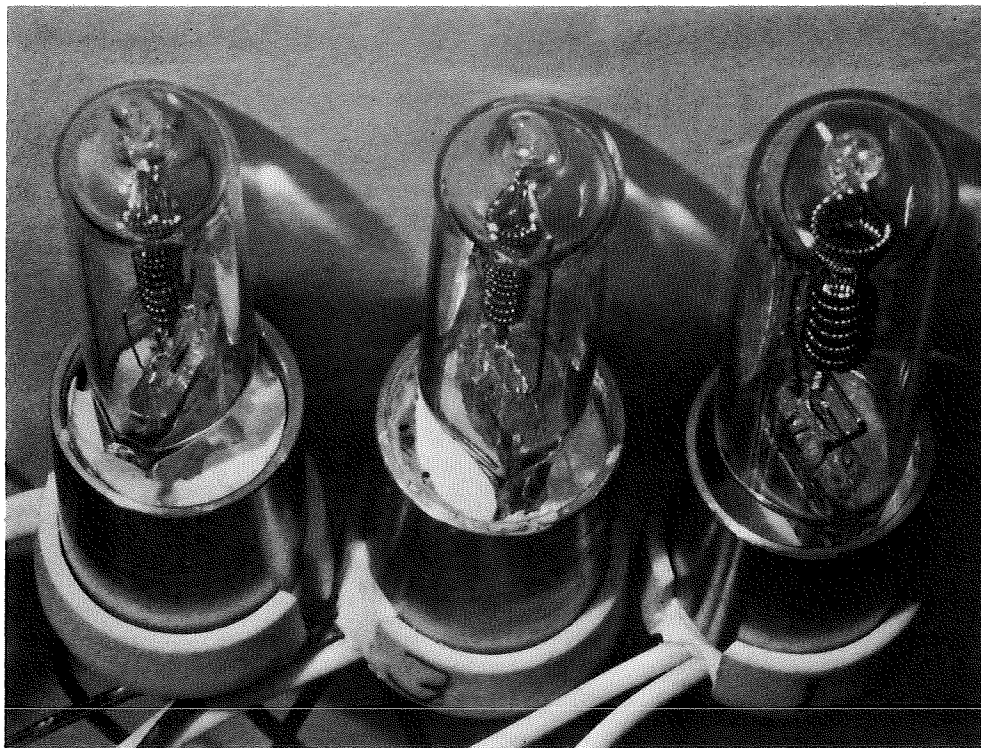
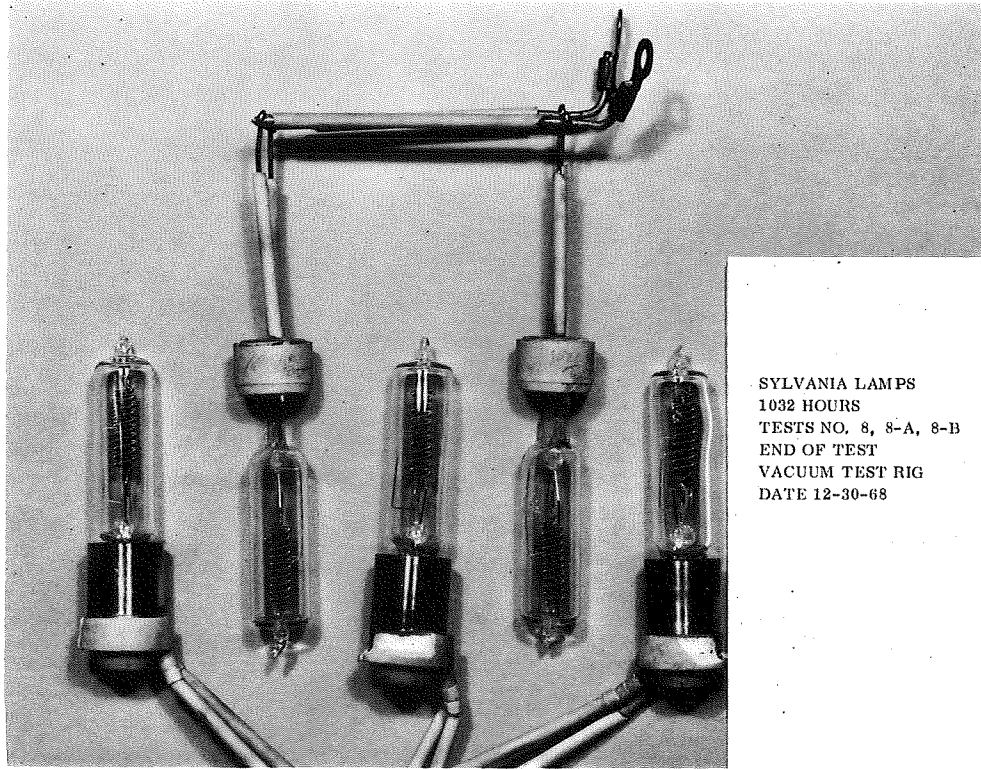
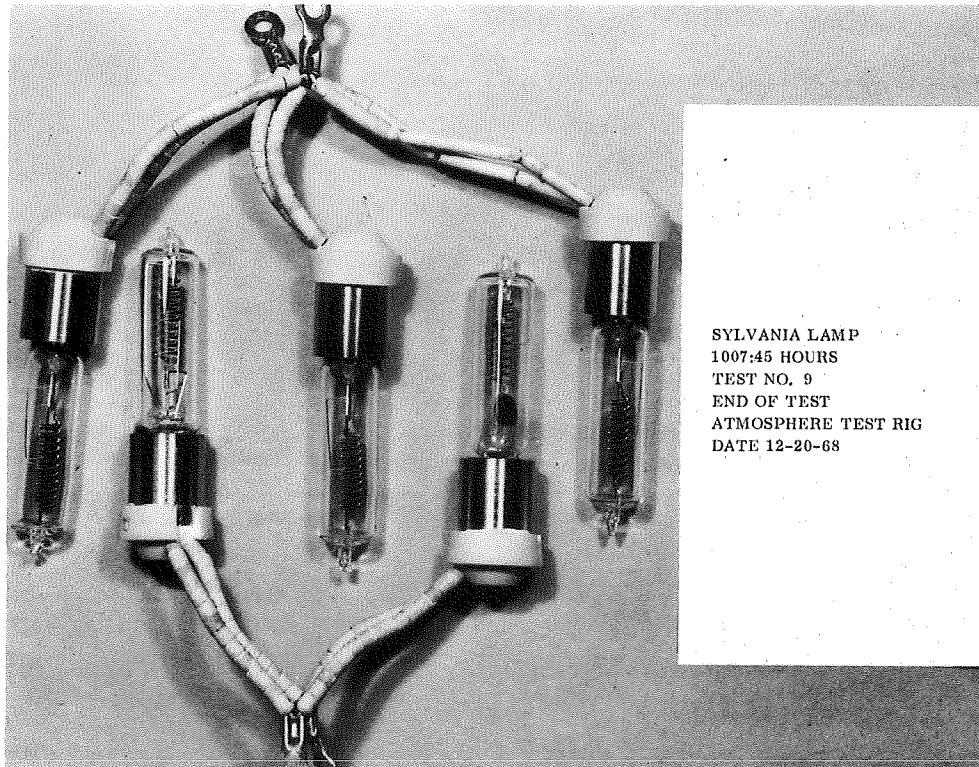


FIGURE 46. TYPICAL VOIDS IN BASE SEAL POTTING



SYLVANIA LAMPS
1032 HOURS
TESTS NO. 8, 8-A, 8-B
END OF TEST
VACUUM TEST RIG
DATE 12-30-68

FIGURE 47. SYLVANIA LAMPS AFTER 1032-HOUR VACUUM TEST



SYLVANIA LAMP
1007:45 HOURS
TEST NO. 9
END OF TEST
ATMOSPHERE TEST RIG
DATE 12-20-68

FIGURE 48. SYLVANIA LAMPS AFTER 1007-HOUR ATMOSPHERE TEST

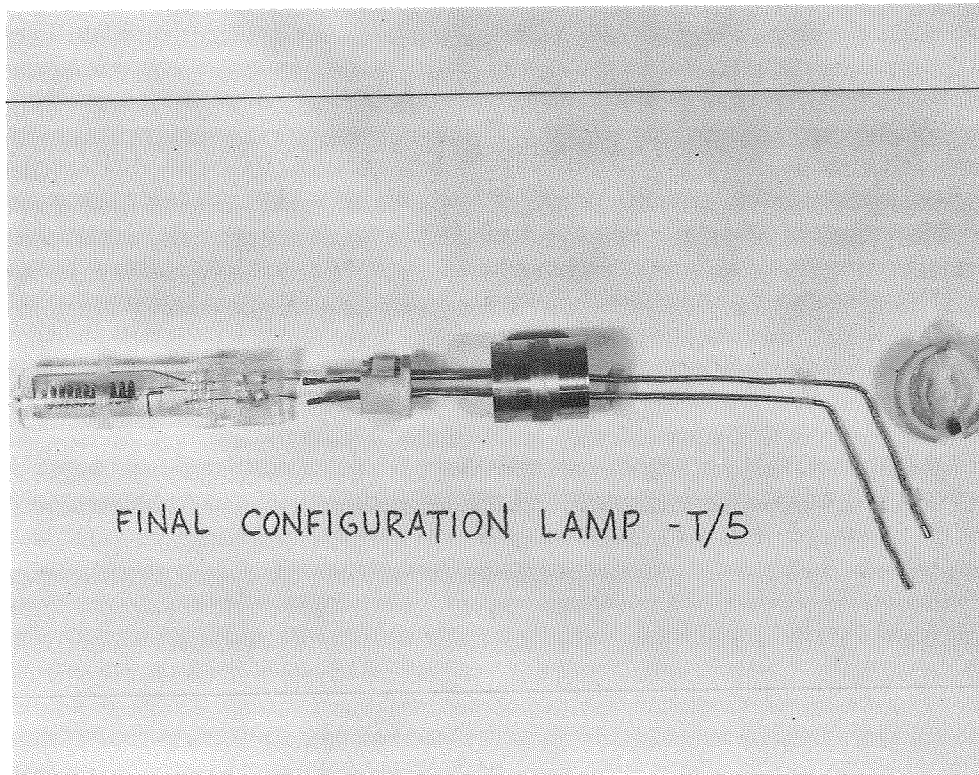


FIGURE 49. FINAL CONFIGURATION LAMP

The capsule is potted into Sylvania's "Trans-Lux" base arrangement using Sauereisen 31. Components include a 0.750-inch OD stainless steel sleeve, ceramic cap, and stranded bare-nickel lead wires spot welded to the platinum-clad molybdenum pins which protrude from the capsule. Unplated copper lugs were staked to the nickel leads to facilitate connection to the buss bars in the lamp modules.

As stated previously, the lamps shown in Figures 47 and 48 were used in the final vacuum and air environment tests. Only three final configuration lamps were on hand and hence two ceramic base lamps were used to fill out the complement in the vacuum test. Two of the three final configuration lamps had accumulated 1032 hours of operation during this test. All five of the final configuration lamps used in the air test had accumulated 1007 hours.

All lamps used in both tests had operated at 76 to 80 volts, a target temperature of 1700°F, and were still in operating condition. Time did not allow the tests to run to failure; therefore life expectancy of the final configuration lamp was not determined.

6.5 LAMP MODULE DESCRIPTION

The heater consists of 12-lamp modules fabricated by Aerometrics. (A list of their drawings is included as Table VII.) The body of the lamp module (Fig. 50) is made from 6061 aluminum stock with 24 modified spherical reflectors, 2-1/2 inches in diameter by 1-inch deep machined into the face. A 1/4-inch diameter cooling water passage was drilled through the entire 61.44-inch length of the lamp module on each side of the lamp holes and cross-drilled and weld-plugged as necessary for continuity. A cross section of the module is shown in Figure 51.

The lamps are installed from the back (or outside) of the lamp module after removing the cover. The 0.750-inch OD stainless steel sleeve on the lamp base fits into the 0.755-inch OD hole in the module and the ceramic cap bottoms out on the flat surface at the back of this hole. This close fit is intended to promote the transfer of heat from the lamp base. The electrical leads are attached to copper buss bars which run the length of the module. Teflon is used as insulating material. The perpendicular member on the inside of the aluminum cover allows expansion while retaining the lamps.

TABLE VII

LIST OF AEROMETRICS DRAWINGS

Drawing Number	Description
1005250	Body
1005253	Insulator, Teflon
1005265	Cover
1005266	Buss Bar
1005276	No Drawing Generated
1005283	Assembly, 24-Lamp Module
1005283	Clamp, Center, Teflon
1005284	Clamp, End, Teflon

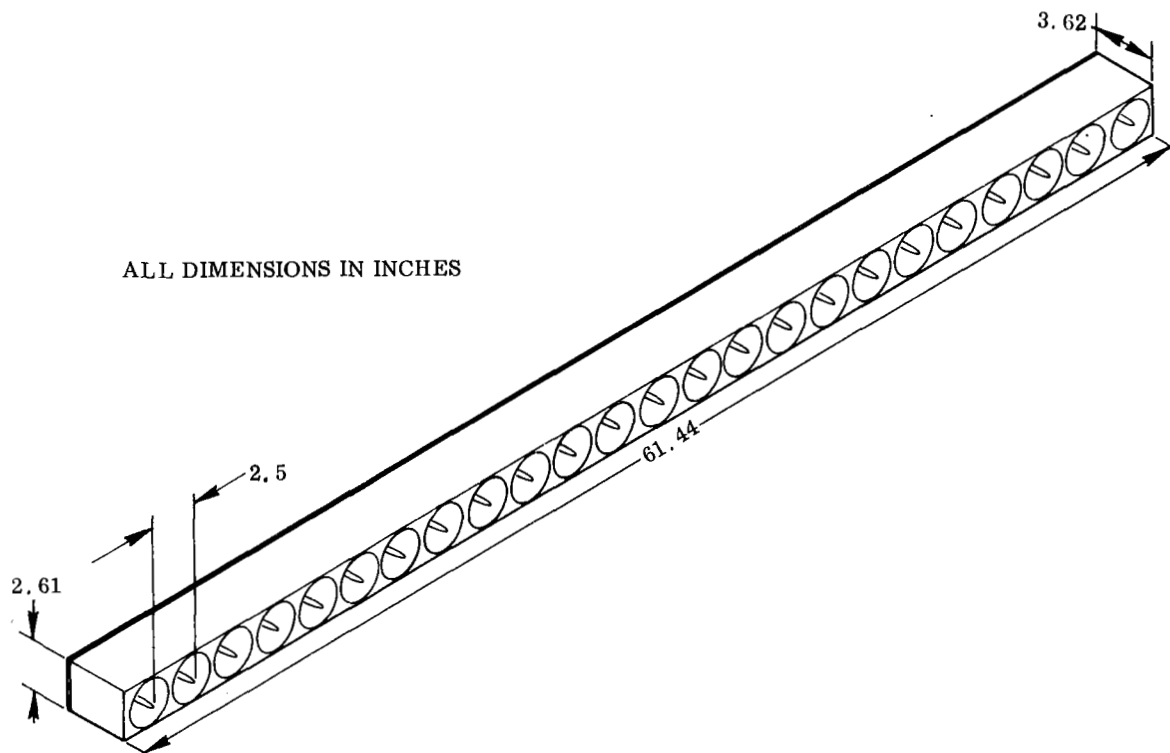


FIGURE 50. LAMP MODULE

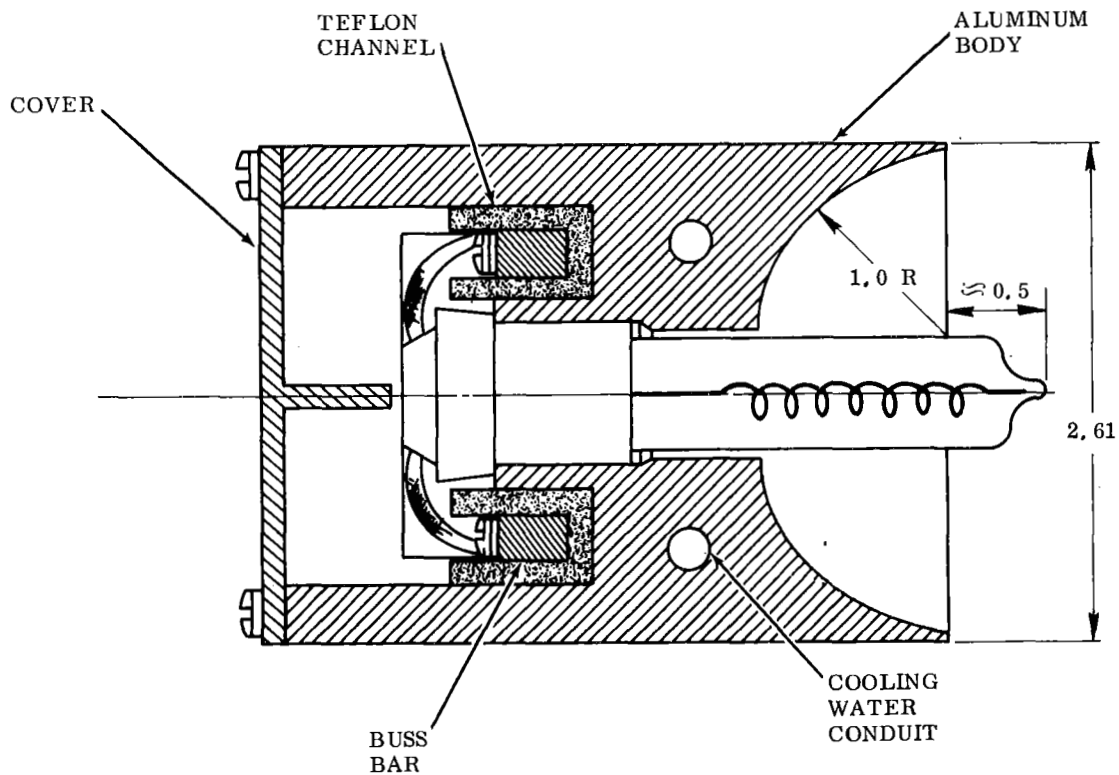


FIGURE 51. CROSS SECTION OF LAMP MODULE

6.6 DESCRIPTION OF THE IODINE CYCLE

The following brief statements describe the operation of the tungsten filament, iodine cycle, quartz tube lamp:

- Quartz temperature must be below 1832°F for the iodine vapor to pick up condensed tungsten; 1832°F is also the quartz devitrification threshold. Quartz temperature must exceed 480°F for the iodine-tungsten reaction to take place and prevent tungsten deposition on the quartz.
- Filament temperature must be above 2240 to 3140°F (investigators disagree) to dissociate the tungsten halide, allow the tungsten to deposit on the filament, and the iodine to continue the cycle. The filament will fail when the crystalline deposits change its resistance significantly.
- The filaments must be hotter than 2240°F to prevent rapid attack by the iodine vapor which happens when the tungsten-iodine cycle does not function.

6.7 OPERATING CONDITIONS

If all 288 lamps are operating and consuming 120 kw (the rated capacity of the control system), the power input to the average lamp will be 416 watts. As shown in Figure 52, the corresponding operating voltage is 83. Figure 52 also shows that the operating voltage corresponding to a filament temperature of 3140°F (3600°R), dissociation temperature for tungsten halide, is 38. Operation below this value is not recommended. Finally, it should be noted that the quartz envelope temperature must not exceed 1832°F, the theoretical value at which devitrification starts; the filament operating temperature at 80 volts is 4100°F; and a portion of the lamp view angle sees a U-tube plane that has a 1700°F design temperature. The module water must cool the reflector surfaces in addition to cooling the lamp bases.

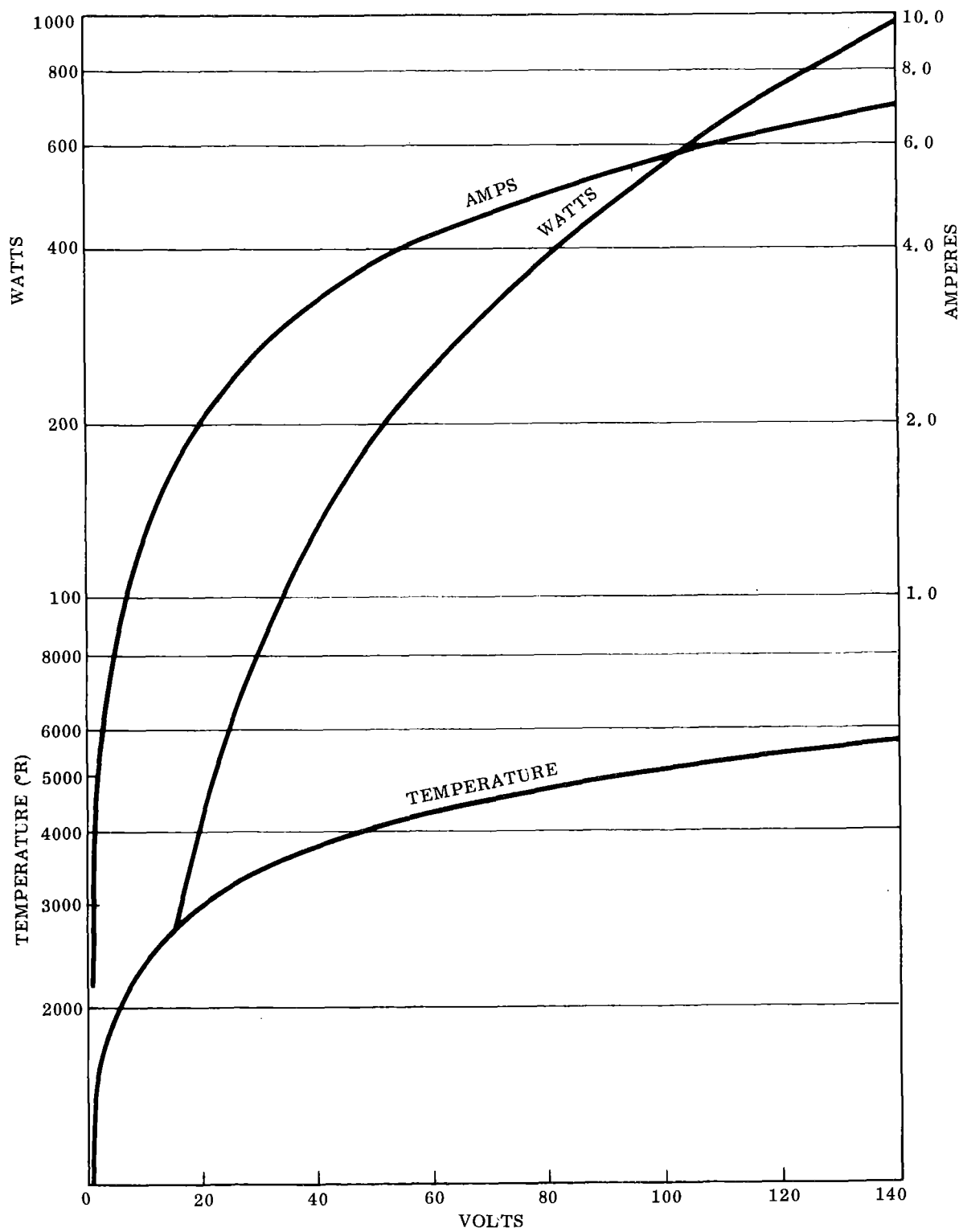


FIGURE 52. AMPERES, WATTS, AND AVERAGE FILAMENT TEMPERATURE VERSUS OPERATING VOLTAGE

7

SURFACE COATING

Early deliberations indicated that the prime heat exchanger surfaces should have a surface coating:

- To provide high surface absorptivity and thereby reduce the power requirements.
- To equalize the heat exchanger performance between air and vacuum operation.
- To minimize the loss of chrome and manganese from the heat exchanger surface during vacuum operation.

7.1 COATING SELECTION

Of all the coatings which had the proper characteristics, a Solar-developed, high-emittance coating, SE-8A, was selected for evaluation. This coating was developed under AFML Contract AF33(615)-76-C-1211 for use on superalloy reentry and hypersonic vehicle heat shields.

Although the function of the coating was to efficiently radiate absorbed energy, Kirchoff's law of radiation in a small wave length interval states that if the emittance is high, the absorptance must be high. It was assumed, therefore, that SE-8A would be a high absorptance coating since the λ for maximum energy radiation varies only from 2.310 microns at 1800°F to 1.074 microns at 4400°F (a typical tungsten filament operating temperature).

7.2 COATING DESCRIPTION

SE-8A is a silica-base ceramic coating which adheres to the oxides (chromium oxide, etc.) on the surface of the substrate. It must be applied in a thickness of 1 to 2 mils and fired at 1850°F in air or in argon. The composition of this coating includes:

<u>Parts</u>	<u>Addition</u>	<u>Purpose</u>
40	TiO ₂	Active
0.02	Nb ₂ O ₅	Active
60	S5210	Frit
6	Clay	Binder
65	Water	Vehicle

7.3 COATING TESTS

Solar's experience with SE-8A prior to the conduct of this program included many hours of use in jet engine combustion chambers (an oxidizing atmosphere) and a few hours of use in vacuum where the significant emittance data were obtained. Accordingly, tests were run in the Research Laboratories at Solar to fill the information gaps and determine the suitability of SE-8A for the specific application. These tests included:

- As-fired absorptivity (control) - determine surface absorptance of coated Inconel 600 specimens as-fired in air and in argon over the wave length band of 0.3 to 8.5 microns. (Most of the tungsten filament energy is radiated in the wave band between 0.3 and 3.5 microns.)
- Thermal stability - determine absorptance and coating weight loss of both types of specimens after exposure to 100 hours at 1800° F and a vacuum level of 10^{-6} Torr.
- Thermal cycling - determine absorptance and appearance of both types of specimens after 20 thermal cycles between 300 and 1700° F in vacuum over 100 hours.

A summary of the test results are as follows:

- Absorptivities were above 0.9⁽¹⁾ in the region of interest.
- The argon-fired surfaces were smoother than the air-fired surfaces.
- The weight loss for both types of specimens appeared to level off with time. Weight loss for the air fired specimens was somewhat greater.
- Argon firing was recommended.
- A 1000-hour thermal cycling test with weight measurements at 200-hour intervals was recommended to better establish the shape of the weight loss curve with time.

The 1000-hour test was conducted but proved to be inconclusive because coating spall occurred in the pattern of the grid on which the specimens were fired. Therefore,

1. The Radiant Energy Transfer Group, Space Science Laboratory, General Dynamics-Convair, under the direction of Dr. J. T. Neu measured the spectral reflectance of specimen surfaces over a range of wave lengths. Solar converted these measurements to absorptance.

a second 1000-hour test was run with uncoated, single-coated, and double-coated specimens. The results from this test were:

- Instead of a slow, steady, weight loss due to vaporization of chromium and manganese as expected, the uncoated specimen exhibited almost no weight change.
- After 240 hours of exposure, spalling was observed on the double-coated specimen; after 846 hours, 78 percent of the original coating weight had been lost.
- Up to 846 hours of exposure, the single-coated specimen had a coating weight loss of only 6.6 percent and this value had been constant for the last 700 hours. Upon completion of the test at 1014 hours, the coating had spalled with a weight loss of 65 percent.
- The spall was probably due to either crystallization of the coating forming cristobalite which is the equilibrium phase of silica at the test temperature or due to the loss of bond as a result of vaporization of chromium oxide from the interface.

Since the SE-8A coating did not satisfactorily endure 1000 hours of exposure, the coating was deleted.

7.4 COATING PERFORMANCE DURING HEATER MODULE TESTS

To simulate actual operating conditions during the heater module tests, the lamps "looked at" Inconel 600 targets that had been coated with SE-8A. After the major difficulties had been resolved, it was noticed that the water-cooled reflectors accumulated contaminants at a decreasing rate for the first 150 hours of target operation. X-ray diffraction analysis, determination of the most volatile of the coating constituents, and examination of the coating weight loss test results, all pointed to a single source. Oxides of potassium, sodium, and lithium (in that order) were probably leaving the 1-1/2 mil thick coating and depositing on the cooled reflectors.

7.5 EFFECT ON PERFORMANCE OF DELETING THE COATING

The effect of deleting the surface coating on thermal performance was investigated by Ray Burns of NASA LeRC. His analysis is included as Appendix B.

REFERENCES

1. Kays, W. M. , "Convective Heat and Mass Transfer"; McGraw Hill (1966) p. 173.
2. Kreith, F. , "Principles of Heat Transfer"; International Textbook (1958) pp 346-7.
3. Berggren, L. , Stress Analyses of The Brayton Cycle Gas Heating System, Task II - Detail Design; Solar Report M-1981 (August 1968).
4. Weil, N. A. , et al. , "Analysis of U-Shaped Expansion Joints", ASME Journal of Applied Mechanics (March 1962) p. 115.
5. Duffy, T. E. , NASA Brayton Cycle Radiant Gas Heating System; Control System Analysis, Solar Report M-1973 (April 1968).
6. Evans, D. M. , et al. , NASA Brayton Cycle Gas Heating System; Task II, Detail Thermal Design, Solar Report M-1974 (August 1968).

APPENDIX A

NASA REVIEW OF SYSTEM THERMAL DESIGN

REVIEW OF BRAYTON CYCLE GAS HEATING SYSTEM THERMAL DESIGN⁽¹⁾
(In Response to Reference 6)

By

Raymond K. Burns
Lewis Research Center

SUMMARY

The conservation equations describing the heat transfer within the exchanger were presented. The solution procedure used by Solar was outlined in order to indicate the approximations made in their analysis. The effects of these approximations on the final results were then discussed.

It was concluded that because of radiation exchange between the various surfaces of the enclosure and of reflections of the radiation emitted by the lamps, and because of transfer of heat across the dividing shield between the inlet and outlet sides of the tube bundle, the actual flux and temperature distributions will be smoother than those calculated by Solar. The tube wall temperatures should then more closely approach the desired isothermal condition than the results of their analysis indicate. The approximations made all appear to be conservative assumptions. However, because of these approximations it was not necessary to actually perform a complete radiation analysis of the enclosure. The analysis is therefore incapable of indicating whether or not hot spots will develop anywhere within the exchanger. Also the analysis is valid only for blackened tubes.

-
1. This review was made before the decision to eliminate the high absorbtivity coating on the gas tube surfaces. Appendix B includes further discussions of the effect of tube surface absorbtivity on temperature distributions.

CONSERVATION EQUATIONS

Given the required input and output gas temperatures, the gas properties, and the flow rate, a heat exchanger using an array of radiant heat sources can be described by the following equations:

A heat balance on a tube from inlet ($x = 0$) to a position x , yields,

$$\int_0^x q(x) dx = wc_p (T_g(x) - T_g(0)) \quad (1)$$

where $q(x)$ is the net heat input rate to a tube per unit length.

A heat balance on an incremental length of tube yields,

$$q(x) dx = h(x) 2\pi r dx (T_w(x) - T_g(x)) \quad (2)$$

The local heat transfer coefficient, $h(x)$, can be evaluated from a correlation of experimental results in the form,

$$h(x) = f(T_w(x), T_g(x)) \quad (3)$$

Finally the net heat input rate to the tubes per unit length, $q(x)$, is determined by performing a radiant heat transfer analysis of the entire enclosure. The resulting distribution of $q(x)$ depends on the arrangement of radiant heat sources and power input to them; on the entire enclosure geometry; and on the surface conditions and boundary conditions imposed upon each surface of the enclosure. It should be noted that $q(x)$ can vary from tube to tube.

Equations (1) to (3) and the radiation analysis of the enclosure can then be used to determine the unknown quantities, $T_w(x)$, $T_g(x)$, $h(x)$, and $q(x)$. Two boundary conditions imposed on the system of equations are

$$T_g(0) = T_{g \text{ in}} \quad (4)$$

$$T_g(L) = T_{g \text{ out}} \quad (5)$$

where L is the length of the tubes. Substituting equations (4) and (5) into equation (1) yields:

$$\int_0^L q(x) dx = wc_p (T_{g \text{ out}} - T_{g \text{ in}}) \quad (6)$$

In this particular case, the tube length, L , has also been specified so that equation (6) provides a constraint on the distribution $q(x)$. Finally, it is required that

$$T_w(x) \leq 1700^\circ\text{F} \quad (7)$$

The heat exchanger geometry and power input to the radiant heat sources must be such that equations (6) and (7) are satisfied.

Equations (1) and (2) can be rearranged to obtain more convenient forms,

$$T_g(x) = T_g(0) + \frac{1}{wc_p} \int_0^x q(x) dx. \quad (1a)$$

$$T_w(x) = T_g(x) + \frac{q(x)}{2\pi r h(x)} \quad (2a)$$

Equations (1) and (2) assume the following:

1. Negligible heat transfer resistance of the tube walls in the radial direction.
2. Negligible heat conduction in the axial direction.
3. The quantities $q(x)$, $h(x)$, and $T_w(x)$ are assumed to be circumferentially averaged quantities, and $T_g(x)$ is the local bulk temperature of the gas.

SOLUTION OF THE CONSERVATION EQUATIONS

Equations (1) to (3) and the radiant heat transfer analysis of the enclosure are coupled and must therefore be solved simultaneously. The required gas flow length can be minimized by maintaining the tube wall temperature distribution at a constant value close to the allowable maximum of 1700°F . This can be accomplished by arranging the radiant heat sources so that the net heat input rate to the tubes varies exponentially. This is the approach taken by Solar. In summary, the heat exchanger must

be designed to yield a variation of $q(x)$ which is as close to exponentially decaying as possible, which satisfies equation (6), and which yields a solution of equations (1) to (3) for which the temperatures of the enclosure do not exceed 1700°F .

SOLAR'S SOLUTION PROCEDURE

The analysis made by Solar did not include all of the coupling between the radiant transfer analysis and equations (1) to (3) and therefore yields an approximate solution. Their approach will be briefly outlined in order to indicate the assumptions and the effects of these assumptions on the solution obtained.

Solar assumed that the $q(x)$ consists only of the absorbed fraction of the radiation which is directly incident on the tubes from the radiant heat sources. This assumption neglects:

1. All inter-reflections of radiation within the enclosure.
2. All radiation exchange between the tube surfaces and other parts of the enclosure.

The first implicitly assumes that the effective absorptivity of the tube bundle and the shield behind it is unity and that the effect of the end walls of the enclosure is negligible. The second assumes that all nonadiabatic surfaces of the enclosure are at the same temperature.

In addition it was assumed that the dividing shield between the inlet and outlet sides of the U-tube bundle is an adiabatic surface. This simplifies the radiation analysis by allowing independent consideration of each side of the exchanger. The results obtained, however, show that this is not an adiabatic surface.

All surfaces and the radiant heat sources were assumed to be diffuse.

An estimate of the validity of these assumptions and the effect on the results can be obtained by considering the final results. This will be discussed in the next section.

With these assumptions the $q(x)$ distribution was determined for various arrangements of the radiant sources until one was found which satisfied equations (6) and (7). During this design process it is necessary to determine the tube wall temperature in order to check the requirement of equation (7).

The method used by Solar, which involves calculating a fictitious β and determining a temperature limit line, has no valid basis. It consists of calculating a fictitious β by solving the following equations:

$$hpL \Delta T_{\log} = \frac{q_o}{\beta} (1 - e^{-\beta L})$$

$$q_o = hp (T_w - T_{g \text{ in}})$$

using $T_w = 1700^\circ\text{F}$. This is equivalent to solving for β using:

$$e^{-\beta L} = \frac{T_w - T_g(L)}{T_w - T_g(o)}$$

and the required $T_g(L)$ and $T_g(o)$ values. Then using this value of β , the curve

$$q = q_o e^{-\beta x}$$

is supposed to represent a limit line which must not be crossed by the actual $q(x)$ distributions if the tube wall temperature is to be kept below 1700°F . That this cannot be true can be seen by considering equations (1a) and (2a). The value of $T_w(x)$ is a function not only of $q(x)$ but of its integral with respect to x . The tube wall temperature at a point x depends not only on $q(x)$ at that point but on the entire distribution up to that point. It cannot then be stated that T_w has a certain value at x when $q(x)$ crosses any specific curve at point x . This procedure appears however to have been a satisfactory tool in their design process because the actual $q(x)$ distribution did not significantly depart from an exponential variation. If the entire calculations had been performed on a digital computer it would have been as easy and more desirable to use equations (1a) and (2a) to check the requirement of equation (7).

Since the T_w distribution was actually calculated by Solar after the radiant source arrangement was finalized, the discussion of this fictitious β procedure in the report was unnecessary.

SOLUTIONS OBTAINED BY SOLAR

The overall heat balance for each case considered by Solar shows that the net heat input to the system equals or exceeds that required to heat the gas to the specified outlet temperature. The system losses were calculated using the maximum

allowable enclosure temperature and are therefore conservative. If, however, the tube surface emissivity were lower so that a significant fraction of the radiation incident on the tubes is reflected back to the water cooled lamp modules this calculation of radiation losses should be reexamined.

The remaining question is whether or not the 1700°F maximum temperature will be exceeded anywhere in the exchanger. According to the temperature distributions presented in the Solar report, the temperature maximum is not exceeded in any of the cases considered. The temperature and flux distributions presented however, clearly reflect the assumptions made in the radiation analysis of the enclosure. If radiation interchange between the enclosure surfaces and interreflections of the radiation emitted by the lamps had been included, the net flux to the tubes would not vary as rapidly with distance as those shown in Figure 25 of the Solar report. The neglect of radiation interchange and interreflections is also shown by the temperature distributions shown in Figure 33 of the report. The variations in temperature indicated would be reduced by radiation exchange between the tube surfaces and other parts of the enclosure. Because of the large insulated surface in the plane of the radiant sources, the overall view factor between any two positions along the tubes may be quite significant. There would then be a significant exchange of energy between different points on the tubes and the temperature distributions would be more uniform than those shown in Figure 33.

For the cases shown in Figures 33c and 33d the temperatures indicate that there will also be a net heat transfer across the dividing shield between the inlet and outlet sides of the U-tube bundle, and therefore the temperatures will be further equalized throughout the exchanger.

These factors which have been neglected in the radiation analysis all would tend to make the enclosure temperatures more uniform than the results presented in the Solar report would indicate.

As stated previously, it was assumed that $T_w(x)$ was a circumferentially averaged quantity. Since the heat input rate $q(x)$ actually will vary around the circumference of a tube, there will be an induced circumferential temperature distribution. Solar made some calculations of this circumferential distribution in order to check the possibility that tube surface temperature may somewhere exceed 1700°F when the average is below that limit. However, the applicability of the circumferential flux distribution used in that calculation is very questionable. The calculations, however, indicate that this circumferential variation of temperature is probably small except near the tube inlet.

MODULE FLUX DISTRIBUTION TEST

The assumption was made that the radiant sources are diffuse. Solar measured the angular distribution of flux from a module and showed that it approached being diffuse. The results shown in Figure 15 and 16 of the report, however, are presented in a misleading manner. More information could be obtained from such a comparison if both curves were normalized with respect to the same quantity (such as the total flux output of a module). At any position, x , a direct comparison could then be made between the actual module flux and the prediction made using the diffuse assumption.

APPENDIX B

EFFECTS OF TUBE SURFACE ABSORPTIVITY

THE EFFECTS OF TUBE SURFACE ABSORPTIVITY ON THE THERMAL
PERFORMANCE OF THE BRAYTON CYCLE GAS HEATING SYSTEM⁽¹⁾

By

Raymond K. Burns
Lewis Research Center

ABSTRACT

A simple model was used to determine the sensitivity of the thermal performance of the heat exchanger to a decrease in the gas tube surface absorptivity. This model was necessary to include the effects of interreflections and radiation exchange within the enclosure. These factors become significant when the tube bank surface does not approximate a black surface, and they were not included in the design analysis performed by Solar. The results show the qualitative variation of tube surface temperature and flux with absorptivity with all other factors held constant. They also indicate the effect of heat transfer across the U-tube bank dividing shield and the areas of the exchanger where high temperatures may become critical.

-
1. This analysis was performed for the early 16-lamp module radiant source configuration presented in Reference 6; however, the trends are valid for the 24-lamp module configuration.

INTRODUCTION

The radiation analysis performed by Solar assumed that the net flux to the tubes could be approximated by the absorbed fraction of the radiation which is directly incident on the tubes from the heat sources. This neglects all inter-reflections within the enclosure and all radiation exchange between the tube surfaces and other parts of the enclosure. Because of these assumptions the analysis performed by Solar is, in one respect, conservative since radiation which could reach the tube bank by reflection from the insulated enclosure walls is neglected and since radiation initially reflected from the tube bank is assumed not to return. The total energy leaving the lamps then exceeds the sum of the total energy absorbed by the tube bank and the losses from the system. In other words the Solar analysis does not include a complete heat balance for radiation energy. But because reflections and radiation exchange have been neglected, the analysis of Solar may not be conservative in its estimates for tube wall temperatures.

As a result of the assumptions, the distribution of net flux to the tubes in their analysis is a direct function of the radiant heat source arrangement i. e. , the net flux at a particular point is a function only of the geometric view factor from that point to the lamp modules. For a tube bank which is close to being black, the effects of reflections are small and the desired exponential heat flux distribution can be maintained by arranging the radiant sources according to an analysis such as Solar's. However when the absorptivity of the tubes is reduced and reflected radiation becomes significant, the procedure used by Solar becomes inadequate since the reflections could significantly alter the net heat flux distribution to the tubes. Including the effects of inter-reflections and radiation exchange considerably complicates the radiation analysis because of the coupling between various points on enclosure surfaces. If the tube bank is divided into n nodal areas, it is necessary to solve n simultaneous nonlinear equations to determine the flux distribution on the tube bank.

In order to obtain some information about the effect of tube surface absorptivity on the tube surface temperatures, solutions have been obtained for a simple model of the exchanger. The effects of reflections and radiation interchange are included by simultaneously determining the flux at several parts of the tube bank. One side of the exchanger was divided into either four or five nodes. The radiant heat sources were taken as one node and the insulated enclosure walls were taken as another. Either two or three nodes were then considered on the tube bank surface. They were considered simultaneously, including radiation exchange and reflections between them. By continually increasing the number of nodes, the model would approach the actual case and the radiation analysis would become more exact. It follows that the solutions which were obtained are the first approximations to the exact, complete radiation analysis including radiation exchange and inter-reflections.

In order to make the results obtained using this model correspond as closely as possible to the actual case, the area of the heat source node is taken as the actual total lamp module area. For each of the nodes considered on the tube bank, the geometric view factor to the modules was obtained from the calculations made by Solar. Also the gas temperature at each point considered in the tube bank plane was taken from the Solar calculations. Since the gas temperature is a function of the net heat flux distribution, it actually should be determined simultaneously with the radiation enclosure analysis. Since this was not done for the solutions presented here, they are not complete solutions, but are intended only to show the effect of tube surface absorptivity while all other factors are held constant.

As in the analysis made by Solar, the heat transfer across the dividing plane between the inlet and outlet sides of the U-tube bundle is neglected in order to permit independent analysis of the inlet and outlet sides of the exchanger. The effects of this assumption on the results will be discussed later. The effective absorptivity of the tube bank and the shield behind it was calculated in the same manner as in the Solar analysis.

The details of the formulation and solution procedure for the five node case are given in the Appendix.

RESULTS

The exchanger was designed by Solar to operate with a tube absorptivity of 0.9 or above. In order to approach a condition of constant tube wall temperature, the radiant heat sources were arranged to obtain a heat flux distribution to the tubes which decays exponentially in the flow direction. Factors not included in the Solar analysis, which would be expected to further equalize the tube wall temperature throughout the exchanger are radiation exchange between various parts of the enclosure and heat transfer across the dividing shield. When the emissivity of the tube surface is reduced, the role of reflection becomes more important and the effectiveness of radiation interchange in equalizing the temperatures is reduced. It follows that for a given arrangement of the radiant sources, the net flux distribution will vary with changes in the absorptivity of the tube surfaces. The purpose of this analysis is to estimate the extent of the variation of tube wall temperature when the tube surface absorptivity is reduced in the exchanger designed by Solar.

In Figure 1 the change in net flux as a result of reflections and radiation exchange is shown at various positions along the flow length as the tube absorptivity is decreased from 0.9. The locations at $X = 8.4$, 25.6 , and 42.7 are on the inlet side of the exchanger and the other three are on the outlet side. On both sides, the reflections of radiation cause a decrease in flux in the higher flux regions and an increase at the lower end. As expected, when the tube surfaces are made more

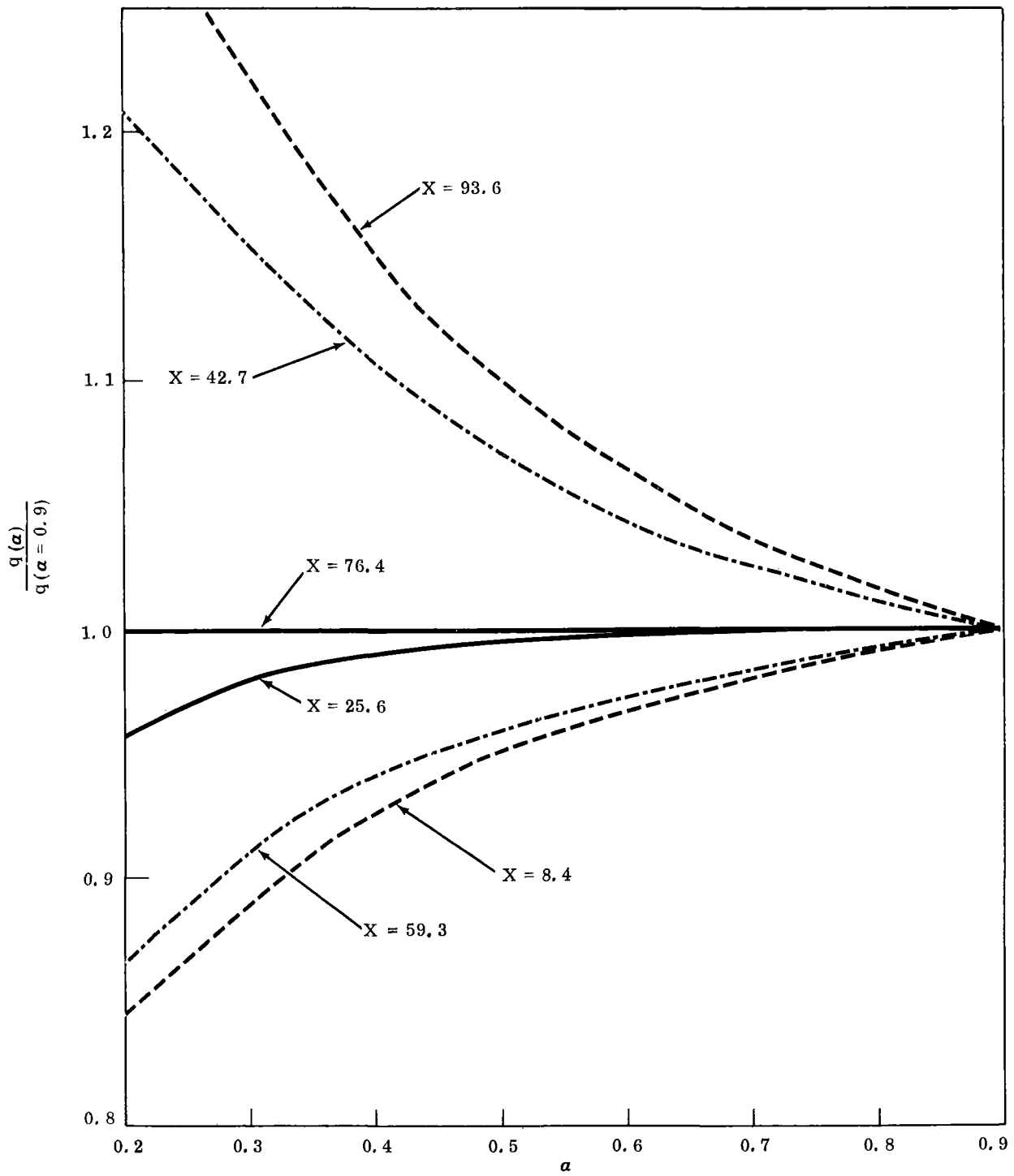


FIGURE 1. CASE II - He-Xe

reflective the flux distribution for a given radiant source arrangement becomes more uniform. If the exponential variation of the flux is to be maintained at lower tube absorptivities the radiant heat source arrangement would have to be changed.

The corresponding temperatures are shown in Figure 2. By considering the curves for each side of the exchanger, it is seen that the temperatures become more nonuniform as the absorptivity is decreased as would be expected from the consideration of the changes in the flux distribution. One of the assumptions made in the analysis was that the shield between the two sides of the U-tube bundle is an adiabatic surface. This obviously would not be true unless the shield was perfectly reflecting or unless the flux incident on each side of the shield was equal. Figure 2 shows that at the top portion of the exchanger the temperature difference between the tubes across this shield increases and at the bottom it decreases. As the tube surface absorptivity decreases it becomes more and more advantageous to allow heat transfer across this plane at the top of the exchanger. This would decrease the temperature at one of the hottest regions of the exchanger, the outlet region, and increase the temperature and input flux near the exchanger inlet. For this reason it would be advantageous to keep the effective surface absorptivity of this shield at the top of the exchanger as high as possible. One way to accomplish this would be to use a shield with a pattern of holes in it at the upper portion of the exchanger. Nearer to the bottom of the exchanger, the heat transfer across the shield is smaller and not as significant a factor.

In Figure 3 some temperature results are shown for the model which included two nodes on the tube bank. The curves show the same qualitative behavior as in Figure 2. A comparison of Figures 2 and 3 can be used to indicate the behavior as the number of tube plane nodes is increased. The indication is that the qualitative behavior shown in Figures 2 and 3 correctly predicts the behavior of a more exact or complete solution and that the amount of change in the tube surface temperatures increases toward the ends of the exchanger. It should be noted that the present model does not correctly account for the insulated end walls. The effect of these walls should be small except in the regions close to them.

In Figure 3 some points are shown for which the gas temperature was arbitrarily changed. In every case, the change in the tube surface temperature was smaller than the change in the gas temperature.

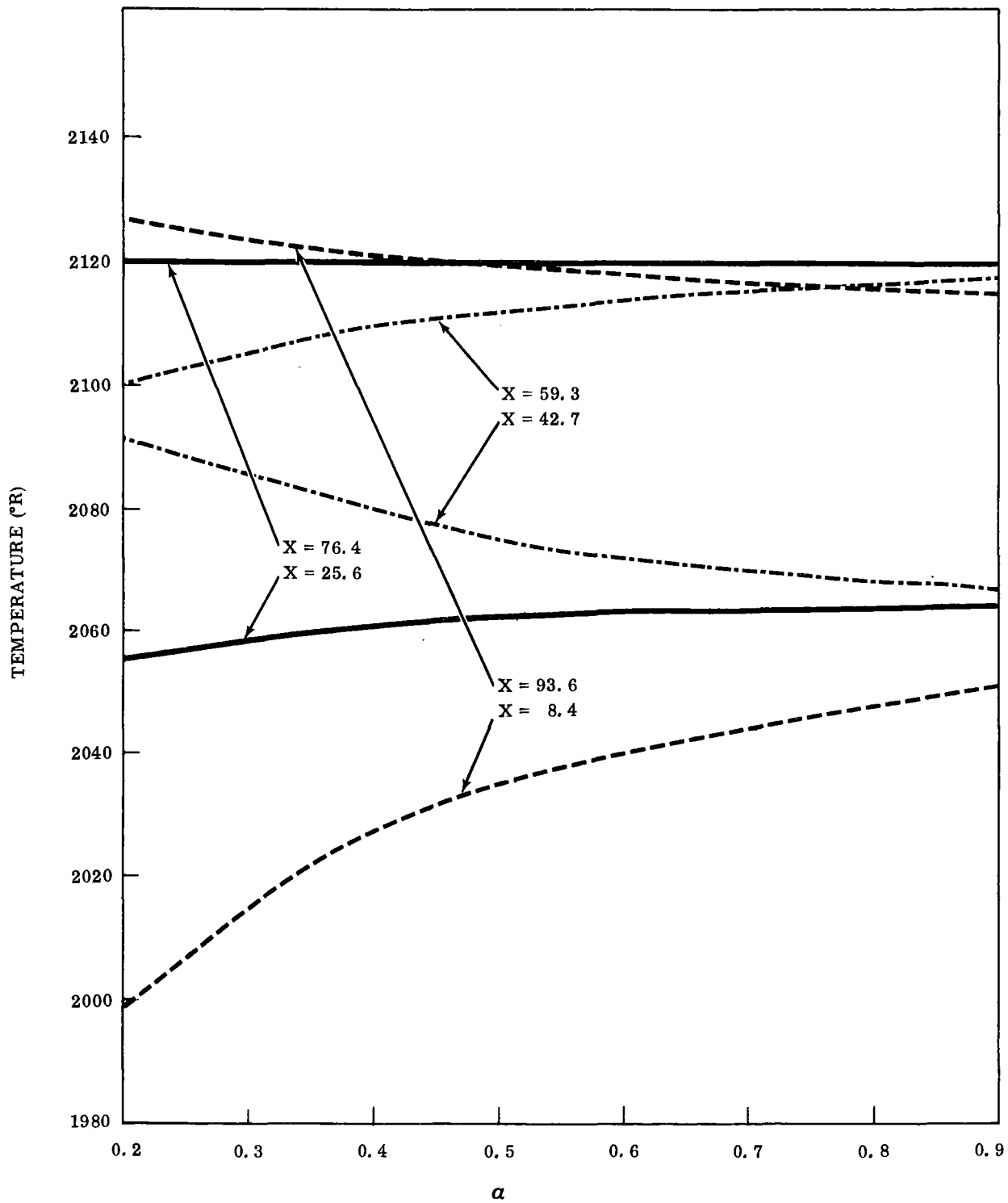


FIGURE 2. CASE II - He-Xe

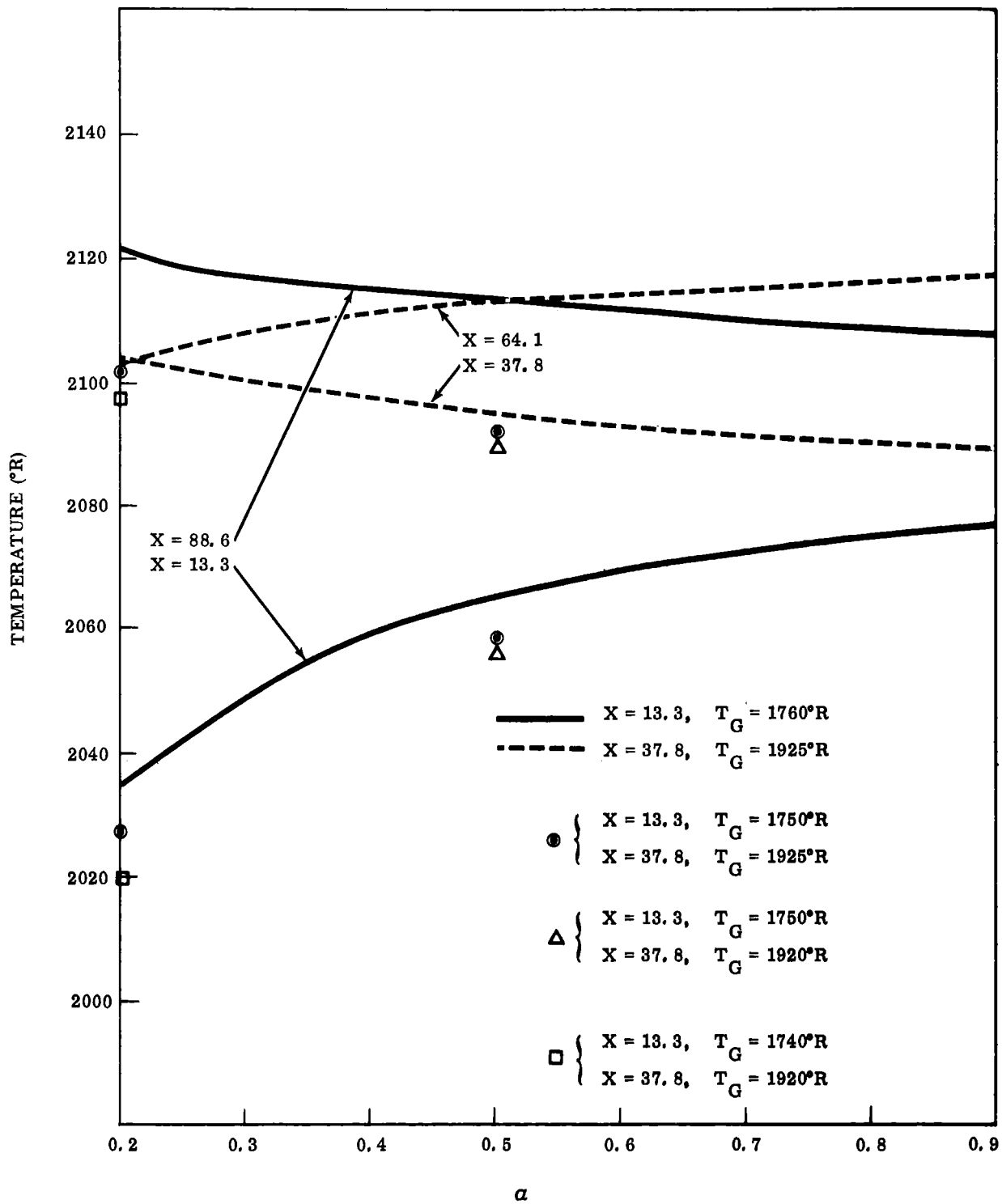


FIGURE 3. CASE II - He-Xe

CONCLUSIONS

Because of the limitations on the tube surface temperature, the temperature changes which are of most interest are those which increase. The increases indicated on the outlet side of the exchanger are small, and in the actual exchanger these temperatures, near the outlet, should be lower due to the heat transfer across the dividing plane, an effect which was not considered in this analysis. The increase in temperature shown on the inlet side, at the lower end of the exchanger, is however larger. The temperatures across the shield at this point will be at about the same level or slightly higher. The heat transfer across the shield at the bottom of the exchanger therefore will not help the conditions as it will at the top. This area will probably then become the most critical temperature region.

Figures 2 and 3 show that the temperature changes produced by reducing the tube surface absorptivity from 0.4 to 0.2 are about half that produced by reducing the absorptivity from 0.9 to 0.2. The thermal performance of the exchanger should therefore be much more sensitive to changes in absorptivity at values below about 0.4 than above. For this reason the tube surface absorptivity should be kept above about 0.4. The surface should also be diffuse in order to reduce the possibility of developing local hot spots.

As already stated, the heat transfer across the dividing shield is advantageous at the top of the exchanger. This is because the radiant heat sources are arranged in a manner such that the heat flux to the tubes near the inlet is below the desired exponential variation. This is even more so when the tube surface absorptivity is reduced and inter-reflections become more important. For this reason the absorptivity of the dividing plane surface or the effective absorptivity of the plane should be as high as possible in the upper part of the exchanger.

Because the required outlet gas temperature is so close to the maximum allowable tube wall temperature, the exchanger must operate close to the maximum temperature. If this maximum is not to be exceeded, the design must be accurate. Neither the analysis performed by Solar nor the present estimate of the effect of surface absorptivity on the performance attains the level of confidence required for such close design. It is only reasonable therefore that a sufficient number of thermocouples be installed to monitor the surface temperatures of the tube walls throughout the exchanger during the initial operation, both in air and in vacuum. An obvious part of the exchanger to be monitored closely is the outlet region. The present calculations show that with lower surface absorption, the lower end of the exchanger, especially on the inlet side, may be the most critical and should also be monitored closely.

APPENDIX

The formulation for the five node model is presented here for reference.

Node 1 represents the heat source and has an area equal to the actual total lamp module area on either side of the exchanger. Node 2 is assumed to be adiabatic and represents the insulated enclosure walls in the plane of the modules. Nodes 3, 4, and 5 represent three areas in the tube plane at three specific points along the tube length. The view factors from each of these nodes to the modules and the gas temperature at each node was obtained from the calculations made by Solar. The remaining view factors and node areas are obtained by requiring them to satisfy the reciprocity and sum rules of flux algebra. The results are:

$$F_{11} = 0$$

$$F_{12} = 0$$

$$F_{13} = F_{31} / (F_{31} + F_{41} + F_{51})$$

$$F_{14} = F_{41} / (F_{31} + F_{41} + F_{51})$$

$$F_{15} = F_{51} / (F_{31} + F_{41} + F_{51})$$

$$F_{21} = 0$$

$$F_{22} = 0$$

$$F_{23} = (1 - F_{31}) / \left[(1 - F_{31}) + (1 - F_{41}) + (1 - F_{51}) \right]$$

$$F_{24} = (1 - F_{41}) / \left[(1 - F_{31}) + (1 - F_{41}) + (1 - F_{51}) \right]$$

$$F_{25} = (1 - F_{51}) / \left[(1 - F_{31}) + (1 - F_{41}) + (1 - F_{51}) \right]$$

$$F_{31} = \text{Specified}$$

$$F_{32} = 1 - F_{31}$$

$$F_{33} = 0$$

$$F_{34} = 0$$

$$F_{35} = 0$$

$$F_{41} = \text{Specified}$$

$$F_{42} = 1 - F_{41}$$

$$F_{43} = 0$$

$$F_{44} = 0$$

$$F_{45} = 0$$

$$F_{51} = \text{Specified}$$

$$F_{52} = 1 - F_{51}$$

$$F_{53} = 0$$

$$F_{54} = 0$$

$$F_{55} = 0$$

$$A_1 = \text{Specified}$$

$$A_3 = A_4 = A_5 = A_1 / (F_{31} + F_{41} + F_{51})$$

$$A_2 = 3A_3 - A_1$$

Using this information and the emissivity of each surface, the Hottel or "over all" view factors are obtained. It is assumed that each surface is gray.

The heat balance on each node then yields, after algebraic rearrangement:

$$h' \left(T_3 - T_{G_3} \right) = A \sigma T_3^4 + B \sigma T_4^4 + C \sigma T_5^4 + D \quad (1)$$

$$h' \left(T_4 - T_{G_4} \right) = E \sigma T_3^4 + F \sigma T_4^4 + G \sigma T_5^4 + H \quad (2)$$

$$h' \left(T_5 - T_{G_5} \right) = K \sigma T_3^4 + L \sigma T_4^4 + M \sigma T_5^4 + N \quad (3)$$

where:

$$A = \frac{\tau_{32} \tau_{23}}{(\tau_{23} + \tau_{24} + \tau_{25} + \tau_{21})} - \tau_{31} - \tau_{32} - \tau_{34} - \tau_{35} \quad (4)$$

$$B = \frac{\tau_{32} \tau_{24}}{(\tau_{23} + \tau_{24} + \tau_{25} + \tau_{21})} + \tau_{34} \quad (5)$$

$$C = \frac{\tau_{32} \tau_{25}}{(\tau_{23} + \tau_{24} + \tau_{25} + \tau_{21})} + \tau_{35} \quad (6)$$

$$D = \frac{\tau_{32} \tau_{21} \left(\frac{q_1}{\epsilon_1} + \sigma_{T_1}^4 \right)}{(\tau_{23} + \tau_{24} + \tau_{25} + \tau_{21})} + \tau_{31} \left(\frac{q_1}{\epsilon_1} + \sigma_{T_1}^4 \right) \quad (7)$$

$$E = \frac{\tau_{42} \tau_{23}}{(\tau_{23} + \tau_{24} + \tau_{25} + \tau_{21})} + \tau_{43} \quad (8)$$

$$F = \frac{\tau_{42} \tau_{24}}{(\tau_{23} + \tau_{24} + \tau_{25} + \tau_{21})} - \tau_{41} - \tau_{42} - \tau_{43} - \tau_{45} \quad (9)$$

$$G = \frac{\tau_{42} \tau_{25}}{(\tau_{23} + \tau_{24} + \tau_{25} + \tau_{21})} + \tau_{45} \quad (10)$$

$$H = \frac{\tau_{42} \tau_{21} \left(\sigma_{T_1}^4 + \frac{q_1}{\epsilon_1} \right)}{(\tau_{23} + \tau_{24} + \tau_{25} + \tau_{21})} + \tau_{41} \left(\sigma_{T_1}^4 + \frac{q_1}{\epsilon_1} \right) \quad (11)$$

$$K = \frac{f_{52} f_{23}}{(f_{23} + f_{24} + f_{25} + f_{21})} + f_{53} \quad (12)$$

$$L = \frac{f_{52} f_{24}}{(f_{23} + f_{24} + f_{25} + f_{21})} + f_{54} \quad (13)$$

$$M = \frac{f_{52} f_{25}}{(f_{23} + f_{24} + f_{25} + f_{21})} - f_{51} - f_{52} - f_{53} - f_{54} \quad (14)$$

$$N = \frac{f_{52} f_{21} \left(\sigma T_1^4 + \frac{q_1}{\epsilon_1} \right)}{(f_{23} + f_{24} + f_{25} + f_{21})} + f_{51} \left(\sigma T_1^4 + \frac{q_1}{\epsilon_1} \right) \quad (15)$$

and

$$\sigma T_2^4 = \frac{\left(f_{23} \sigma T_3^4 + f_{24} \sigma T_4^4 + f_{25} \sigma T_5^4 + f_{21} \sigma T_1^4 + \frac{f_{21} q_1}{\epsilon_1} \right)}{(f_{23} + f_{24} + f_{25} + f_{21})} \quad (16)$$

In the above equations T_{G_i} is the gas temperature at node i and q_1 is the flux output of the heat source at node 1. The reflector temperature and emissivity at node 1 are specified. The heat transfer coefficients appearing in these equations have been modified to account for the difference in surface area between the actual tubes and the effective tube plane as follows:

$$h_1 = \frac{Ph}{C}$$

where h is the value calculated by Solar, P is the tube circumference and C is the tube bank pitch.

Equations (1) through (3) are rewritten as follows:

$$T_{3/i+1} = \left[\frac{h'(T_{3/i} - T_{G_3}) - B\sigma T_{4/i}^4 - C\sigma T_{5/i}^4 - D}{\sigma A} \right]^{\frac{1}{4}} \quad (1a)$$

$$T_{4/i+1} = \left[\frac{h'(T_{4/i} - T_{G_4}) - E\sigma T_{3/i}^4 - G\sigma T_{5/i}^4 - H}{\sigma F} \right]^{\frac{1}{4}} \quad (2a)$$

$$T_{5/i+1} = \left[\frac{h'(T_{5/i} - T_{G_5}) - K\sigma T_{3/i}^4 - L\sigma T_{4/i}^4 - N}{\sigma M} \right]^{\frac{1}{4}} \quad (3a)$$

and solved simultaneously by iteration.

APPENDIX C

HEATER MODULE LIFE TESTS - PROGRESS REPORTS

SOLAR

DIVISION OF INTERNATIONAL HARVESTER COMPANY
2200 PACIFIC HIGHWAY, SAN DIEGO, CALIFORNIA 92112

RESEARCH MEMORANDUM

R68H-1557-1 March 20, 1968

TO: T. L. Stockham (G-5)

cc: R. L. Neher
J. E. Benawa
Ref. File

From: 
R. L. Neher
Sr. Research Engineer, Ext. 732

SUBJECT: PROGRESS REPORT NO. 1 - HEATER MODULE LIFE TEST
Week Ending 3-18-68

Reference: Brayton Cycle Heater Program - S.O. 6-2933-7

General

This program is in initial planning and test equipment design stage only.

It should be noted that the D.P.E. dated 1/23/68 Desmon/Neher, was based on a module size of 3" x 8" x 12" with subsequent change to 9" x 10" x 16" in accordance with heat target drawing dated 3/8/68 by Marchese. Since the initial vacuum chamber selection was based on the smaller specimen size a new chamber will have to be procured or fabricated. We have located a chamber that will accommodate the new size but in-house research scheduling may not permit full five (5) month uninterrupted usage.

We are proceeding with a minimum usage of six (6) week anticipated as discussed with Stockham/Desmon by M. Gould.

Equipment Status To Date

1. Chamber Modification - Fabrication of base plate scheduled to start week of 3/18/68 pending receipt of material.
2. Heat Target - Test section received 3/15/68.
3. Power Source - (4) auto-transformers vari-ac available. Wiring and check out scheduled for week of 3/25/68 pending receipt of Heater Module.

RLN:cm

SOLAR

DIVISION OF INTERNATIONAL HARVESTER COMPANY
2200 PACIFIC HIGHWAY, SAN DIEGO, CALIFORNIA 92112

RESEARCH MEMORANDUM

R68H-1557-2

April 15, 1968

TO: T. L. Stockham (F-5)
L. G. Desmon (F-5)

From: R. L. Neher
Senior Research Engineer, Ext. 732

cc: J. E. Benawa
R. L. Neher
Ref. File

SUBJECT: PROGRESS REPORT NO. 2 - HEATER MODULE LIFE TEST
WEEK ENDING 4-12-68

Reference: Brayton Cycle Heater Program - S.O. 6-2933-7

Preliminary tests were conducted to verify system output characteristics during this report period. Total exposure at temperature was 3 hours and 15 minutes as shown in attached data sheet.

Test data from initial runs indicated low convection heat transfer from heat target area. Cooling radiator (fin) to be installed adjacent to the target area to provide additional cooling.

System checkout scheduled for week of 4/15 with subsequent start of Life Test if system check is satisfactory.

Figures 1 through 3, respectively, (attached) show (1) Test System Schematic, (2) Thermocouple Layout and (3) Power Source and Instrumentation Wiring Diagram.

RLN:cm

Attachments

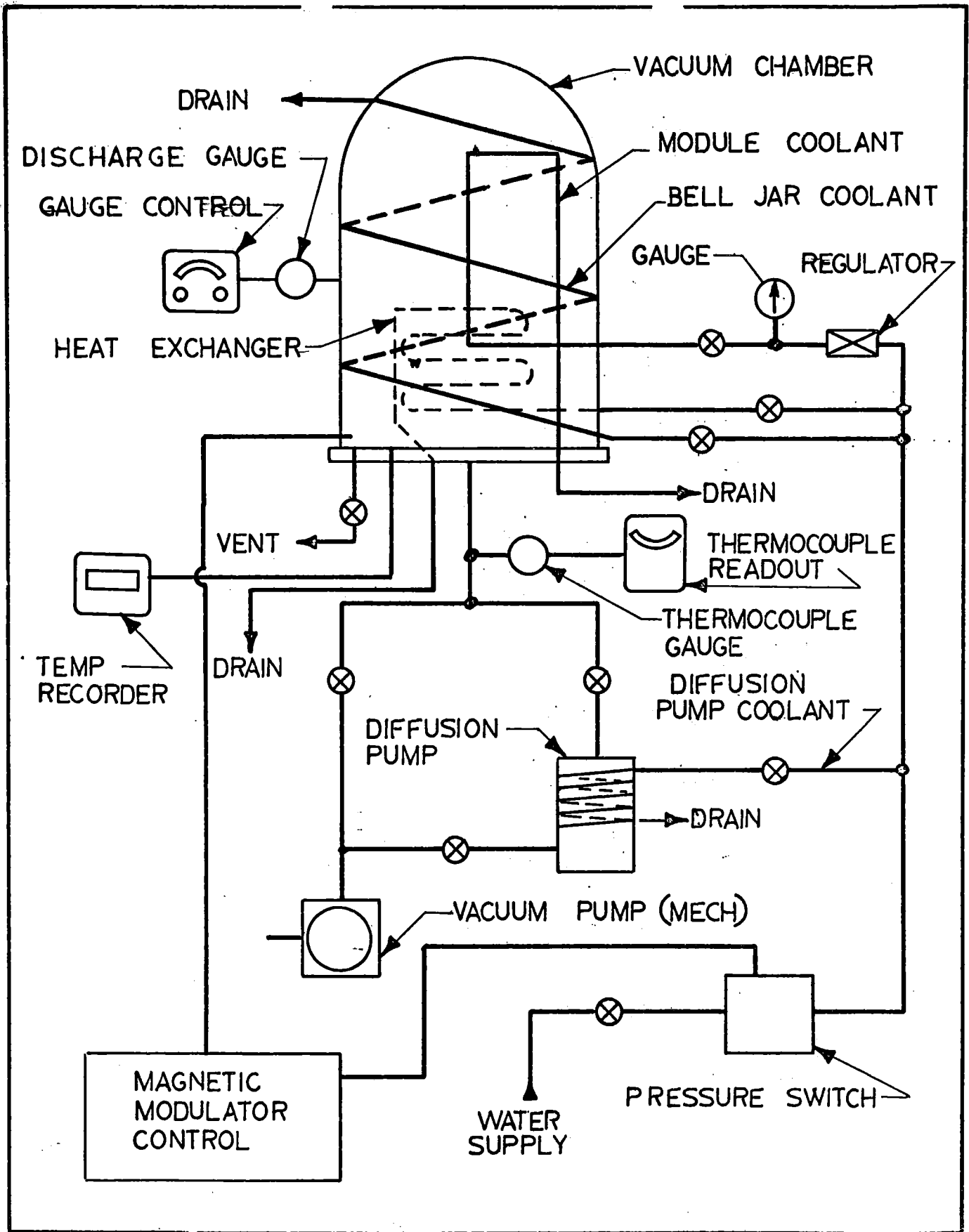


FIG. 1
TEST SYSTEM SCHEMATIC

LOCATION	T. C. NO.
INSULATION	1-6
TARGET	2-3-4-5
MODULE	9-10-11-12
COOLANT	7-8

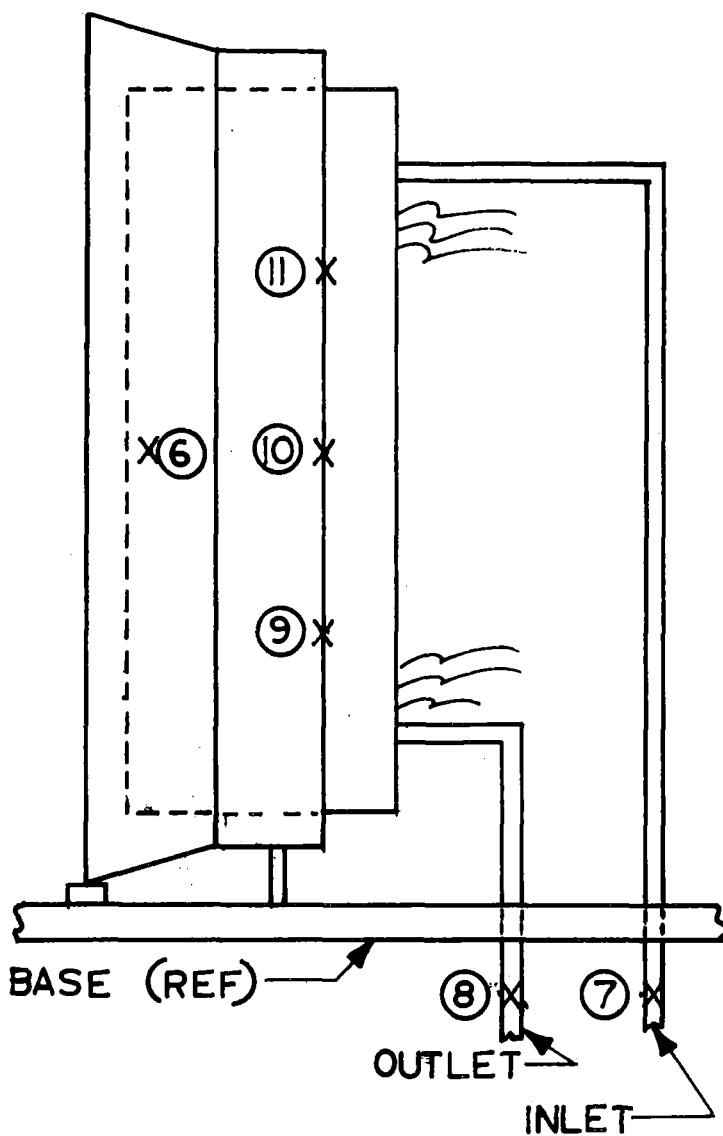
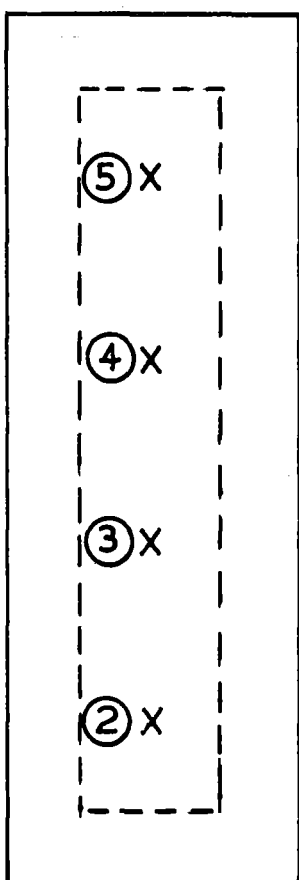
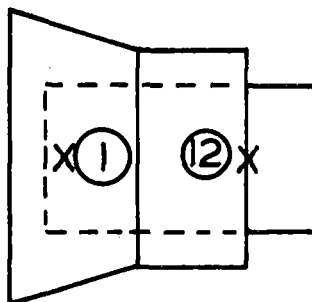


FIG. 2
THERMOCOUPLE LOCATIONS

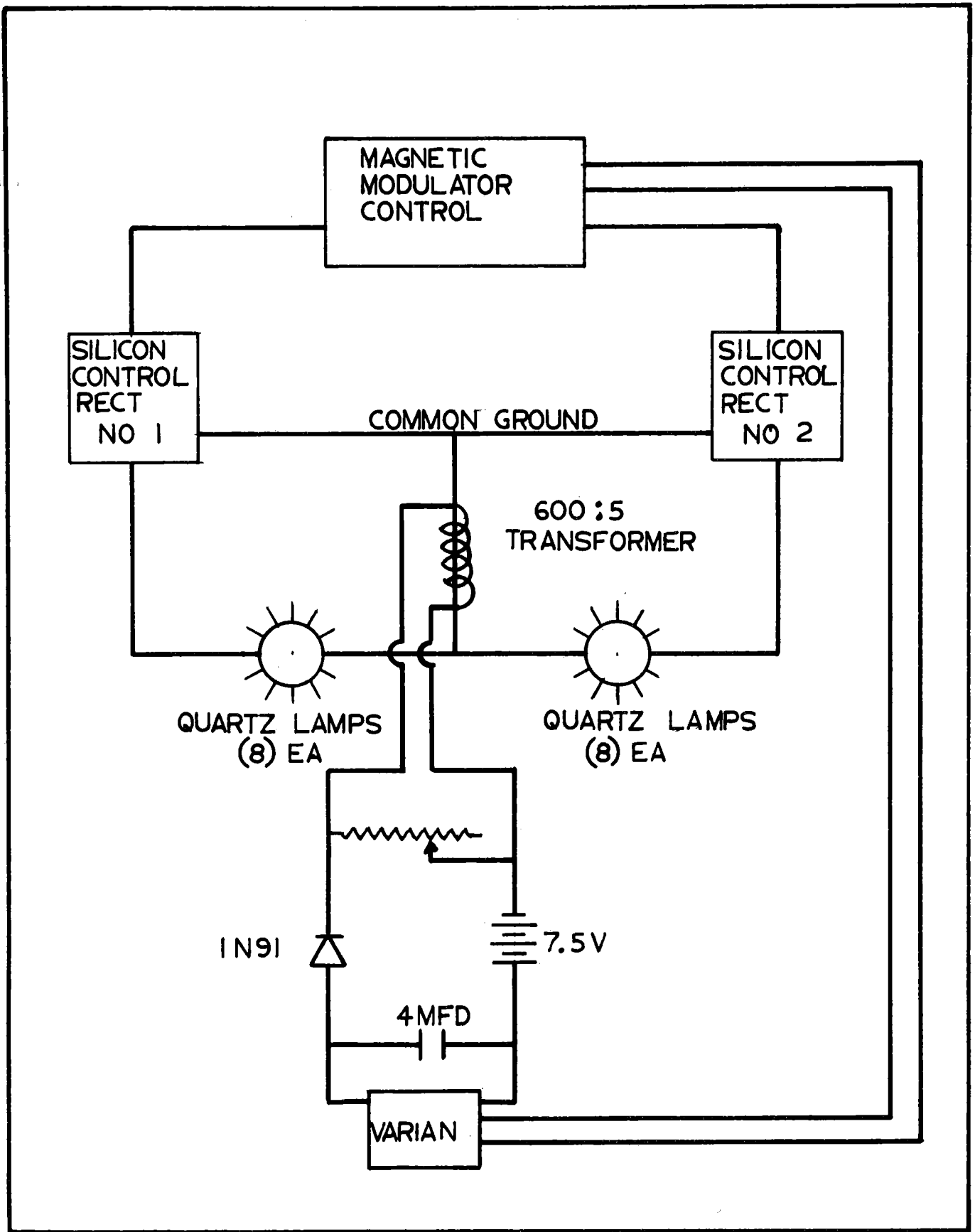


FIG. 3-A
POWER SOURCE SCHEMATIC

BRAYTON HEATER MODULE LIFE TEST

System Discussion

Power to lamps derived from 115V AC through SCR units, stepped down to required voltage. Voltage is variable through MMC from 0 - 115V AC. Max. current obtained from each SCR is 50A; test thus requires two SCR's as total current = 76A.

MMC has provisions for automatic shutdown by opening N.C. shutdown terminals.

Three protective devices are utilized:

1. Water Pressure Switch

In the event water pressure fails or falls below prescribed limit N.O. switch opens MMC and thus shuts down entire system. If water pressure is raised to set level of switch MMC will resume operation at the same level as before shutdown occurred.

2. Vacuum Switch

In case of vacuum failure below a desired level MMC will shut down until vacuum is restored.

3. Current Level Detector

Consists of a 600:5 current transformer, balance battery, level set load pot, IN536 diode, Varian recorder, N.C. switch set at 20% of Varian scale.

In the event of current increase or decrease Varian recorder will sense D.C. change and will drive toward N.C. Switch. System is calibrated so that a Δ of 6% in total current will actuate N.C. Varian Switch and cause complete shutdown of system. Power can only be restored by manually resetting the Varian. This is to enable operators to determine elapsed time for one or more failed lamps and also protects against Voltage $\Delta > 6\%$; as follows: $I = \text{Current}$, $E = \text{Voltage}$, $R = \text{Resistance of Lamps}$

$I = \frac{E}{R}$. as R is fixed any ΔE will be directly: to I and Varian senses any

ΔI , thereby protecting test against over-voltage or under-voltage. ΔI of 6% or ≈ 4.8 amps = 1 lamp current. Current increase or decrease $< 6\%$ can be read on Varian recorder by operator as $\Delta/O = 1.1$ amp.

* 6% = (I° F 1 lamp)

ENGINEERING DATA SHEET

SADI 965 REV 4/64

HEATING MODULE - LIGHT TEST

NUMBER 1 OF 8 PAGE

DATE 4-10-68

OBSERVER CUSTARD / MESSING

PROJECT S.O. 6-2933-7

AROMATIC LAMPS -

"Pre-Lin System Shut Down"

TIME	DATE	MIRROR LEVEL (Discn. Gage)	GLASPER TIME (MINUTES) (NR. MASTER)	TEMPERATURE (C/A) SEE FIG. 1 FOR LOCATION								AMP		REMARKS		
				TOP FIL 1	BOT. MOD. 2	BOT. CAN. MOD. 3	TOP CAN. MOD. 4	TOP MOD. 5	R.S. CAN. FIL 6	H ₂ O IN 7	H ₂ O OUT 8	L	R			
0910	4/10	5-M	3070.4											40		
0930		500-M	20 MIN.													MAX TEMP 1700 F.
1125		200-M	55 MIN											32		MAX TEMP 1530 F.
1200		50-M														
TOTAL GLASPER TIME 55 MIN w/ MAX TEMP 1530-1700 F.																
1420	4/10	2x10 ⁻⁴														MAX TEMP 1490 F.
1430		6-M	1 HR. 5 MIN	300	1382	1470	1505	1405	330	58	72	33	33			
1440		17-M	1' 10"	365	1390	1480	1475	1405	415	60	70	32	32			
1 HR 15 MIN / 440-6 F																
TOTAL GLASPER TIME 1 HR. 15 MIN. 4/10/68																
0805	4/11	8x10 ⁻⁴														- DIFFUSION PUMP ON.
0830		3x10 ⁻⁴														- HARTON (Lamps).
0845		7x10 ⁻³	15 MIN	80	1320	1460	1450	1418	172	58	72	34	34			
0855	50-M	5x10 ⁻³	25 MIN	255	1360	1490	1510	1465	308	58	72	34	34			
0908																STOP ADJ. AMP.
0909/0915		2x10 ⁻³	30 MIN.	472	1380	1537	1545	1505	502	60	70	33	34			
0930		2x10 ⁻³	45 MIN.	535	1372	1525	1585	1492	530	60	90	34	34			INCREASE H ₂ O FLOW TO MEDIUM
0945			60 MIN.	530	1380	1535	1542	1500	562	58	68	34.5	34			
GLASPER TIME = 1 HR.															STOP - VOLTAGE SURGE w/ OUT OFF	
1000	4/11	8x10 ⁻⁴		550	1265	1525	1545	1508	562	58	70	33.8	34.2			
1015		9x10 ⁻⁴	15 MIN.	540	1195	1475	1505	1495	560	58	72	35	35			
1030		1x10 ⁻³	30 MIN	555	1252	1502	1535	1500	562	56	72	34	34			
1045		2x10 ⁻³	45 "	535	1252	1508	1530	1490	562	56	71	31.5	32			
1100			60 MIN	552	1250	1503	1532	1495	562	58	72	34.2	34.2			STOP - ADD COOLING COIL.
TOTAL GLASPER TIME (4/10 & 4/11) = 3 HR 6 AND 15 MIN.																

SOLAR

DIVISION OF INTERNATIONAL HARVESTER COMPANY
2200 PACIFIC HIGHWAY, SAN DIEGO, CALIFORNIA 92112

RESEARCH MEMORANDUM

R68H-1557-3

September 17, 1968

TO: T. L. Stockham (F-5)
L. G. Desmon (F-5)

From: 
D. H. Sanders
Research Engineer, Ext. 731

cc: J. E. Benawa
R. L. Neher
File (JHS)
Ref. File

SUBJECT: PROGRESS REPORT NO. 3 - HEATER MODULE LIFE TEST
WEEK ENDING 8-23-68

Reference: Brayton Cycle Heater Program - S. O. 6-2933-7

Continued testing was conducted through July and August as shown in Chart, page 2.

This chart is a breakdown and condensation from the laboratory data sheets kept as a running record of times, modifications, lamp failures and lamp changes.

The chart does not reflect the manhours and minor problems encountered during test - such as tear down and set-up, modification of insulation techniques and polishing module between tests.

A description of the general system is discussed in Progress Report No. 2.

JHS:cm

SOLAR

DIVISION OF INTERNATIONAL HARVESTER COMPANY
2200 PACIFIC HIGHWAY, SAN DIEGO, CALIFORNIA 92112

RESEARCH MEMORANDUM

R69H-1557-8

January 15, 1969

TO: L. G. Desmon (F-5)

cc: J. E. Benawa
R. L. Neher (2)
File (1)

From: 
R. L. Neher
Senior Research Engineer, Ext. 732

SUBJECT: PROGRESS REPORT NO. 8 - HEATER MODULE LIFE
TEST SUMMARY - PERIOD 12-27-68 through 1-15-69

Reference: Brayton Cycle Heater Program - S. O. 6-2933-7

Attached are the Heater Module Life Test Summary for Vacuum (Sheet 1) and Atmosphere (Sheet 2) Environment Testing to date.

Original test data sheets are on file in the Experimental Physics Lab.

RLN:cm

Attachments

Module Description	Test Run	Total Hrs/Run	Accum. Hours	Avg. Temp.	Max. Temp.	Period Start/Stop	Remarks and Observations
1. 5 Lamp Module	5-5B	*	145	1610	1760	8/28 - 8/30	* See Test Data Sheets No. 5 through 5B.
2. 5 Lamp Module - (5) New Lamps (Bar Machine - Large Dia.)	#6	2:33	2:33"	1650	1710	9/05 - 9/05	Lamps w/Sylvania Potted and Welded Leads (Soft Ni Wire). See Test Data Sheet #6. Photograph 58-4589 and 68-4604.
3. 5 Lamp Module - (5) New Lamps (Ceramic Coated)	#6A	45:00		1605	1720	9/09 - 9/11	See Data Sheet #6A for Inspection After Test Run.
	#6B	48:15	93:15	1580	1610	9/16 - 9/18	Lost (1) Lamp #3 Position (Leads at Base) - See Data Sheet #6B.
4. 5 Lamp Module - (1) Lamp Replaced	#6C	287:45		1600	1755	9/18 - 10/01	See Data Sheet #6-C.
		4 lamps	381:00				
		1 lamp	287:45				
	#6-D	29:00		1650	1740	10/02 - 10/03	
		4 lamps	410:00				
		1 lamp	316:45				
	#6-E	97:30		1630	1705	10/04 - 10/08	
		4 lamps	507:30				
		1 lamp	414:15				
	#6-F	177:10		1680	1730	10/10 - 10/21	Total accumulated hours was 684 Hours 40 Minutes for (4) Lamps and 591 Hours, 25 Minutes for (1) Lamp. All lamps returned to hold area with (2) subjected to further test in atmosphere - see atmosphere test run #8.
		4 lamps	684:40				
		1 lamp	591:25				
5. 5 Lamp Module - Vacuum (3) S. S. Sleeve Lamps	#7	01:00	<1000	1485	1485	10/22 - 10/27	Test Run #7 Using Module and Lamps of Atmos. Test. Total Exposure to Atmosphere Test Prior to Start of Vacuum Run was: 2 Lamp - Ceramic - 753 Hours, 2 Lamp - SS Sleeve - 74 Hours, 20 Minutes See Atmos. Test 1 Lamp - SS Sleeve - 67 Hours Data Sheet #7D-7E. Lamp #4 SS Sleeve Failed.
	#7-A	25:00	26:00	1660	1680	10/23 - 10/24	Replaced #4 Lamp with New SS Sleeve Lamp and Continued Test Run. SS Lamp # failed. Base Joint Weld Failure.
	#7-B	280:45	306:45	1660	1680	10/25 - 11/06	Lamp Failed (SS Sleeve) - All lamps forwarded to Engineering (L. Desmon) for Vendor Evaluation.
							NOTE: Total Elapsed Time Ceramic Lamps - 306 Hours, 45 Minutes Vacuum 753 Hours, 55 Minutes Atmosphere. Total Exposure = 1060 Hours, 40 Minutes.
6. 5 Lamp Module - (5) New Sylvania	#8	610:30	610:30			11/8 12/6	(5) New Sylvania Lamps (3) SS and (2) Ceramic. Total Exposure Time was 610 hours and 30 min. Without failure. Lost (1) ceramic base lamp which was replaced with new ceramic base lamp for Test Run 8-A. Also replaced 2nd lamp with loose Ni wire at weld joint. See Data Sheet #8.

SOLAR

Module Description	Test Run	Total Hrs/Run	Accum. Hours	Avg. Temp.	Max. Temp.	Period Start/Stop	Remarks and Observations
1. 5 Lamp Module	#7	451:40		1670°F	1710°F	9/11 - 9/30	New 750W Lamps Sylvania (Modified) - Ceramic Base Ni Wire
	#7-A	25:50	477:30	1680	1740	9/30 - 10/7	Replaced (1) Lamp with a New Brass Base Lamp - No Failure - See Run #7-A.
	#7-B & #7-C	201:10	678:40	1650	1725	10/3 - 10/15	Removed Brass Base Lamp and 2 Ceramic -- Replaced with (3) New SS Sleeve Lamps - See Data Sheet #7B and 7C. Total Hour Brass Base Lamp was 201 Hours, 10 Minutes.
	#7-D	3:05		1600	1720	10/17 - 10/17	(3) New SS Sleeve Lamp Identified Per Dwg. #1503 - 750W Flexlead Teflon Coated
	#7-E	4:15		1450	1565	10/18 - 10/18	(2) Original Ceramic Base Lamp. Stop to Pot Inside of SS Sleeve Lamps to Top of Sleeve
	#7-F	67:00	7:20	1640	1695		(3) SS Sleeve Lamps Fully Potted. (1) SS Sleeve Lamp Failed During This Run. Replaced With New SS Sleeve Lamps. See Data Sheet 7-E and 7-F.
	#8	167:20	167:20	1640	1740	10/28-11/4	End Test 7-F with Lamps and Module Transferred to Vacuum Environment Test - See Test Data Sheet #7-Vacuum. All Lamps Functional. Total Accumulated Time in Atmosphere Environment: Ceramic Base Lamps = 753 Hours SS Sleeve Lamps = 74 Hours, 20 Minutes
2. 5 Lamp Module	#9	1007:45	1007:45	1680	1705	11/5 - 12/20	(5) New SS Lamps - 300 W, 60V w/5 Clip Restraints (T-4's) Test Run #8 Stop - No Failure T-4 Lamps. Remove module and replace lamps with Flexlead, non insulated Ni Wire partially potted SS Sleeve over Ceramic Base - Final Configuration for Test Run #9. Total Exposure Time of 1007 hours, 45 minutes without failure with intermediate inspection. See Test Data Sheet #9. END OF TEST
							NOTE: Photograph 69-0011 shows condition of lamps after life test of 1000 hours.

(A)

APPENDIX D

SINGLE-LAMP, LIFE-TEST - SUMMARY REPORT

BRAYTON CYCLE SINGLE-LAMP, LIFE-TEST SUMMARY REPORT

1.0 Introduction

A T4, 750-watt, 120-volt, quartz-iodine lamp was selected at random from a shipment of lamps from Aerometrics. It was mounted in a test fixture which would allow testing in both vacuum and air environments. A target of Inconel 600 two inches from the tip of the lamp was instrumented with chromel-alumel thermocouples to measure the output from the lamp.

Three individual tests were performed: two in vacuum and one in air. An as-received potted lamp failed in 50 hours in vacuum conditions from power lead problems. A Solar potted lamp with a modified design at the power lead connections was operated for 600 hours in vacuum of 1×10^{-4} Torr. The same lamp was then tested in an air environment for an additional 1400 hours before filament failure caused termination of the life test. The operating power level of the test was 53 percent of the rated power of the lamp.

2.0 Experimental Procedure

An as-manufactured (by Sylvania) standard 750-watt quartz iodine lamp was procured. This lamp had been potted in a ceramic insulator base with Sauerisen No. 31 potting material. The power leads consisted of stranded nickel wire, spot welded to the molybdenum pins at the base of the lamp and covered with plastic type insulating sleeving. A lamp holder was machined from aluminum (T-6061) bar stock and designed for water cooling at the base. The concave reflector, which was 2.5 inches in diameter, was polished with -325 grit aluminum oxide-water paste to a surface finish of 5 to 7 microinches (RMS). The lamp holder was inserted into a target assembly which positioned the lamp two inches from, and normal to the target end plate. The target portion of the assembly was fabricated from Inconel 600 material and instrumented with three chromel-alumel thermocouples, two on the end plate and one on the side area of the target assembly; oven dried fiberfrax was used to insulate the target area. The target assembly was sealed into a port in a vacuum facility using an O-ring and bolted flange. Figure 1 shows the test apparatus in place. Power to the lamp was adjusted using a 12.5-amp, 115-volt, Variac in series with a Raytheon 500-watt line voltage regulator. Voltage and amperage were indicated on a Weston AC voltmeter and ammeter. Periodically, the temperature, voltage, and current of the system were monitored and recorded.

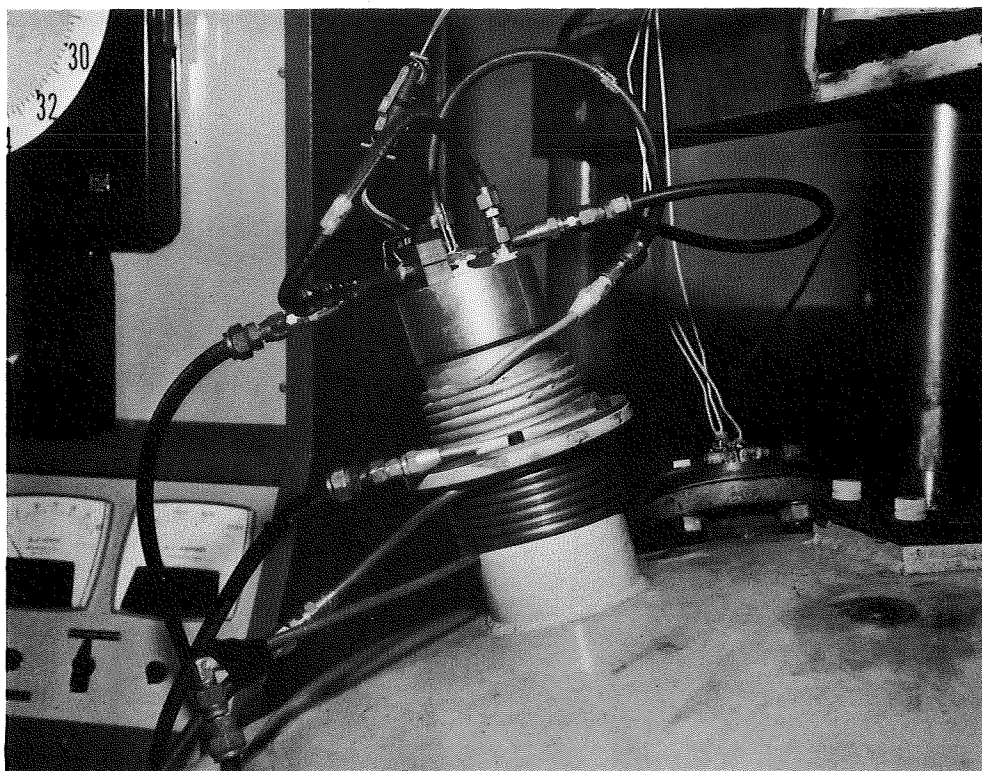


FIGURE 1. LAMP LIFE TEST APPARATUS

3.0 Test of Aerometrics Potted 750-Watt Lamp

An electrical lead junction of an as-received lamp which was depotted is shown in Figure 2. The difficulties in making this connection by spot welding are obvious from the oxidation, crushing, and delamination of the molybdenum pins of the lamp; each wire of the stranded extension leads must be securely welded to the lamp-pin to prevent a high-resistance point and local heating of the spot weld area.

The lamp was inspected after 39.5 hours of testing and the conditions were as follows:

- Lamp - normal, no apparent change from start of test
- Reflector surface - covered with a very thin opalescent film, easily removed with acetone
- Target - satin-grey metallic surface with bright crystalline area 0.5-inch in diameter (apparently hottest area) just off-center of target end plate.

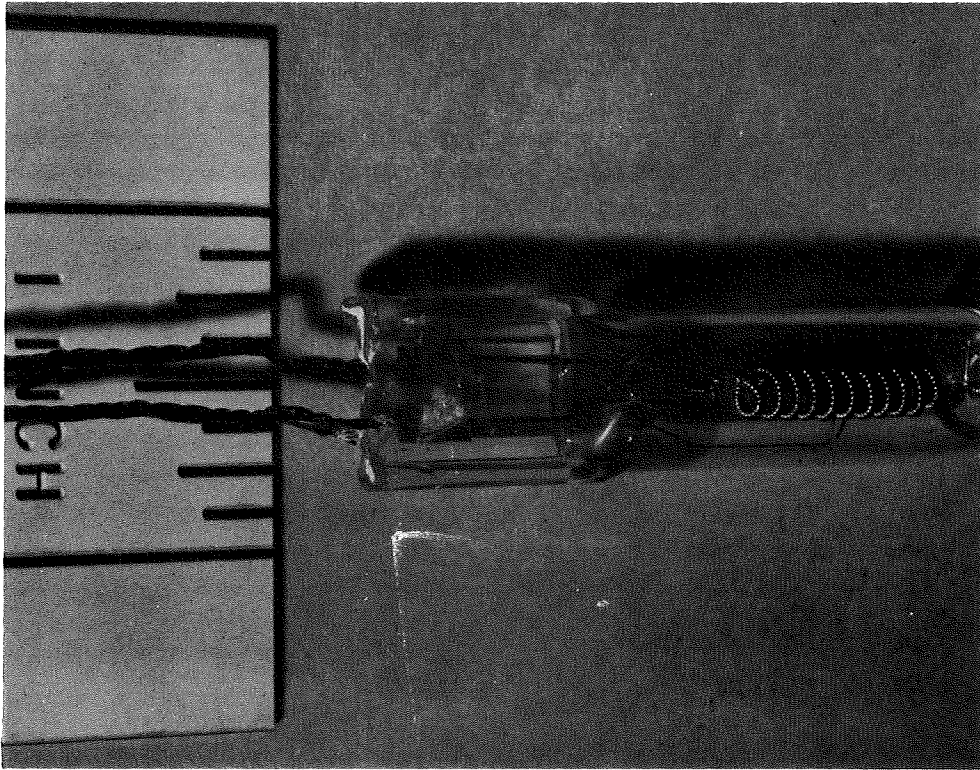


FIGURE 2. DEPOTTED QUARTZ LAMP; As-Received

The test was restarted at 1700° F target temperature. Operating conditions after cleaning the reflector were nearly identical to the original conditions; i. e. , 76 volts, 1700° F. At 12 hours operation after restarting the test, the stranded nickle leads burned off at the base of the bulb. The area was covered with a black, apparently carbonaceous material (Fig. 3). Total life for this lamp configuration was 51.5 hours, all under vacuum conditions; the major cause of failure appeared to have been an inferior spot weld at the juncture of the stranded leads and molybdenum pins at the base of the lamp. The plastic type sleeving in this area was apparently responsible for the black carbonaceous deposit.

Measurements using a thermocouple of 0.005-inch diameter chromel-alumel wire, spot welded to a lamp base pin, indicated that a temperature of 350 to 500° F occurs on the lead pins when the lamp is operated at 80 volts in air. In a vacuum environment and the pin insulated by the potting material, the temperature in the area will be high enough to cause deterioration of the plastic type sleeving. Charring of the sleeving in this area probably caused arcing between the pins contributing to the failure.

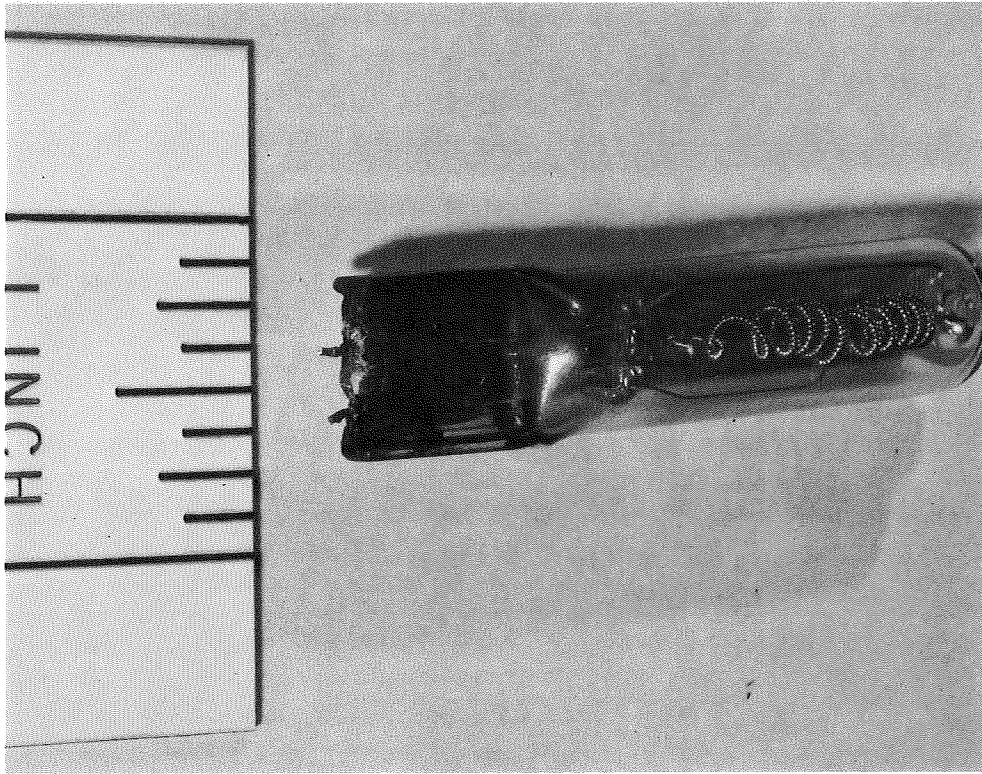


FIGURE 3. AEROMETRICS-POTTED QUARTZ LAMP AFTER 51.5 HOURS OPERATION AT LOW PRESSURE

4.0 Test of Solar-Potted 750-Watt Lamp - 600 Hours at Low-Pressure

To correct the apparent problems associated with the previous test lamp, the following changes were made to a new 750-watt, 120-volt, T4 lamp:

- Solid 1/16-inch diameter nickel lead wires were brazed to the lamp power pins using Easyflow-3 silver brazing alloy
- Fused alumina insulators were placed over the nickel lead wires in the hot areas
- The lamp was potted with Sauerisen No. 31 into a single (instead of a two-part) insulator

The lamp was then sealed into the lamp holder. A new Inconel 600 target base was installed in the target assembly, instrumented with three new chromel-alumel thermocouples, and sealed into the vacuum facility. The life test was started at a pressure of 4×10^{-5} Torr and run continuously except for seven periodicals

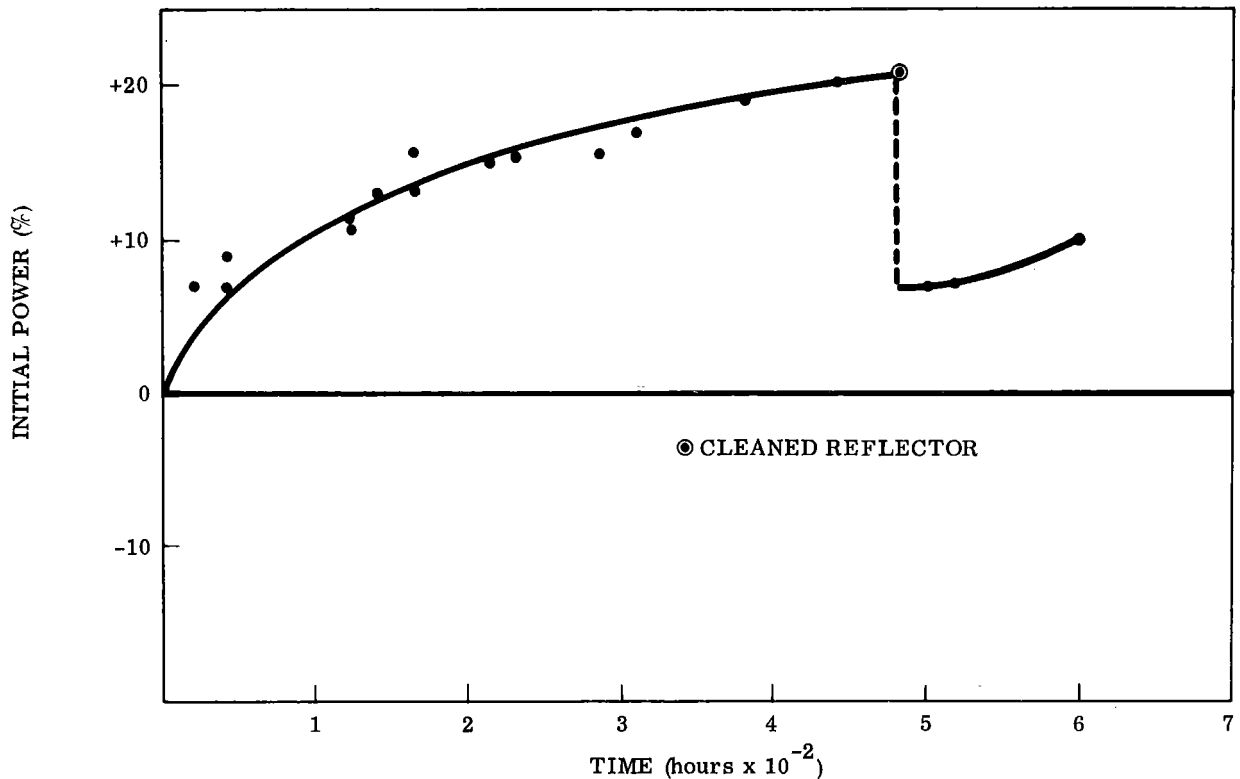


FIGURE 4. POWER REQUIREMENT TO MAINTAIN 1700°F TARGET TEMPERATURE VERSUS TIME

interruptions to inspect the lamp, reflector, and target. A plot of power requirement to maintain a maximum target temperature of 1700°F versus time for this 600-hour test is shown in Figure 4; the power requirement at 480 hours of operation in vacuum had increased about 20 percent over the original value to maintain a target temperature of 1700°F. Wiping the opalescent film from the cold reflector surface reduced the power required to sustain the 1700°F target temperature by 65 percent, to a value only 7 percent greater than that required at the initiation of the test. After 600 hours of low-pressure operation, the test was terminated. Examination of the lamp, reflector, and target showed:

- No apparent change in the bulb or filament.
- The reflector, when wiped free of the film, was apparently unaffected.
- The target was a matte-grey in color, with a darker grey spot 3/4-inch in diameter near the center of the target face. A slight bluish ring on the target wall near the flange area (colder zone) had formed.

A calibration check of the chromel-alumel thermocouple which indicated the maximum target temperature during the 600-hour test was made and the results are shown in Figure 5. The maximum deviation from the reading of a new couple was +10°F and occurred at 1400°F. At 1700°F, the aged couple exhibited a +4°F differential; well within the normal accuracy for standard thermocouple wire.

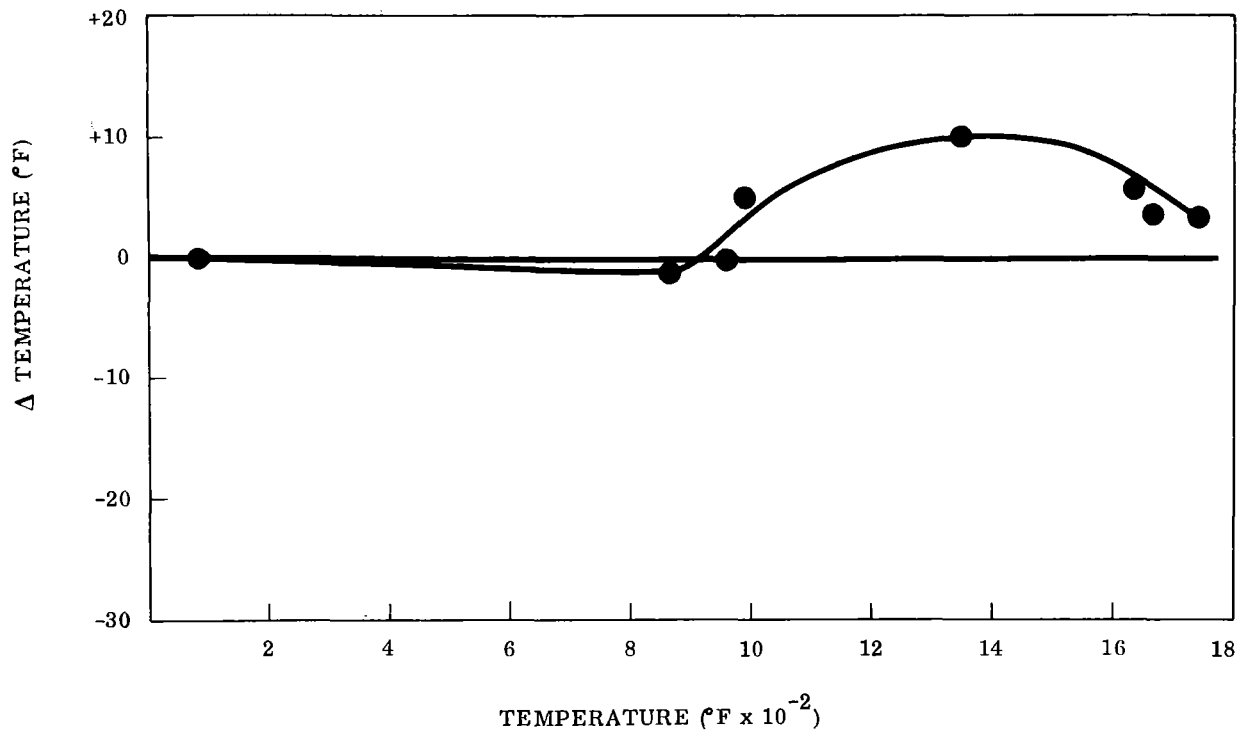


FIGURE 5. THERMOCOUPLE CALIBRATION, LOW PRESSURE TEST

5.0 Test of Solar Potted 750-Watt Lamp - 1400 Additional Hours in Air

The same lamp and assembly was set up for testing in air; the target face had been bead-blasted and new thermocouples installed. The outside area of the target was insulated to a thickness of approximately 1.5 inches with fiberfrax. A 500-watt hot plate was placed under the target face to subsidize the heat losses. The reflector surface was cleaned and represented approximately the same finish as before the low pressure test.

After about 15 hours of operation, it was apparent that greater than 80 volts would be required to maintain a 1700°F target temperature. Oxidation of the target resulted in an increase in the absorbtivity and emittance of the target. Film formation on the reflector further reduced the efficiency of the unit. A decision was made to hold the 80-volt input to the lamp constant and run to equilibrium conditions; at this point the reflector was cleaned and the test resumed.

After 304 hours operation in air, the target temperature dropped to about 1550°F and was holding steady. The test was temporarily terminated for relocating the test and cleaning the reflector surface. The reflector was cleaned using acetone with fiberfrax as the abrasive. The maximum target temperature ranged from 1740

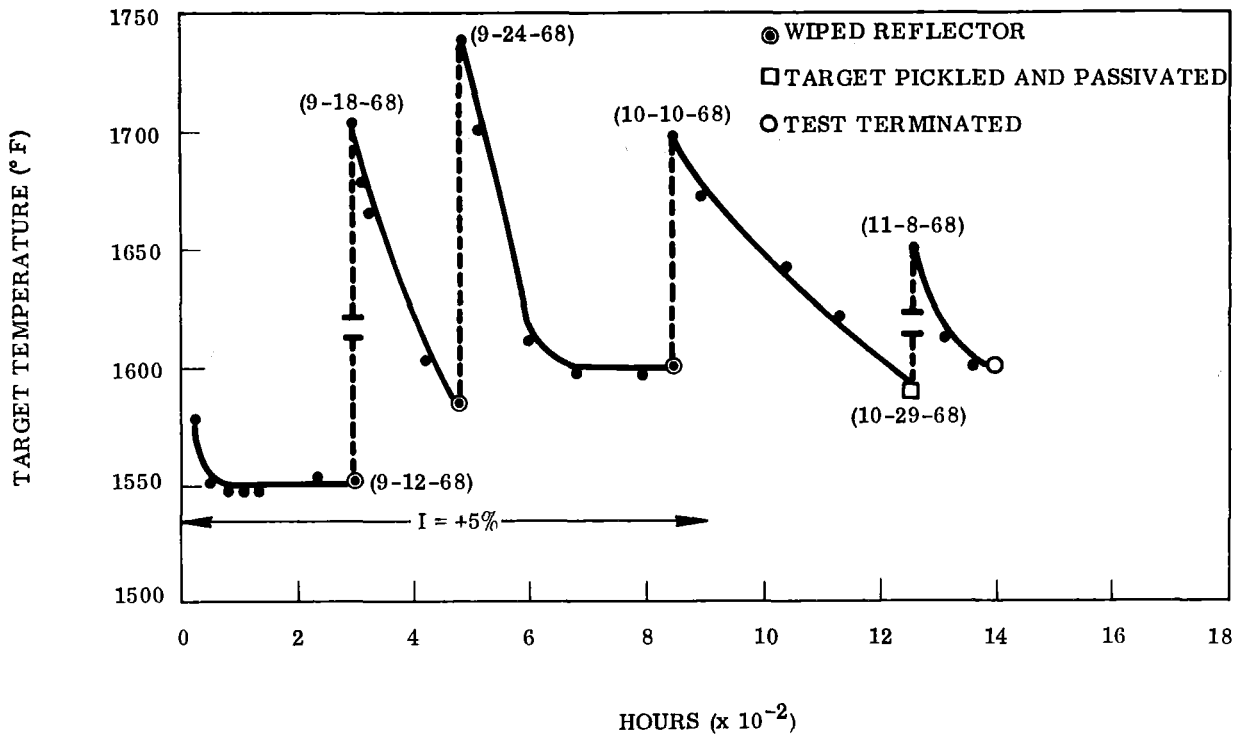


FIGURE 6. TARGET TEMPERATURE VERSUS HOURS, AIR OPERATION

to 1590°F (at a constant value of 80 volts); the higher temperatures occurred after cleaning the reflector. Within 200 hours, the target temperature decreased to approximately 1600°F. Figure 6 shows a plot of the maximum target temperature versus hours of air operation. The reflector surface was cleaned periodically and always resulted in increased target temperature. The loss in thermal efficiency was apparently due to a redeposition of volatile materials on the cold reflector. X-ray analysis of the deposit wiped from the reflector surface showed the following elements to be present:

<u>Primary Material</u>	<u>Small to Trace Amount</u>	
Potassium	Lead	Silicon
Chlorine	Zinc	Phosphorous
	Copper	Calcium
	Nickel	Chromium
	Iron	Sulfur
	Aluminum	

During the 600-hour air environment test, the amperage in the lamp circuit increased approximately 10 percent. With voltage constant at 80 volts, the starting

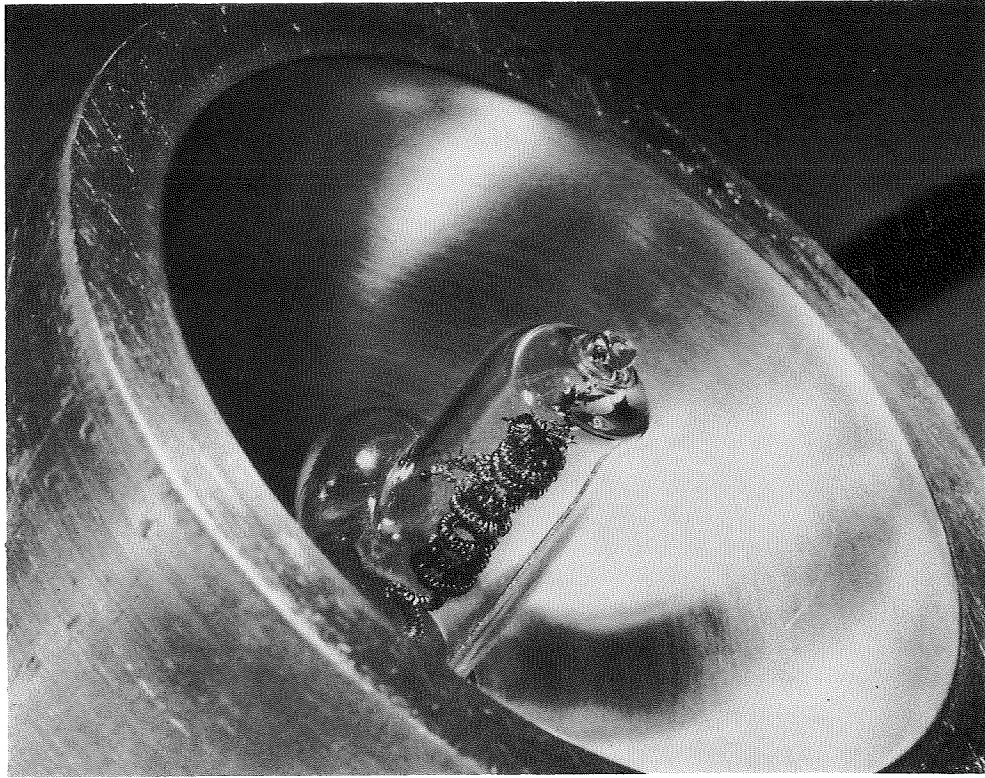


FIGURE 7. SOLAR-POTTED QUARTZ LAMP AFTER 1994 HOURS OPERATION IN AIR AND VACUUM

current in the circuit was 5.2 amps and, after about 1300 hours, the current was 5.8 amps. At 1200 hours, the first noticeable change in the lamp filament was observed. Small crystalline or dendritic formations of bright metallic material (tungsten) were observed over about 50 percent of the filament. The primary area showing the crystals was from mid-point of the filament to the terminal end near the tip of the lamp envelope.

Failure at 1400 hours occurred about mid-point of the filament and caused the quartz envelope to soften and bubble. The lamp envelope was deformed, but intact, and the filament was operable but damaged; Figure 7 shows the lamp after termination of the life test. The total time of operation at approximately 80 volts input to the lamp was 1994 hours, of which 600 hours were accumulated in a low-pressure environment and 1394 hours at ambient pressure in an air environment.

6.0 Conclusions

The 750-watt, quartz-iodine lamp, as supplied by Aerometrics at the initiation of this program was not designed to perform reliably in the Brayton Cycle Heater. Better engineered designs which correct the problems encountered in this

test program, i. e. , improved lead wire attachment, and the elimination of the organic type sleeving material in the hot areas, led to a more reliable product. The tungsten filament, iodine cycle system appears to be the limiting factor on the life of the lamp when adequate power connections and sleeving materials are used. Other tests had previously revealed that the configuration and size of the concave reflecting surface is also a major lamp life factor.

FINAL REPORT DISTRIBUTION LIST

NASA Lewis Research Center
 21000 Brookpark Road
 Cleveland, Ohio 44135
 Attention:

W. T. Wintucky Mail Stop 500-201	(3)	Technology Utilization Office Mail Stop 3-19	(1)
D. G. Beremand Mail Stop 500-201	(1)	P. A. Thollot Mail Stop 500-201	(1)
H. O. Slone Mail Stop 500-201	(1)	T. A. Moss Mail Stop 500-201	(1)
D. R. Packe Mail Stop 500-201	(1)	J. E. Dilley Mail Stop 500-309	(1)
V. F. Hlavin Mail Stop 3-14	(1)	Library Mail Stop 60-3	(2)
B. Lubarsky Mail Stop 3-3	(1)	Report Control Office Mail Stop 5-5	(1)
L. G. Gertsma Mail Stop 500-202	(1)		

NASA Lewis Research Center Plum Brook Station Taylor Road Sandusky, Ohio 44870 Attention: J. C. Nettles Mail Stop 1441-1	(10)	National Aeronautics and Space Administration Washington, D. C. 20546 Attention: H. D. Rothen Code RNP	(1)
---	------	--	-----

NASA Scientific and Technical Information Facility
 Post Office Box 5700
 Bethesda, Maryland 20014
 Attention: Acquisitions Branch (SQT-34054) (1 + Reproducible)

NASA Ames Research Center Moffett Field, California 94035 Attention: Library	(1)	Battelle Memorial Institute 505 King Avenue Columbus, Ohio 43201 Attention: Library	(1)
NASA Goddard Space Flight Center Greenbelt, Maryland 20771 Attention: Library	(1)	Bureau of Naval Weapons Department of the Navy Washington, D. C. 20025 Attention: Code RAPP	(1)
NASA Manned Spacecraft Center Houston, Texas 77058 Attention: Library	(1)	Institute for Defense Analyses 400 Army-Navy Drive Arlington, Virginia 22202 Attention: Library	(1)
NASA Marshall Space Flight Center Huntsville, Alabama 35812 Attention: Library	(1)	SAMSO Los Angeles Air Force Station Los Angeles, California 90045 Attention: Library	(1)
NASA Langley Research Center Langley Station Hampton, Virginia 23365 Attention: Library	(1)	Aerospace Corporation P. O. Box 95085 Los Angeles, California 91745 Attention: Library	(1)
U. S. Army Engineer R&D Labs Gas Turbine Test Facility Fort Belvoir, Virginia 22060 Attention: Library	(1)	Massachusetts Institute of Technology Cambridge, Massachusetts 02139 Attention: Library	(1)
Air Force Systems Command Aeronautical Systems Division Wright-Patterson Air Force Base, Ohio 45433 Attention: Library	(1)	Brookhaven National Laboratory Upton, Long Island, New York Attention: Library	(1)
Power Information Center University City Science Institute 3401 Market Street, Room 2107 Philadelphia, Pennsylvania 19104	(1)	Argonne National Laboratory P. O. Box 299 Lemont, Illinois Attention: Library	(1)
Jet Propulsion Laboratory 4800 Oak Grove Drive Pasadena, California 91103 Attention: Library	(1)	Oak Ridge National Laboratory P. O. Box X Oak Ridge, Tennessee 37830	(1)

National Bureau of Standards (1)
Washington, D. C.
Attention: Library

Sandia Corporation (1)
P. O. Box 5800
Albuquerque, New Mexico 87115
Attention: Library